12-1-2021 2:00 PM

Metal Ligand Cooperative Complexes for Acceptorless Dehydrogenation of Amines

Matthew D. Hoffman, *The University of Western Ontario*

Supervisor: Blacquiere, Johanna M., *The University of Western Ontario*

A thesis submitted in partial fulfillment of the requirements for the Master of Science degree in Chemistry

Abstract

Complexes of the type [M(Cp/Cp*)(MeCN)($P^{R}_2N^{R'}_2$)]PF_6 (M = Fe, Ru) were synthesized and/or tested towards acceptorless dehydrogenation (AD) of amines. The primary amine benzylamine can undergo AD to form a mixture of products, and a selection of catalysts were employed in an attempt to control product selectivity. As a result, trends in product distribution were observed by modifying the primary and secondary coordination spheres on the catalyst. A new complex, [Fe(Cp)(MeCN)($P^{Ph}_2N^{Ph}_2$)]PF_6 (**3a**) was synthesized and characterized and was found to be a completely selective dehydrogenation catalyst. This is the first example of an iron catalyst capable of selective dehydrogenation without the need for an exogenous base. Mechanistic analysis was conducted using *in-situ* IR spectroscopy to elucidate the reaction rate order, and rate-determining step for [Ru(Cp)(MeCN)($P^{Ph}_2N^{Ph}_2$)]PF_6 (**1a**) using indoline. The results of these mechanistic studies suggest that the catalytic mechanism for **1a** is a cooperative outer sphere mechanism.

Keywords

Ruthenium(II), Iron(II), synthesis, homogeneous catalysis, acceptorless dehydrogenation, AD, primary amines, *N*-heterocycles, MLC, metal-ligand cooperative, tunability, H_2, rate analysis, VTNA, mechanism, imine, nitrile, selective, selectivity, P2N2

Summary for Lay Audience

A catalyst is a substance that helps make chemical reactions easier. The chemical reaction focused on in this Thesis removes H_2 from molecules and releases it as hydrogen gas. However, there is more than one possible product, and there are many factors that determine the amounts of each product formed. To understand why a particular product is favoured over another, multiple different catalysts were tested. A new catalyst was made and is like a previously known catalyst. The new catalyst has iron in its structure, instead of the previously known catalyst, which had ruthenium. The iron catalyst was the most selective out of all the catalysts tested and is one of the first examples of an iron catalyst capable of doing this reaction. Studies to understand more about how these catalysts work were conducted, and the tested catalysts react differently compared to other known catalysts used for H_2 removal. The reason why they act differently is because of the way the structure around the metal was designed. This structure can be fine-tuned to make a chemical reaction more efficient. Using iron as a cheap alternative to precious metals like ruthenium, and further modification of the iron catalyst, could result in cheaper, more effective catalyst with a variety of different applications. Some applications include using a catalyst to store and release hydrogen as a potential fuel source, as well as employing catalysts for more eco-friendly synthesis of pharmaceuticals.

Co-Authorship Statement

All experiments were performed by M. Hoffman, except for catalytic data for **1d** which is published data from a previous paper published in our group.[80] Chapters 1-6 were written by M. Hoffman and edited by J. M. Blacquiere.

Acknowledgements

First, I would like to thank Dr. Johanna Blacquiere. Ever since I started as a volunteer research student in her lab four years ago, Johanna has been my mentor and guide for all things chemistry. Her wisdom and guidance have shaped me into the student and chemist I am today, and I cannot thank her enough. I would like to thank Dr. James Stubbs, who helped convince Johanna to let me work in her lab and acted as my first mentor at the beginning of my chemistry career. I would also like to take this time to thank everyone in the Blacquiere group (past and present) for your support, and for all the jokes and memories we shared together. I would like to thank Nick Henao, Benjamin Bridge, Devon Chapple, and Kyle Jackman. We've all been in this lab for about the same amount of time, and I appreciate all your help and support throughout the years. I would like to thank Shane Cochrane for always being around to answer any of my questions, and to chat during long reaction times (not like you really had a choice, since your lab is connected to ours). I would also like to thank my family and friends for their unwavering support and encouragement throughout the years. I would like to thank my two cats Henry and Theo for being my writing buddies these past few months. Special thanks to Mat Willans, the NMR facility manager, and Kristina Jurcic, the MALDI-MS facility manager. Finally, I would like to thank my best friend and fiancée, Lauren Micallef. You have been instrumental in keeping me motivated, focused, and sane these past months. I appreciate everything you do for me and am so grateful to have you in my life. Thank you for everything.

Table of Contents

List of Charts

List of Tables

List of Schemes

List of Figures

List of Appendices

List of Abbreviations

Å (angstrom)

AD (acceptorless dehydrogenation)

ADC (acceptorless dehydrogenative coupling)

Ar (aryl)

ATR-FTIR (Attenuated Total Reflectance –Fourier Transform Infrared)

BAr^{F}_{4} (Tetrakis(3,5-bis(trifluoromethyl)phenyl)borate)

Bn (benzyl)

$BnNH_2$ (benzylamine)

COSY (correlation spectroscopy)

Cp (cyclopentadienyl)

Cp* (pentamethylcyclopentadienyl)

Cy (cyclohexyl)

DAD (double acceptorless dehydrogenation)

DCB (1,4-dichlorobenzene)

DCM (dichloromethane)

DDQ (2,3-Dichloro-5,6-dicyano-1,4-benzoquinone)

DMF (dimethylformamide)

DMSO (dimethyl sulfoxide)

Dppe (1,3, bis-(diphenylphosphino)ethane)

Dppp (1,3, bis-(diphenylphosphino)propane)

GC-FID (Gas Chromatograph – Flame Ionization Detector)

h (hour)

HB (hydrogen borrowing)

HMBC (heteronuclear multiple bond correlation)

HMTA (hexamethylenetetramine)

HSQC (heteronuclear single quantum correlation)

IBX (2-Iodoxybenzoic acid)

IR (infrared)

M (metal)

MALDI-MS (Matrix Assisted Laser Desorption Ionization Mass Spectrometry)

Me (methyl)

MeCN (acetonitrile)

MLC (metal ligand cooperative)

NHC (*N*-heterocyclic carbene)

NMR (nuclear magnetic resonance)

Ph (phenyl)

ppm. (parts per million)

$P^{R}{}_{2}N^{R'}{}_{2}$ (1,5-R′-3,7-R-1,5-diaza-3,7-diphosphacyclooctane)

pKa (acid dissociation constant)

RT (room temperature)

tBu (tert-butyl)

THF (tetrahydrofuran)

TMS (tetramethylsilane)

TOF (turnover frequency)

TON (turnover number)

UV-Vis (ultraviolet-visible)

VTNA (variable time normalization analysis

W (watt)

Chapter 1: Introduction

1.1 Homogeneous Catalysis

A catalyst is a substance that increases the rate of a chemical reaction without being consumed.[1] These transformations proceed at a faster rate than the uncatalyzed reaction, as the presence of the catalyst lowers the activation barrier for a particular transformation. Catalysts are also powerful alternatives to stoichiometric reagents, as they decrease the amount of waste material relative to the uncatalyzed reaction of interest. Homogeneous catalysis is a reaction where the substrate (the starting material(s) of the reaction) and catalyst components are in the same phase.[2] The homogeneous nature of the catalyst allows for easier determination of structure-activity relationships, as well as the ability to characterize and observe the chemical structure of the catalyst by means of analytical methods such as Nuclear Magnetic Resonance (NMR) spectroscopy, which is difficult to do for heterogeneous catalysts.[3] The consequence of these features is that homogeneous catalysts are more versatile, and can be fine-tuned for a specific chemical reaction of interest.

Turnover number (TON) is a unitless term used to define catalyst lifetime.[4] The TON is the total amount of catalytic turnovers a catalyst can perform before dying. It is defined as the number of molecules of product formed divided by the number of active sites per molecule of catalyst.[5] Ideally, a catalyst should have a high TON, which means it could catalyze a reaction many times before dying. Turnover frequency (TOF) is the number of turnovers (TONs) per unit of time and is used to define catalyst efficiency. A higher TOF means that the catalyst is completing more catalytic turnovers per unit of time. It is easier to determine the TOF of a homogeneous catalyst, as the number of active sites is more easily determined compared to a heterogeneous catalyst.

1.2 Amine Oxidation: Methods of Accessing Imines and Nitriles

Imines, nitriles, and *N*-heterocycles are regarded as key motifs in drug design and are present in a diverse array of pharmaceutical compounds.[6–11] Traditional synthesis of imines involves the condensation of an amine with a carbonyl compound, which was

originally reported by Schiff in 1864.[12] Nucleophilic addition of the amine to an aldehyde affords a hemiaminal, which then eliminates water to form the imine (Scheme 1.1). The imine formed can also react reversibly with water to reform the aldehyde and amine starting materials. There are many factors that affect the equilibrium of this reaction, including steric and electronic effects, concentration, solvent choice, and reaction temperature.[13] Conducting the reaction in the presence of a Lewis acid, such as P_2O_5/SiO_2 activates the carbonyl moiety, rendering the Cα more susceptible to nucleophilic attack by the amine.[14] The Lewis acid also acts as a drying agent, which drives the reaction forward by removal of the byproduct H_2O.[11]

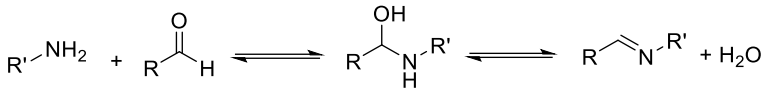

Scheme 1.1. Condensation reaction of an amine and an aldehyde to form an imine and water.

Other traditional methods for synthesis of imines from amines involves reacting an amine with a stoichiometric amount of an oxidizing agent, such as 2-iodoxybenzoic acid (IBX), MnO_2, 2,3-dichloro-5,6-dicyano-1,4-benzoquinone (DDQ), or $HgO\text{-}I_2$ (Scheme 1.2).[15–18] These reactions all gave good to excellent yield of secondary aldimines. A downside of using stoichiometric oxidants in a reaction is that it generates an equivalent amount of waste material (usually toxic), which then has to be removed.[19]

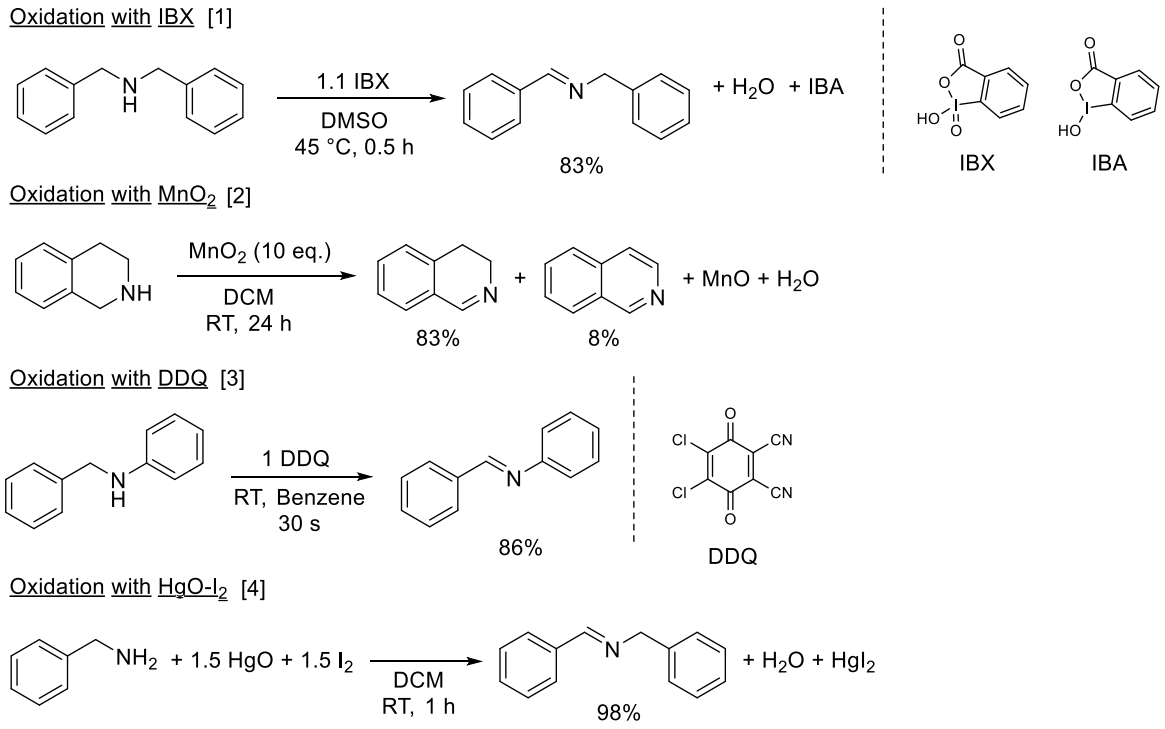

Scheme 1.2. Synthetic methods used to prepare imines from amines/*N*-heterocycles. References: [1][15][2][16][3][17][4][18]

Transition metal catalysts can also be employed for oxidation of secondary amines to imines (Scheme 1.3).[20] One example is Shvo's catalyst which afforded good to excellent yields of secondary ketimines. However, it also required the use of oxidant MnO_2, as well as a super-stoichiometric amount of 2,6-dimethoxyquinone, which acted as a reversible H_2 acceptor.

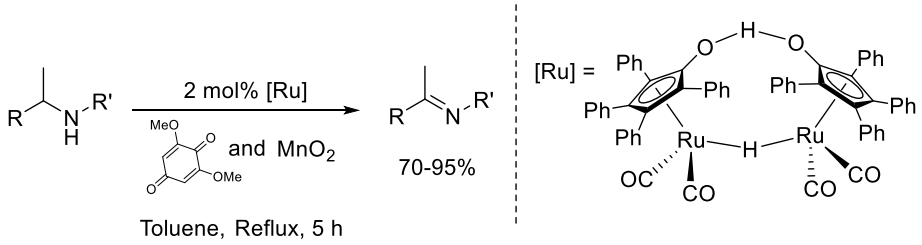

Scheme 1.3. Oxidation of a secondary amine to form a secondary ketimine using Shvo's catalyst, in conjunction to an oxidant, and hydrogen acceptor.[20]

Established methods to synthesize nitriles involves a mix of catalytic, and non-catalytic methods, including ammoxidation, the Sandmeyer reaction, cyanation, dehydration of aldoximes and amides, and the Rosenmund-von Braun reaction.[21–29] Many of the ways to access nitriles have long reaction times, require stoichiometric oxidants, or require the employment of an additive, in conjunction with a catalyst, to afford nitriles. Overall, synthesis of nitriles and imines from amines suffer from a variety of issues, resulting from the use of stoichiometric reagents.

An alternative method to synthesize imines from amines is transfer dehydrogenation. This is a metal-catalyzed reaction where the substrate is oxidized by removal of H_2. An alkene is needed as a stoichiometric additive, which serves as the hydrogen acceptor molecule (Scheme 1.4).

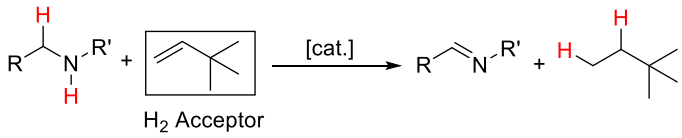

Scheme 1.4. General depiction of catalytic transfer dehydrogenation. Dehydrogenation of a secondary amine in the presence of a sacrificial H_2 acceptor alkene forms the dehydrogenated secondary aldimine product as well as one molecule of hydrogenated alkane.

In 2002, Jensen and co-workers used an Ir(III)-PCP pincer complex,[30] previously used as a catalyst for transfer dehydrogenation of cycloalkanes (Scheme 1.5a).[31,32] Reacting a secondary amine with the Ir(III) catalyst resulted in 64% secondary aldimine as the product. This reaction did however require 200 °C reaction temperatures, 72 h of reaction time, and nearly 10 mol% catalyst loading in order to achieve decent yields. In 2008, Lee and Yi expanded the work done by Jensen, by developing a tetranuclear ruthenium-μ-oxo-μ-hydroxo-hydride complex for transfer dehydrogenation of amines (Scheme 1.5b).[33] This compound was found to be an effective catalyst for dehydrogenation of a wide variety of amines and *N*-heterocycles, with TONs ranging from 35 to as high as 8000. However, temperatures of up to 200 °C, and the presence of a stoichiometric amount of *tert*-butyl ethylene were required for this transformation. Additionally, many of the primary amines

afforded product mixtures of both secondary aldimines and secondary amines. Instead of H_2 transfer to the sacrificial alkene, the imine was instead hydrogenated leading to the formation of the secondary amine product. With benzylamine as a substrate, 59% imine and 29% amine are formed, which is a 3:1 ratio of dehydrogenation to hydrogenation product. Overall, transfer dehydrogenation suffers from harsh reaction conditions, and requires the presence of a stoichiometric equivalent of a sacrificial H_2 acceptor molecule. Furthermore, product selectivity issues arise when the product imine is hydrogenated by the catalyst, to form an amine.

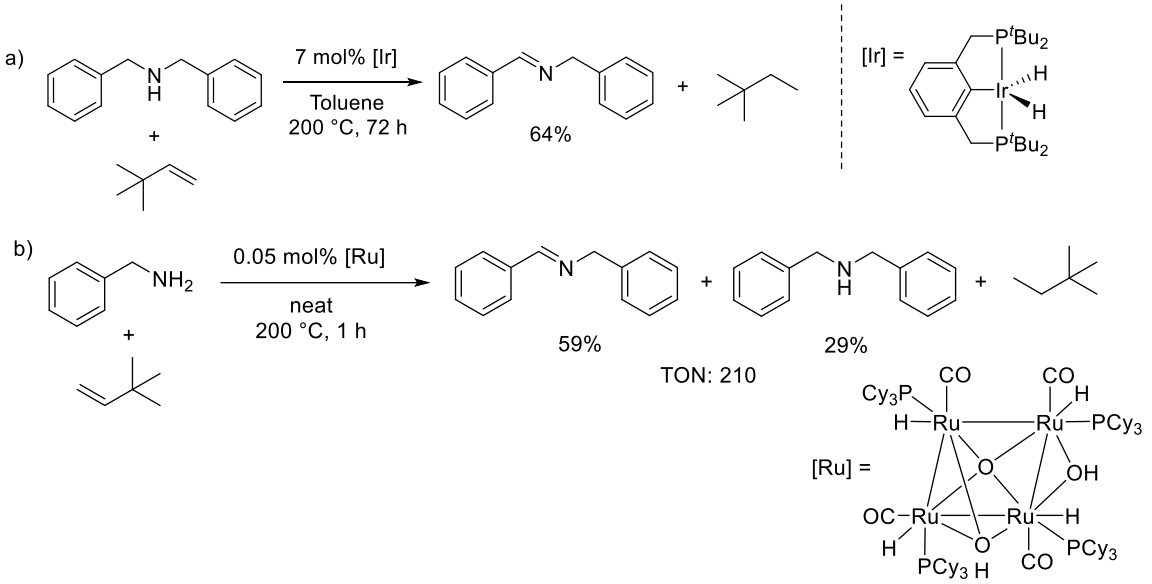

Scheme 1.5. a) Catalytic transfer dehydrogenation of dibenzylamine in the presence of a sacrificial hydrogen acceptor to form a secondary aldimine and an alkane.[30] b) Catalytic transfer dehydrogenation of benzylamine to form a 3:1 mixture of secondary aldimine and secondary amine.[33]

A powerful method of accessing imines catalytically is through acceptorless dehydrogenative coupling (ADC) of alcohols and amines (Scheme 1.6). In an ADC reaction, an alcohol is dehydrogenated to form an aldehyde/ketone, which then reacts with a molecule of amine to generate an imine, releasing water and H_2 as the sole by-products. This improves upon transfer dehydrogenation, as there is no longer a stoichiometric amount of alkane produced.

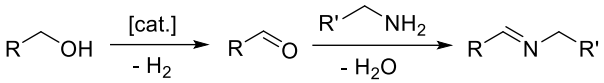

Scheme 1.6. ADC of a primary alcohol in the presence of a primary amine with to form an imine.

In 2010, Milstein employed Ru(II)-PNP pincer complexes for acceptorless dehydrogenative coupling of primary alcohols and amines to form imines (Scheme 1.7a).[34] The catalysts were designed with pyridinyl methylene spacers, which can aromatize/dearomatize to accept/release a proton, which is a key step in the catalytic mechanism. The first step of the proposed mechanism involves the deprotonation of the alcohol proton by the ligand, and addition of the resulting alkoxide anion to the metal center (Scheme 1.7b).[35] Due to the participation of the ligand in the catalytic mechanism, this is an example of metal-ligand cooperative (MLC) catalysis. The generation of water and H_2 as the only by-products of this reaction make it a greener alternative to previously discussed oxidation methods, and very low amounts of catalyst were required to achieve good to excellent isolated yields of secondary imines. One of the greatest benefits of this particular catalyst is the MLC ligand, which serves as an intramolecular base, and avoids the use of an exogenous base. The major drawbacks of this method are high reaction temperatures, and long reaction times, as it takes 52 h in toluene at reflux to generate the secondary aldimine. Acceptorless dehydrogenative coupling of alcohols with amines to form imines has been studied extensively,[36] with many examples of catalysts capable of this transformation.[37–47]

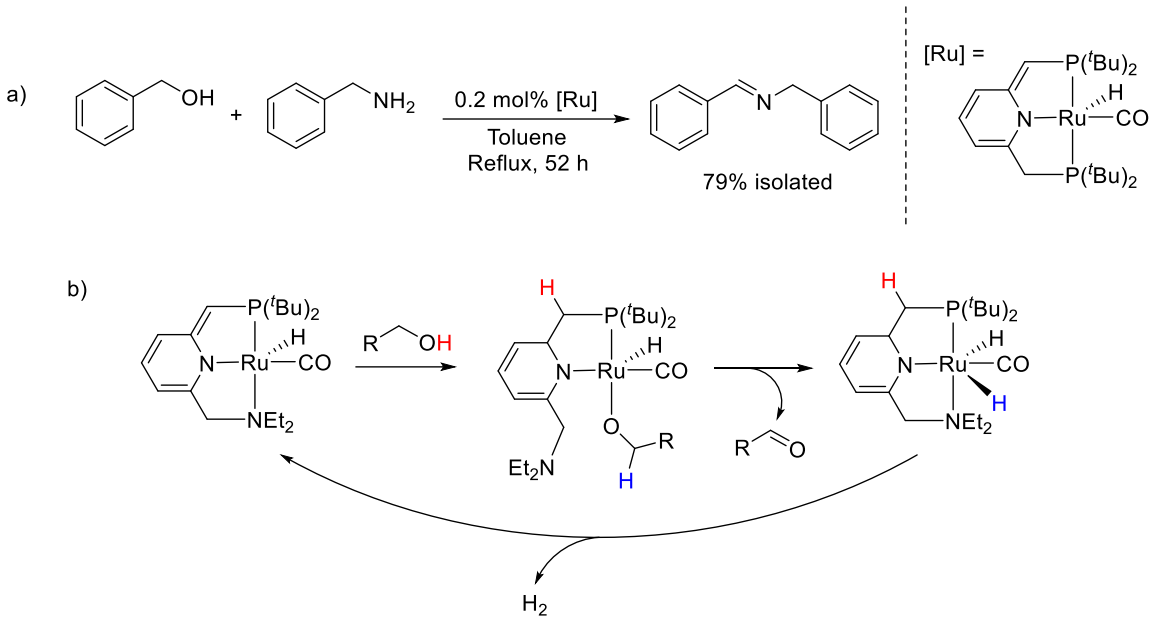

Scheme 1.7. a) Acceptorless dehydrogenative coupling (ADC) of alcohols with amines to form secondary aldimines using a Ru(II)-PNP pincer complex.[34] b) A section of the proposed catalytic mechanism, displaying the metal-ligand cooperative nature of a Ru(II)-PNN pincer complex.[35]A proton (red) and hydride (blue) is transferred from the substrate to the ligand, and metal center, respectively.

1.3 Transition Metal Catalyzed Acceptorless Dehydrogenation of Amines

An alternative method of synthesizing secondary aldimines, and a powerful tool for synthesizing nitriles is by acceptorless dehydrogenation (AD) of primary amines. A primary amine can undergo AD to yield a reactive primary imine (**Im**), which can undergo a condensation reaction with another molecule of starting material to form a secondary aldimine. This secondary aldimine is the acceptorless dehydrogenative coupled (ADC) product. A primary amine can also undergo two dehydrogenations in quick succession to form a nitrile, which is the double AD (DAD) product (Scheme 1.8). This method is a green and atom-economic method to synthesize imines, and nitriles, which avoids the need for a sacrificial H_2 acceptor, or a stoichiometric oxidant.

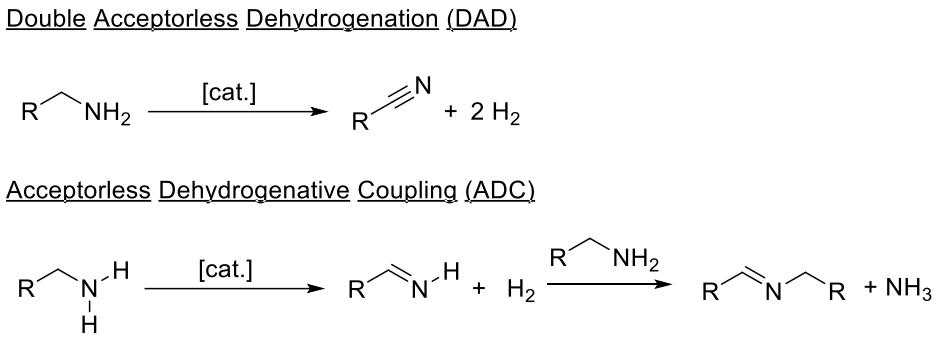

Scheme 1.8. Double acceptorless dehydrogenation (DAD) of a primary amine to form a nitrile, and acceptorless dehydrogenative coupling (ADC) of a primary amine to form a secondary aldimine.

The catalytic mechanism for acceptorless dehydrogenation can occur though either an inner or outer sphere pathway.[48–50] In a proposed inner sphere pathway, the substrate binds directly to the metal center, in this case by coordination of the nitrogen atom (Scheme 1.9a). One molecule of H_2 is released, followed by a β-H elimination to form a primary imine. The primary imine can then undergo another dehydrogenation to form a nitrile or reacts with another molecule of substrate to form the ADC product. The inner sphere pathway requires two coordination sites in total to facilitate the β-H elimination step. An outer sphere pathway is also possible, where the substrate never binds directly to the metal center.[51–53] Instead, a proton and a hydride are transferred to the ligand and metal center, respectively, from the unbound substrate (Scheme 1.9b).

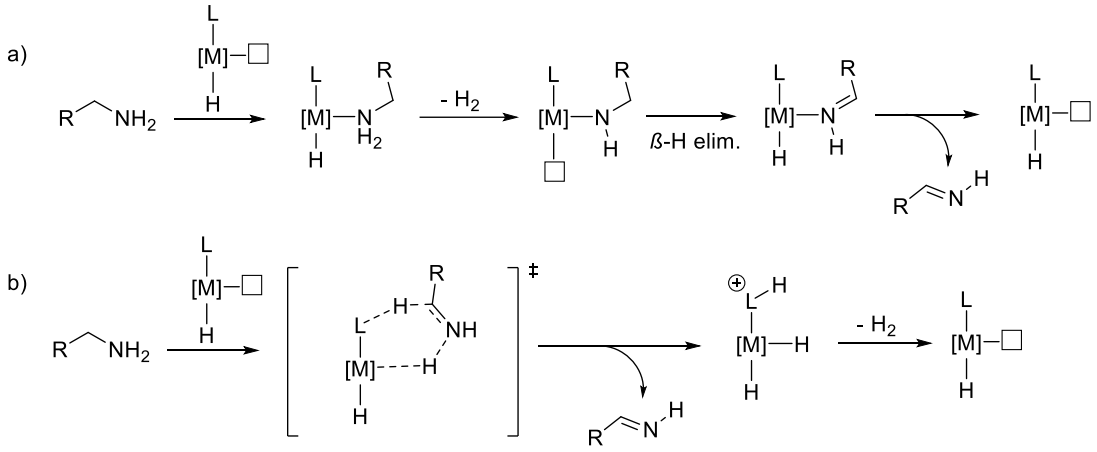

Scheme 1.9. General reaction mechanisms for acceptorless dehydrogenation following a) inner sphere pathway b) outer sphere pathway. Empty squares represent an open coordination site.

One of the first examples of an oxidant-free, base-free, catalytic acceptorless dehydrogenation of primary amines was reported in 2011 by Albrecht.[54] The acceptorless dehydrogenation route is particularly attractive compared to the previous methods, since it avoids the exogenous base and an oxidant pair, or a hydrogen acceptor molecule to drive the reaction forward.[30,55,56] A collection of Ru(II)-NHC complexes were active towards the acceptorless dehydrogenative coupling of primary benzylic amines to form secondary aldimines (Scheme 1.10). Quantitative conversion was achieved by the complex with the normal carbene in 20 h, while quantitative conversion was obtained by the complex with the abnormal carbene in 12 h. Noticeable drawbacks of this reaction, however, was the high temperatures, high catalyst loading, as well as low TONs (20). The proposed catalytic mechanism is inner sphere, based on previous research where similar complexes were used for ADC of alcohols with amines.[57]

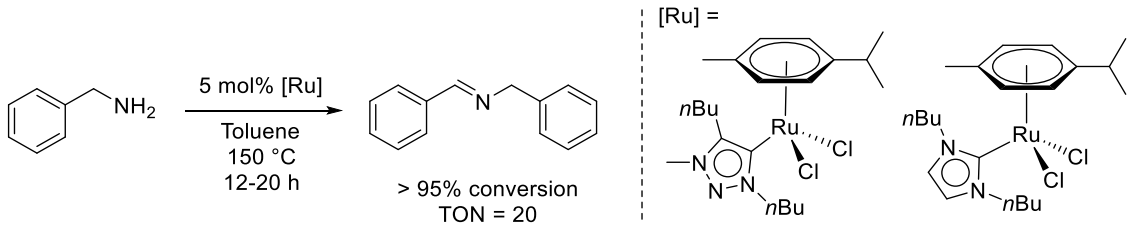

Scheme 1.10. Oxidant-free, base-free, catalytic AD of benzylamine to form homocoupled secondary aldimines.[54]

In 2012, Sadow reported a photocatalytic acceptorless dehydrogenation of primary amines by a rhodium tris(4,4-dimethyl-2-oxazolinyl)phenyl-borate complex (Scheme 1.11).[58] This catalyst was also selective for secondary aldimines, and reactions were performed at room-temperature. Secondary aldimine yields ranged between 77-92% with 10 different primary amine substrates, and TONs ranged from 8-10. Compared to the previous ruthenium-NHC catalysts, the rhodium catalyst was able to form imines at substantially lower temperatures, but the catalyst lifetime was much lower. Mechanistic studies were conducted, and an inner sphere pathway was proposed.

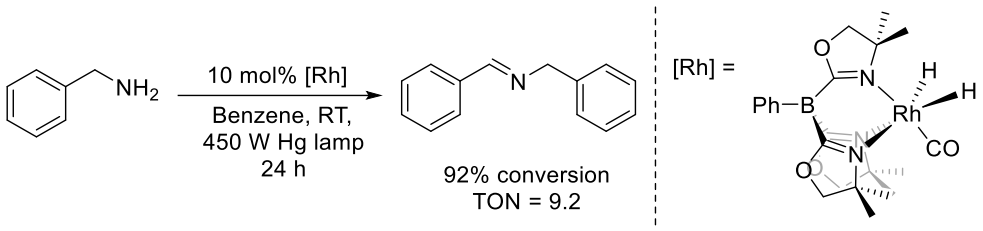

Scheme 1.11. Photocatalytic AD of benzylamine to form homocoupled secondary aldimines.[58]

In 2012, Huang and co-workers developed a new class of Ru(II)-PNP pincer complexes for AD and ADC of primary amines (Scheme 1.12a).[59] An imine arm was incorporated into the backbone of the pincer ligand, which was proposed to increase catalyst activity, by acting as an intramolecular base, driven by aromatization to give a pyridyl ring. The complex bearing an imine-arm (**A**) was compared to a second, known MLC complex that had a PNN pincer ligand with an alkene arm (**B**). For AD of benzylamine, 93% conversion to the coupled imine was observed with complex **A**. Under identical conditions, complex **B** achieved 49% conversion. The mechanism for **B** was previously studied, and the hydrogenated form of the catalyst (**B′**) was isolated, indicating that ligand assists in the dehydrogenation step.[60] The presence of the imine arm significantly increased the reactivity, which was hypothesized to act in the same way as **B** (Scheme 1.12b). Intermediate **A′** is the hydrogenated form of **A**, and releases H_2 to regenerate catalyst **A**. The increased activity of **A** compared to **B** is likely due to the increased acidity of the N-H bond in intermediate **A′**, which results in faster release of H_2, and regeneration of **A**. No mechanistic analyses were conducted to determine whether dehydrogenation occurred via an inner or outer sphere mechanism with **A**, however, the catalytic mechanism for **B** was previously thought to be inner-sphere.[61]

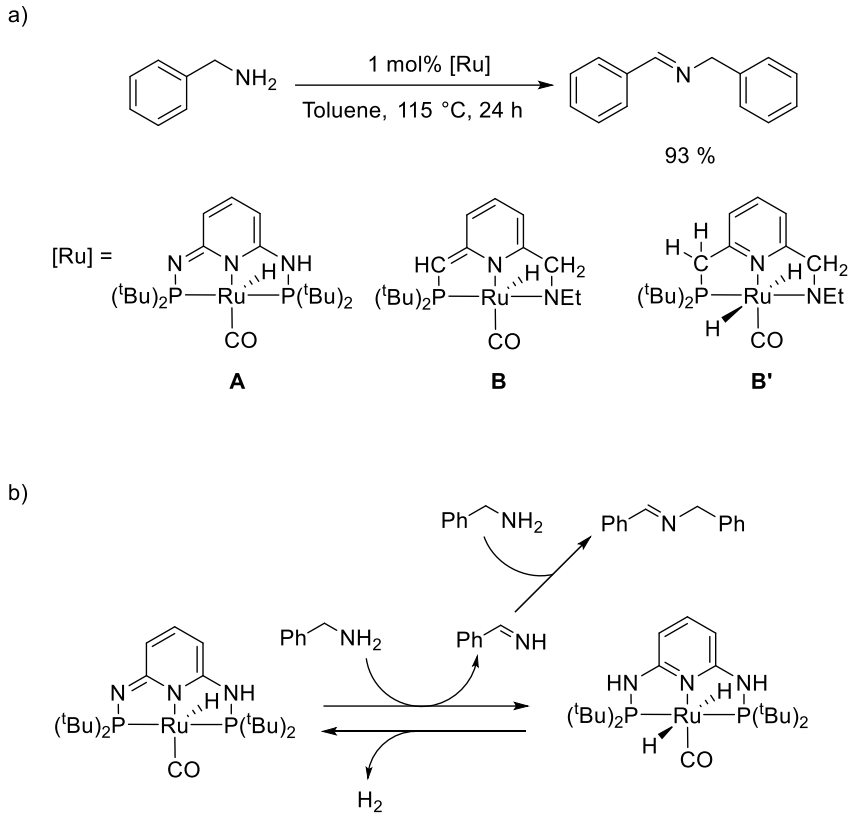

Scheme 1.12. a) Catalytic AD of benzylamine with pincer complexes bearing cooperative imine/alkene moieties to form a secondary aldimine.[59] b) Catalytic AD of benzylamine, with complex **A** to form an imine.[59,60] The complex on the right is a hypothesized intermediate, based on mechanistic studies on complex **B**.

The first example of an oxidant-free, base-free catalytic double acceptorless dehydrogenation of an amine to a nitrile was reported in 2013 by Szymczak (Scheme 1.13).[62] AD of primary benzylic amines lead to the selective formation of nitriles, catalyzed by a Ru(II)-NNN-pincer hydride complex. AD of benzylamine gave 63% conversion to benzonitrile after 24 h in toluene at 1 mol% catalyst loading, which corresponds to a TON of 63. Experimental and computational mechanistic studies conducted by Szymczak in 2016 supports an inner sphere non-cooperative pathway, where both dehydrogenation steps and release of H_2 occurs while the substrate is bound to the metal center.[50] This is facilitated by a labile PPh_3 ligand, which dissociates, allowing for substrate to bind, and for β-H elimination to occur.

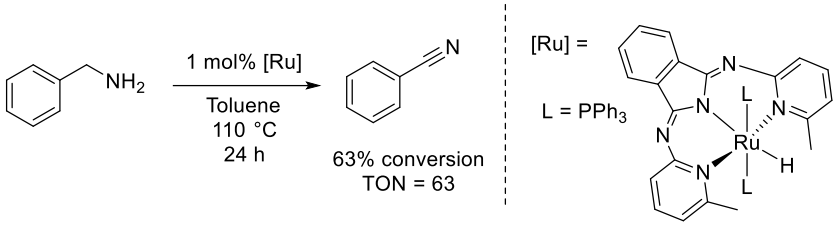

Scheme 1.13. Catalytic AD of benzylamine to form benzonitrile using a Ru(II)-NNN pincer complex.[62]

Mata and co-workers performed a study in 2016, using complexes with the formula [(*p*-cymene)Ru(NHC)Cl_2], which were similar to the complexes used by Albrecht in 2011, except slightly modified NHC ligands were used (Scheme 1.14).[63] All three Ru catalysts employed achieved near-quantitative conversions of a variety substituted benzylamines, and TONs of up to 50 in were obtained under 8 h, with no exogenous base or any other additives. This was also one of the first examples of AD of primary amines that formed a mixture ADC and DAD products. The reactions were conducted at lower temperatures than the Albrecht study, which may be a contributor to the different products observed. With benzylamine as the substrate, a 3:1 distribution of nitrile to secondary aldimine was observed. The AD pathway proceeds via an inner sphere mechanism, similar to the Albrecht Ru-NHC complexes. The presence of secondary imine products indicates a second competing pathway, where after the first dehydrogenation, a molecule of benzylamine intercepts a primary imine, forming the ADC product. The trade-off of lower reaction temperatures, and lower catalyst loadings is off-set by the overall decreased product selectivity.

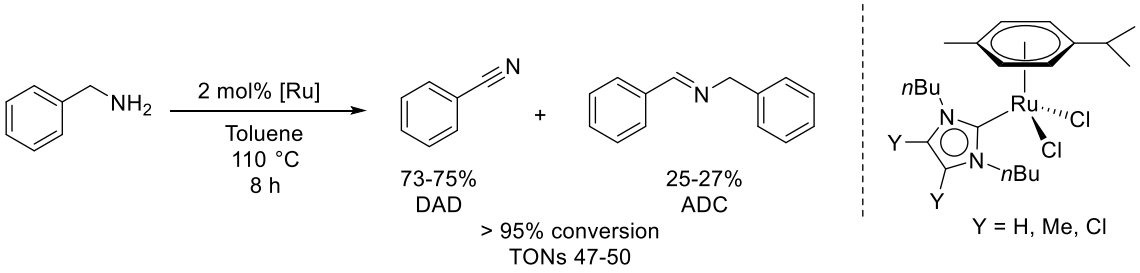

Scheme 1.14. Catalytic AD of benzylamine to form a mixture of DAD and ADC products.[63]

In 2017, AD of primary amines was conducted by Albrecht using iridium(III) complexes bearing a cooperative C,N-bidentate pyridyl-triazolylidene (PT) ligand (Scheme 1.15).[64] The role of the PT ligand was twofold: to act as a hemilabile ligand to increase catalyst lifetime; and to facilitate N-H bond activation of the substrate, by acting as a Lewis base. This cooperative complex **C** was compared to a non-cooperative analogue **D**, which had an aryl ring instead of the pyridyl moiety. Both complexes resulted in high conversions, using a variety of different benzylic amines, with benzylamine achieving 93-97% over 24 h. The use of this catalyst did not result in any DAD products, rather it gave a mixture of dehydrogenated, and hydrogen-borrowing products. Hydrogen-borrowing (HB) occurs when an ADC product is hydrogenated by the catalyst, which forms an amine. Complex **C** gave a 2:1 ratio of ADC product to HB product, while **D** gave a 1:1 ratio. The presence of the cooperative pyridyl moiety resulted in higher selectivity compared to the non-cooperative complex, which was attributed to the pyridyl group acting as a Lewis base and activating substrate bound to the meta center through hydrogen bonding. Based on this interaction, the catalytic mechanism was proposed to be inner sphere.

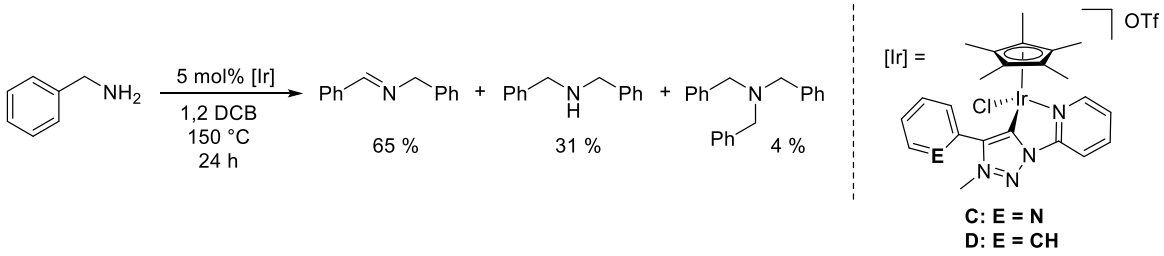

Scheme 1.15. Catalytic AD of benzylamine to form a mixture of ADC and HB products.[64]

A more recent example of AD of primary amines comes from Muthaiah in 2020, who employed ruthenium trichloride in conjunction with an additive, as a catalyst for AD of primary amines to generate nitriles, and secondary amines to form secondary aldimines (Scheme 1.16).[65] The additive was hexamethylenetetramine (HMTA) and its derivatives, which acts as the hydride source, base, and reducing agent required for $RuCl_3$ to act as a suitable catalyst for these substrates. With 0.5 mol% $RuCl_3$ and 1 mol% N-Bn HMTA, 91% isolated yield of benzonitrile was obtained after 24 h. Secondary amines, such as dibenzylamine were also tested, and 74% isolated yield of the secondary imine were

obtained, under the same conditions. The reactivity of this catalyst/additive was also extended to *N*-heterocycles, including indolines, tetrahydroquinolines and tetrahydroisoquinolines. This gave indoles, quinolines, and isoquinolines, respectively, in high isolated yields. The proposed inner sphere mechanism is HMTA and $RuCl_3$ react to form a Ru-$(H)_2$ intermediate, that then reacts with benzylamine to release H_2 to form a Ru(H)(NHBn) adduct. Two successive β-H eliminations and release of a second molecule of H_2 generates the nitrile as the final product.[66]

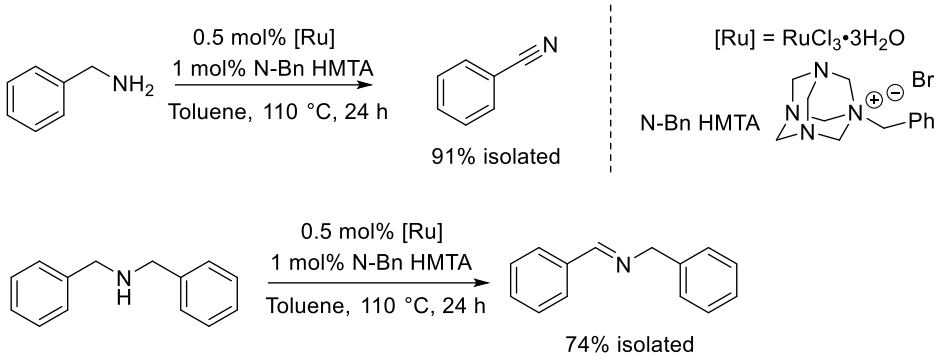

Scheme 1.16. Catalytic AD of benzylamine and dibenzylamine, to form a nitrile, and secondary aldimine, respectively.[65]

Overall, catalysts that have been employed for the AD of primary amines suffer in one, or more of the following categories: low yields, product selectivity, require an additive, poor atom economy, harsh reaction conditions. Furthermore, the field of AD of primary amines is a relatively new, and developing field of research, with few examples of catalysts capable of this transformation.[50,58,59,62–65,67–79] In all the examples discussed above, and in general, AD of amines occurs via an inner sphere pathway. There are currently very few examples of catalysts that are proposed to act through an outer sphere mechanism.[79,80] Catalytic AD of *N*-heterocycles is also a growing field of study, with applications in synthesis, as well as hydrogen storage molecules for energy applications.[81–92] However, the types of *N*-heterocyclic substrates employed generally lead to only one AD product, thus selectivity is not an issue in those applications.

1.4 Tunable $P^{R}_{2}N^{R'}_{2}$ Ligands as Proton Shuttles used in Catalysis

Metal-ligand cooperative (MLC) catalysis is a catalytic transformation where both the metal center and the associated ligand participate in bond formation/cleavage steps.[93] Examples of metal-ligand cooperative catalysis already exists in nature, in the form of hydrogenase enzymes that catalyze reversible heterolytic cleavage of H_2. In the case of [Fe-Fe]-hydrogenase, H_2 is cleaved due to an interaction between one of the iron centers, and a secondary amine located in the secondary coordination sphere. The secondary coordination sphere can be defined as the atoms in the ligand framework that are not directly attached to the metal center.[94] The basic amine acts as a proton shuttle, removing H^+ from dihydrogen bonded to the iron atom, resulting in a protonated amine, and a new iron-hydride bond (Scheme 1.17). The concept that a ligand can participate in a chemical reaction at the metal center though proton-shuttling has inspired catalyst design strategies to incorporate acid/base groups on the supporting ligand framework.

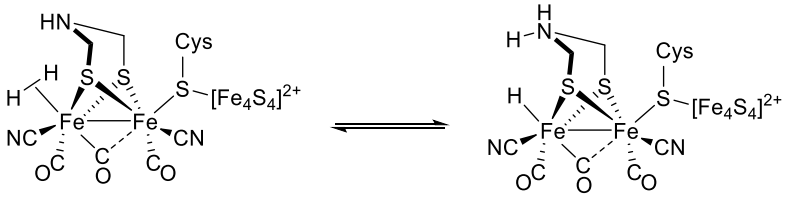

Scheme 1.17. Reversible heterolytic cleavage of H_2 using [Fe-Fe] hydrogenase, an example of metal ligand cooperative (MLC) catalysis.[93]

One example of a ligand designed for proton-shuttling is the 1,5-R′-3,7-R-1,5-diaza-3,7-diphosphacyclooctane ($P^{R}_{2}N^{R'}_{2}$) ligand used extensively by DuBois and Bullock *et al.* (Scheme 1.18).[95] The $P^{R}_{2}N^{R'}_{2}$ ligand has two basic tertiary amines, and two phosphine groups. In late transition metal $P^{R}_{2}N^{R'}_{2}$ complexes, the ligand binds to the metal center via the two P atoms. The two non-coordinated N atoms on the ligand can reversibly shuttle protons to and from the metal center and were inspired by the [Fe-Fe] hydrogenase system. The amine groups are located in the secondary coordination sphere and can be tuned to increase their basicity, by changing the R′ groups. The electronics of the metal center can also be tuned, through modification of the primary coordination sphere, by changing the R groups on the phosphorus atoms. The primary coordination sphere is defined as the atoms

that are directly attached to the metal center, and affect the electronic and geometric properties of the metal center.[94]

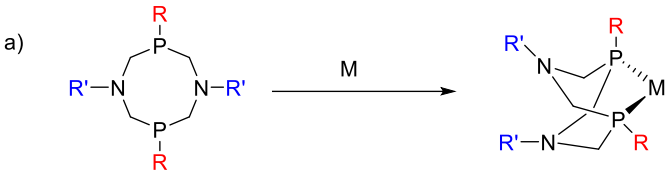

Scheme 1.18. Structure of the $P^{R}{}_{2}N^{R'}{}_{2}$ ligand and coordination to a metal via the phosphine groups.

In 2012, complexes of the type $[Fe(Cp)(H_2)(P^{Ph}{}_{2}N^{R'}{}_{2})]BAr^{F}{}_{4}$ (Tetrakis[3,5-bis(trifluoromethyl)phenyl]borate) were synthesized, and the role of the ligand in the heterolytic cleavage of H_2 was assessed.[96] In the proposed catalytic mechanism of these complexes, H_2 cleavage is reversible, and facilitated by the $P^{R}{}_{2}N^{R'}{}_{2}$ ligand, which acts as a proton shuttle. An equilibrium between an Fe-H_2 complex **II** and a complex bearing a hydride on the metal center, and a proton on the pendant amine **I** is postulated (Scheme 1.19a). To assess whether there was an equilibrium between **II** and **I**, H_2/D_2 scrambling experiments were conducted (Scheme 1.19b). Complex $\mathbf{II^{Bn}\text{-}[H_2]}$ under 1 atm H_2 was subjected to 3.0 mL D_2. After 15 min, complex $\mathbf{II^{Bn}\text{-}[HD]}$ started to form. After 12 h 22 °C, the ratio of the H_2:HD:D_2 complexes of $\mathbf{II^{Bn}}$ was 38:51:11. Complex $\mathbf{II^{Ph}\text{-}[H_2]}$ was also tested, and a 28:51:20 ratio of H_2:HD:D_2 complexes were observed after 12 h. A third complex, bearing a non-cooperative $P^{Ph}{}_{2}C_5$ ligand, $\mathbf{II}^{\mathbf{PPh_2C_5}}\mathbf{\text{-}[H_2]}$ was also tested, and there was no evidence of any formation of any $\mathbf{II}^{\mathbf{PPh_2C_5}}\mathbf{\text{-}[HD]}$. This result confirms that H_2 cleavage is reversible and is facilitated by the pendant amine of the $P^{R}{}_{2}N^{R'}{}_{2}$ ligand. Similar studies were conducted with complexes of the formula $[Ru(Cp^{*})(H_2)(P^{R}{}_{2}N^{Bn}{}_{2})]BAr^{F}{}_{4}$, where R = Ph and *t*Bu, and heterolytic H_2 cleavage was facilitated by the pendant amine on the $P^{R}{}_{2}N^{Bn}{}_{2}$ ligand as well.[97]

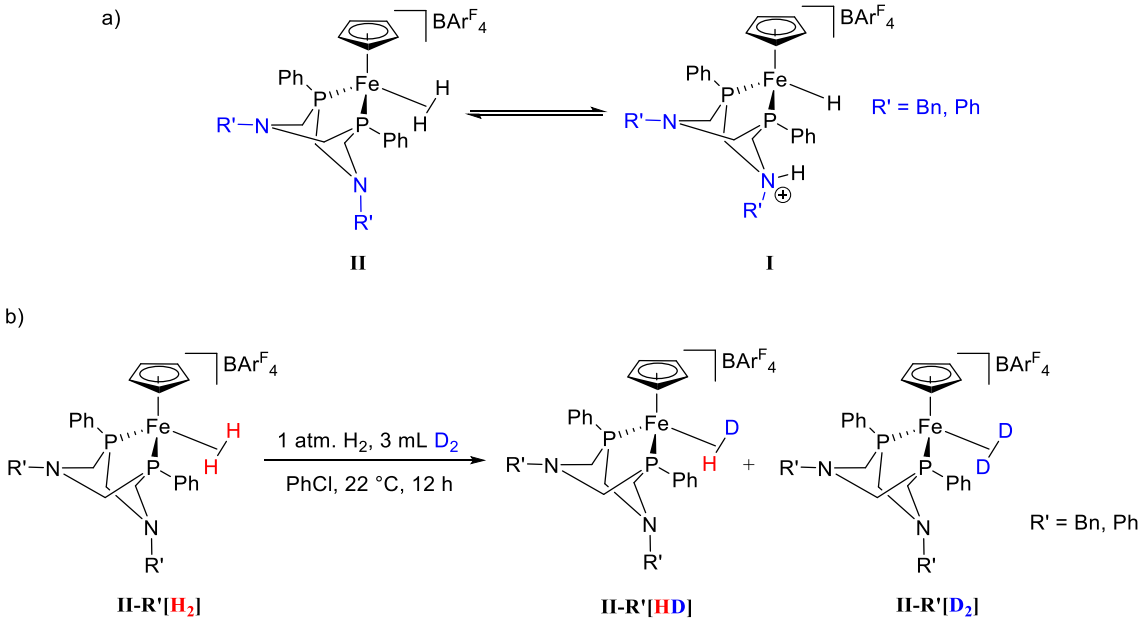

Scheme 1.19. a) Proposed mechanism of reversible heterolytic cleavage of H_2 by $[Fe(Cp)(H_2)(P^{Ph}{}_2N^{R'}{}_2)]BAr^F{}_4$, where R′ = Bn or Ph, and b) H_2/D_2 scrambling experiments with cooperative complexes $[Fe(Cp)(H_2)(P^{Ph}{}_2N^{R'}{}_2)]BAr^F{}_4$ complexes to confirm reversible heterolytic cleavage.[96]

In 2014, Dubois and Bullock were able to isolate an iron-$P^R{}_2N^{Ph}{}_2$ complex that was the direct product of heterolytic H_2 cleavage.[98] An Fe(II) complex with the formula $Fe(Cl)(Cp^{C_4F_4N})(P^{tBu}{}_2N^{tBu}{}_2)$ was reacted with the halide-abstracting agent $NaBAr^F{}_4$ and H_2 to generate complex **E** (Scheme 1.20a). Complex **E** was characterized by single-crystal neutron diffraction, which showed a hydride bonded to the iron center, and a proton located on the pendant amine. The bond distance between the proton and hydride was 1.489 Å, which is slightly longer than an H–H bond distance for a similar H_2 complex $[Fe(Cp^{C_4F_4N})(H_2)(P^{tBu}{}_2N^{tBu}{}_2)]BAr^F{}_4$,[99] and is shorter than if there were no hydrogen-bonding interaction present.[100] This indicates the presence of an intramolecular hydrogen bond in complex **E** between the hydride on the metal center, and the proton on the pendant amine of the $P^{tBu}{}_2N^{tBu}{}_2$ ligand. DFT calculations revealed that complex **E** is 0.65 kcal mol^{-1} more stable than the H_2 adduct (**F**), indicating that reversible heterolytic cleavage occurs rapidly (Scheme 1.20b).

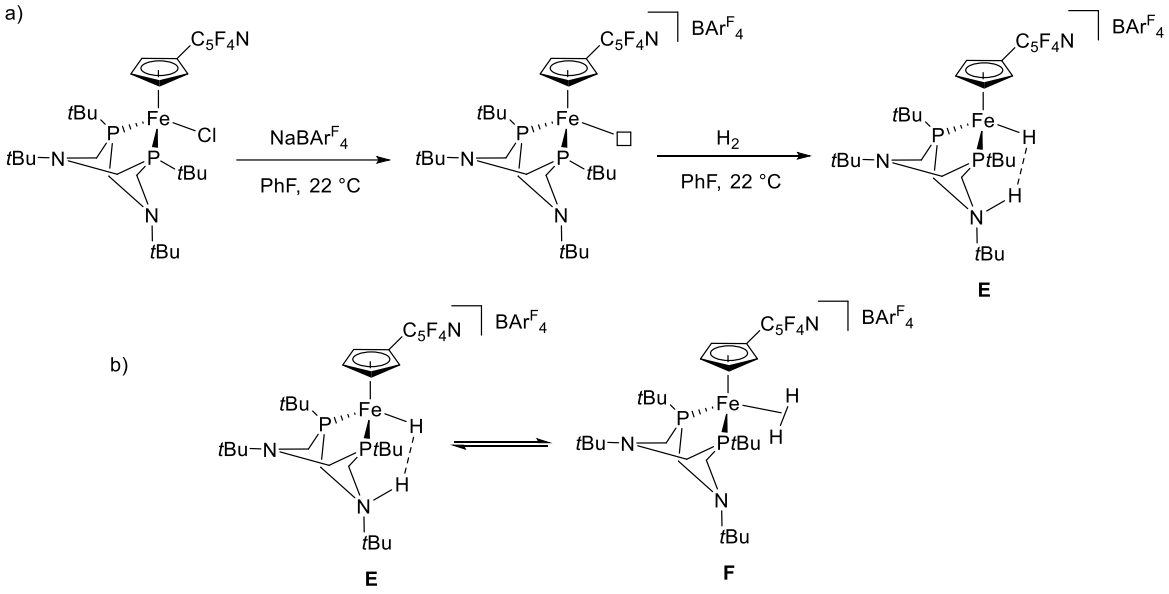

Scheme 1.20. a) Synthesis of complex **E** b) Proposed equilibrium between complex **E** and **F**.[98]

In 2011, complexes of the type $[Ni(P^R_2N^{Ph}_2)(CH_3CN)][BF_4]_2$ were tested for electrocatalytic production of H_2 (Scheme 1.21a).[101,102] The mechanism of H_2 formation is identical to that for the Fe($P^R_2N^{Ph}_2$) complexes discussed above.[96,98] The R groups on the phosphines were changed, and the turnover frequencies (TOFs) of each complex were compared. The complex bearing the Me groups on the phosphines was the highest performing catalyst, with a TOF of 6700 s^{-1}, while the slowest catalyst had 2,4,4-trimethylpentane groups on the phosphine, and gave a TOF of 69 s^{-1}. Strongly-donating phosphine groups resulted in faster rates for production of H_2. In the proposed catalytic mechanism for the $[Ni(P^R_2N^{Ph}_2)(CH_3CN)][BF_4]_2$ complexes, before the release of H_2 there is an intermediate that has a hydride bound to the metal, and a proton on one of the amine groups on the ligand (Scheme 1.21b).[95] The higher electron density on the metal center, as a result of the more donating phosphine ligands, would result in a Ni–H bond that is more hydritic (basic), which reacts faster with H^+ to form H_2. The steric properties of the ligand also had an influence on catalytic rate. When R was the sterically bulky 2, 4, 4-trimethylpentane group, the rate was 69 s^{-1}. This is 100 times slower than when R was a methyl group, which is equally donating. This means that for this reaction, a balance between strong donor group on the phosphine, as well as low steric bulk was essential for quick catalytic turnover.

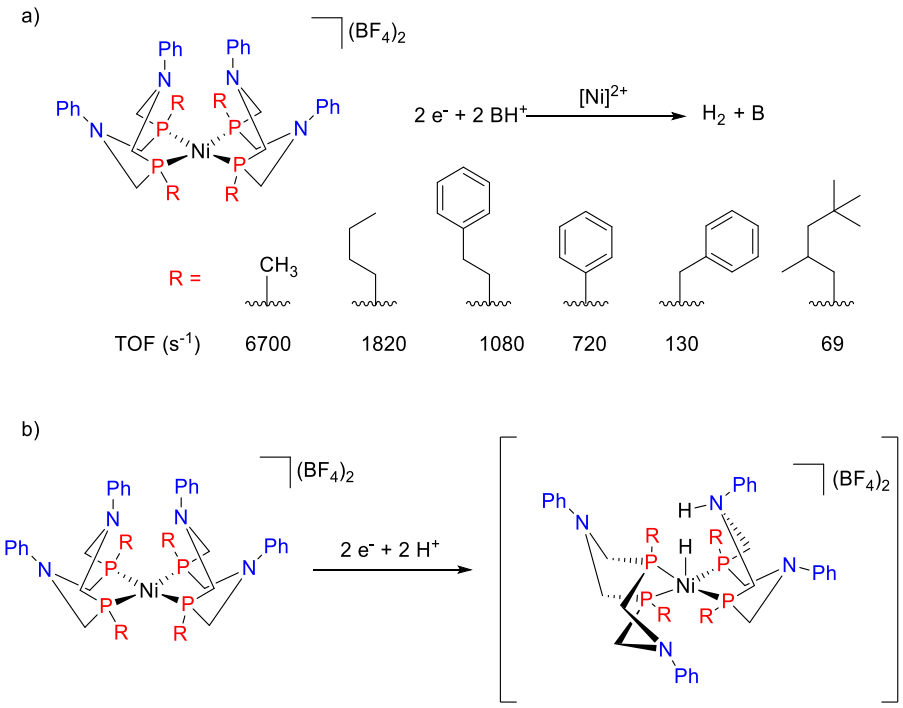

Scheme 1.21. a) Structure of $[Ni(P^{R}{}_2N^{Ph}{}_2)(CH_3CN)][BF_4]_2$ complex, with varied R groups, used in electrocatalytic formation of H_2.[95,101,102] BH^+ = [DMF(H)]OTf. b) Proposed reaction of a $[Ni(P^{R}{}_2N^{Ph}{}_2)_2(CH_3CN)][BF_4]_2$ complex with 2 e^- and 2 H^+ to form the reaction intermediate on the right.[101] The proton on the pendant amine and the hydride on the metal center are brought into close proximity, facilitating H_2 formation via protonolysis of the Ni-H bond.

Nickel(II) complexes bearing cooperative $P^{R}{}_2N^{R'}{}_2$ ligands were also active towards the catalytic oxidation of alcohols.[103] Six nickel phosphine complexes (**G-J**) synthesized by Appel and co-workers were all catalytically active towards the chemical oxidation of diphenylmethanol (Scheme 1.22). Complexes **G-I**, which have one $P^{tBu}{}_2N^{R'}{}_2$ ligand bonded to the metal center, were compared based on their turnover frequencies (TOF). The R′ groups on each of the complexes were changed, to determine the effect of amine basicity on catalyst rate. Complex **G** gave the lowest TOF of 9.4 h^{-1}, followed by **H**, which gave 26.8 h^{-1}, with complex **I** resulting in the highest TOF of 114 h^{-1}. Changing the R′ substituent from Ph to tBu resulted in a 12-fold increase in catalyst rate. This indicated that increased amine basicity has a positive effect on catalyst turnover. The best performing mono-ligated complex **I** can then be compared to a complex bearing a non-cooperative bis-phosphine ligand **J**, to determine the effect of the $P^{R}{}_2N^{R'}{}_2$ ligand on performance. Complex **J** achieved

a TOF of 5.4 h^{-1}, which was 21 times lower than the TOF obtained with **I**. The TOF for **J** was also 2 times lower than the worst performing cooperative mono-$P^{R}_{2}N^{R'}_{2}$ complex **G**. This implies that the intramolecular base has a positive effect on the catalytic rate. Comparing the best mono-ligated complex **I** to the best performing bis-ligated complex **K**, which had a TOF of 0.4 h^{-1} shows that two $P^{R}_{2}N^{R'}_{2}$ ligands was not necessarily better than one. The bis-ligated complex had a rate that was 285 times lower than **I** and this was attributed to the greater prevalence of off-cycle intermediates.[104] The importance of the $P^{R}_{2}N^{R'}_{2}$ ligand, and the tunability of the pendant amine to increase the donor-properties, results in increased performance. This coupled with the cooperative nature of the ligand, results in catalytic rates much higher than the non-cooperative analogues.

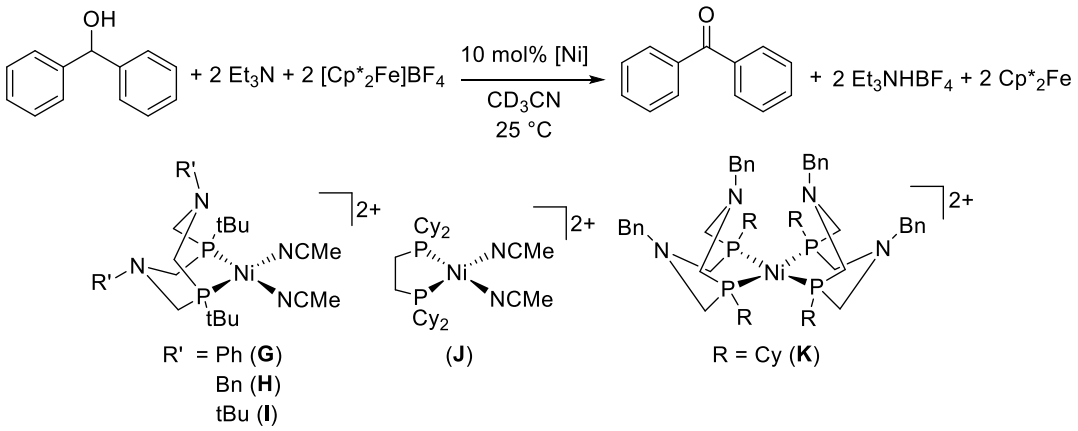

Scheme 1.22. Nickel phosphine complexes for catalytic oxidation of diphenylmethanol to diphenylacetone.

1.5 Ruthenium $P^R_2N^{R'}_2$ Complexes for AD of Primary Amines and *N*-Heterocycles

To further explore the applications of metal-$P^R_2N^{R'}_2$ complexes, our group synthesized a potential MLC catalyst [Ru(Cp)(MeCN)($P^{Ph}_2N^{Bn}_2$)]PF_6 **1d**, and compared it to a known non-MLC catalyst.[80] An example of a non-cooperative catalyst is **4**, as there is no intramolecular base present (Chart 1.1). Catalysts **1d** and **4** were used for AD of primary amines and *N*-heterocycles to determine if catalyst activity and product selectivity were affected by having a $P^R_2N^{R'}_2$ ligand present.

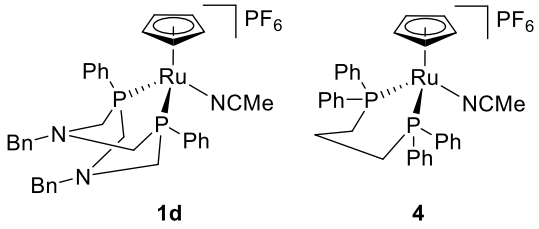

Chart 1.1. Structures of MLC complex **1d** and non-MLC complex **4**, that are active towards the AD of amines and *N*-heterocycles.

If a primary amine, like benzylamine is used for AD, a primary imine (**Im**) and one equivalent of H_2 is formed. This imine can then proceed down three different pathways, which leads to the formation of a mixture of three different products (Scheme 1.23). A second dehydrogenation of **Im** leads to the formation of a nitrile, (**DAD**) and the release of another equivalent of H_2. A condensation reaction between a molecule of **Im** and a molecule of benzylamine, forms a secondary aldimine (**ADC**) and an equivalent of NH_3. Both products **ADC** and **DAD** have either 1 or 2 more units of unsaturation respectively compared to the substrate benzylamine, classifying them both as dehydrogenation products. Hydrogenation of **ADC** can also occur to form a secondary amine, which is the hydrogen-borrowing product (**HB**). The **HB** product is the same oxidation state as the starting material, so it is classified as a hydrogenation product. The selectivity challenge arises when there is a mixture of dehydrogenation products, and hydrogenation products formed by a particular catalyst. Comparing the ratio of **ADC** + **DAD** to **HB** can be used to determine the relative preference of a catalyst for AD or HB products.

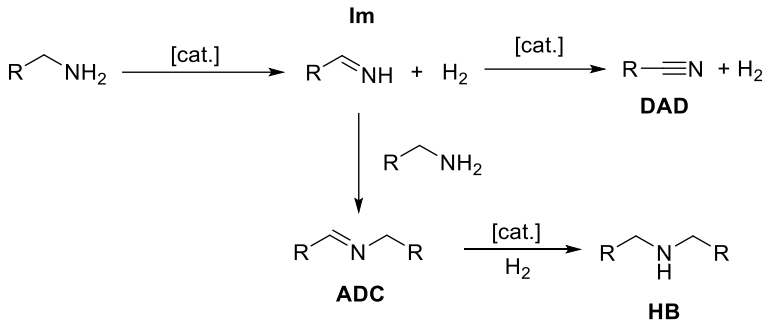

Scheme 1.23. Acceptorless dehydrogenation of benzylamine to form **Im**, which can then react to form **DAD**, or **ADC**. Imine **ADC** can then react with the catalyst and an equivalent of H_2 to form hydrogenation product **HB**.

When complexes **1d** and **4** were used for AD of benzylamine, both afforded a mixture of **ADC**, **DAD**, and **HB** (Scheme 1.24). MLC complex **1d** made an 18:7:1 mixture of **ADC**:**DAD**:**HB**, which is a 25:1 selectivity of AD to HB products. In terms of selectivity, **1d** is more selective for AD products **ADC** and **DAD**. The non-MLC complex **4** made a 7:2:1 mixture of **ADC**:**DAD**:**HB** which was 9:1 selectivity of AD to HB products. Overall, complexes **1d** and **4** were not very different in their selectivities, as both form mainly AD products **ADC** and **DAD**.

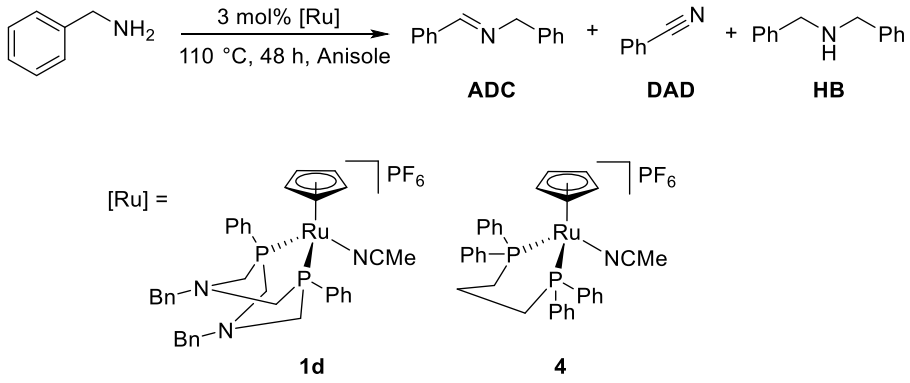

Scheme 1.24. Acceptorless dehydrogenation of benzylamine to form a mixture of products, [Ru] = **1d**/**4**.

The catalytic mechanism for **1d** could be an inner sphere pathway, where the substrate binds directly to the metal center, or outer sphere where the removal of H_2 from the substrate occurs without the substrate binding via the N atom. To determine if an inner sphere pathway was preferred, compound **L** was synthesized by reaction of **1d** with excess benzylamine (Scheme 1.25a). The ^{1}H NMR spectrum of **L** showed a downfield shift of the N*H*$_2$Bn moiety, which was hypothesized to be the result of a hydrogen-bonding interaction between the pendant amine and the substrate bound to the metal center (Scheme 1.25b). If the catalytic mechanism for **1d** was inner sphere, intermediate **L** would have the same, if not better catalytic activity compared to the precatalyst **1d**. Complex **L** was tested for AD of benzylamine and formed 26% less **ADC** than **1d**. The decreased performance of **L** indicated that benzylamine binding to the metal center forms an "off-cycle" intermediate, which is not a species present in the catalytic cycle for **1d**. This evidence suggested that the mechanism for **1d** was either a cooperative, or non-cooperative outer sphere mechanism. If the ligand participated in the catalyst mechanism, then an outer sphere cooperative mechanism was operative. Overall, the mechanism of catalysis for **1d** is still unknown, with only one piece of evidence for the mechanism being an outer sphere pathway.

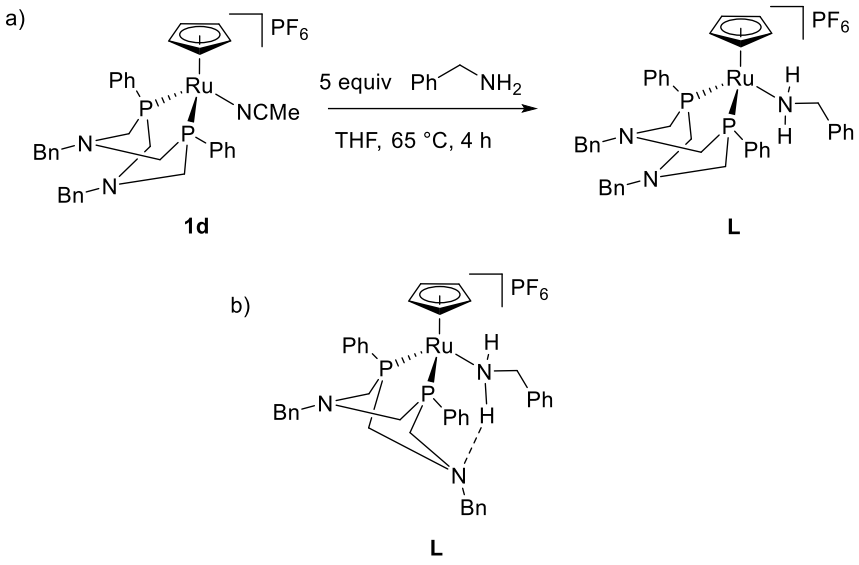

Scheme 1.25. a) Reaction of **1d** with excess benzylamine, to form proposed on-cycle species **L**. b) Proposed hydrogen-bonding interaction between the pendant amine of **L** and a hydrogen atom of bound benzylamine.

For the AD of indoline (Scheme 1.26a), **1d** and **4** gave similar conversions, which left no clear distinct advantage of using one catalyst over the other. However, the use of complex **1a** which has a phenyl in the R′ position (Scheme 1.26b) resulted in higher yields of indole, and in a shorter amount of time than with **1d** or **4**.[105] The increased activity of **1a** towards the AD of indoline indicates that these cooperative ligands have a greater benefit over non-cooperative, but the role of the $P^{R}{}_{2}N^{R'}{}_{2}$ ligand in the catalytic mechanism, including rate studies comparing **1a** to **4** have not been conducted.

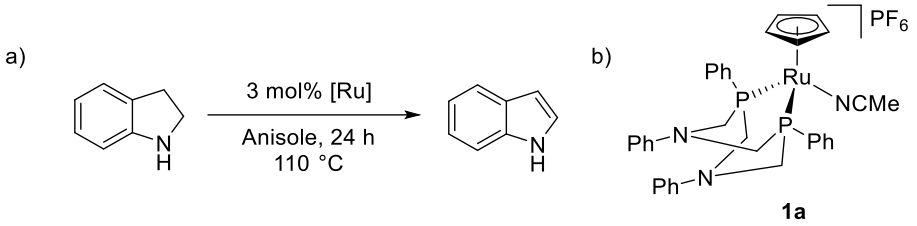

Scheme 1.26. a) Reaction of indoline to form indole using **1a** b) **S**tructure of **1a**, a modified complex based on **1d**, where the Bn substituents on the amine have been replaced with Ph substituents.

1.6 Scope of Thesis

This Thesis outlines the assessment of MLC complexes of the type $[M(Cp/Cp^*)(MeCN)(P^{Ph}{}_{2}N^{Ph}{}_{2})]PF_6$ (M = Fe, Ru) toward the AD of amines. The newly reported synthesis of iron complex (**3a)** will be discussed. AD of benzylamine was conducted with a selection of Ru and Fe complexes, and the product distributions of **ADC**:**DAD**:**HB** were determined. The effect of modifying the primary and secondary coordination sphere on the AD:HB product selectivity was determined.

Currently, more mechanistic information is required to determine the catalytic mechanism of $[M(Cp/Cp^*)(MeCN)(P^{Ph}{}_{2}N^{Ph}{}_{2})]PF_6$ complexes for AD of amines (Scheme 1.27). Out of two proposed pathways: a) outer sphere and b) inner sphere, there was one piece of evidence that supported the outer sphere pathway. The decreased reactivity of **L** supports an inner sphere pathway being unfavourable, but acquiring information on the rate-determining step, and reaction rate order with respect to substrate and catalyst concentrations would help to confirm that the mechanism is outer sphere.

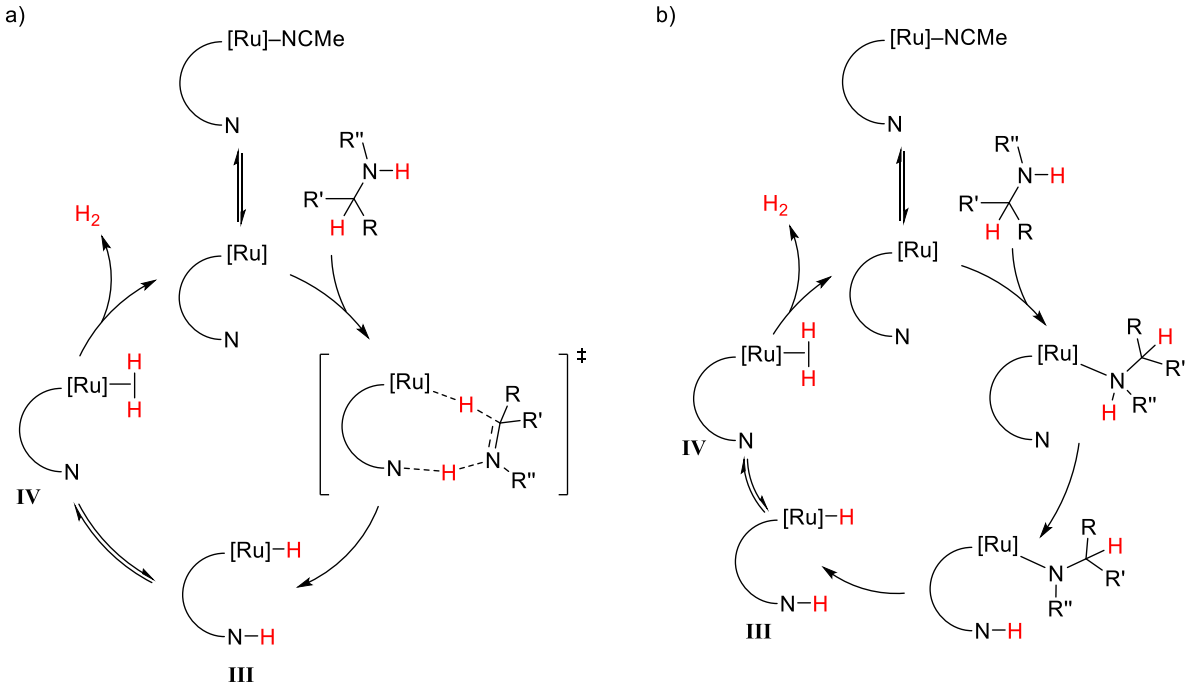

Scheme 1.27. Two possible pathways for AD of amines using [M(Cp/Cp*)(MeCN)($P^{Ph}_2N^{Ph}_2$)]PF_6 complexes. a) outer sphere cooperative pathway b) inner sphere cooperative pathway.

To determine the role of the proposed cooperative $P^{Ph}_2N^{Ph}_2$ ligand, **1a** was compared to non-cooperative complex **4** for the AD of indoline, monitored by *in-situ* IR spectroscopy to determine the differences in catalytic rate, and lifetimes. Variable-Time Normalization Analysis (VTNA) of **1a** for the AD of indoline was conducted to identify the reaction rate order with respect to the catalyst. Mechanistic analysis was also conducted to determine the reaction rate order with respect to the substrate. Product inhibition studies, as well as substrate inhibition studies were also conducted, to provide insight into the catalytic mechanism for the AD of indoline. Kinetic Isotope Effect studies were also conducted with **1a** to distinguish between an innersphere and outersphere mechanism.

Chapter 2: Synthesis and Characterization of [M(Cp/Cp*)(MeCN)($P^{R}_{2}N^{R'}_{2}$)]PF_6 Complexes

2.1 General Synthesis of [Ru(Cp)(MeCN)($P^{R}_{2}N^{R'}_{2}$)]PF_6 Complexes

Cationic ruthenium and iron complexes bearing $P^{R}_{2}N^{R'}_{2}$ ligands that were used in this study are shown below (Chart 2.1). Complexes **1a**, **1b**, **1c**, **3a**, and **4** were synthesized for this study. Complexes **1e** and **1a*** were synthesized by group member Devon Chapple and were determined to be >95% pure by NMR spectroscopy. Complex **3a*** was synthesized by previous group member Benjamin Bridge and was determined to be >95% pure by NMR spectroscopy. Catalytic data for **1d**, which is referenced in Chapter 3, was obtained from a previously published paper within the group.[80] Complex **4** was synthesized following a literature procedure and the $^{31}P\{^{1}H\}$ and ^{1}H NMR chemical shifts matched the known values.[106] Complex **4** was determined to be 92% pure by $^{31}P\{^{1}H\}$NMR spectroscopy, with a minor unknown impurity at 42.1 ppm. The catalytic activity for the 92% pure sample of **4** was tested, and the presence of the impurity did not increase or decrease catalytic activity. This was confirmed using data obtained with a >95% pure sample of **4**. This preliminary data suggested that **4** could be used, without further purification.

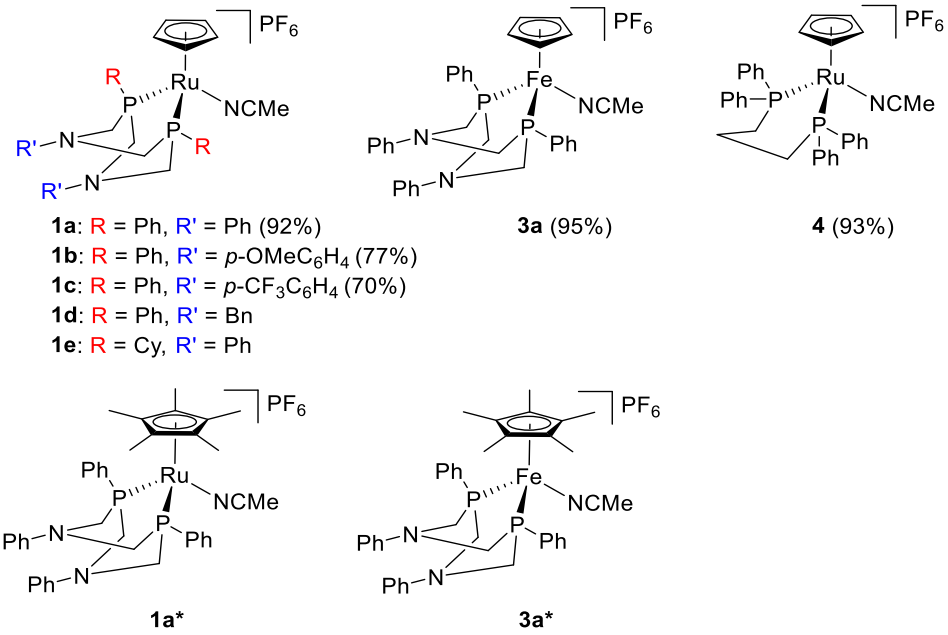

Chart 2.1. Cationic ruthenium and iron complexes employed in this study. Yields for synthesized complexes are shown in parantheses.

The full sequence to make **1a-1c** was previously established, and the synthesis of these compounds was followed with slight modifications. The synthesis of $[Ru(Cp)(MeCN)_3]PF_6$ was performed following a literature procedure where $[Ru(Cp)(Naphth)]PF_6$ was reacted with MeCN in pentane for 1 week.[107,108] The synthesis of complexes with the formula $[Ru(Cp)(MeCN)(P^{Ph}{}_2N^{R'}{}_2)]PF_6$ was performed following a modified literature procedure (Scheme 2.1).[109] Instead of heating the reaction at 60 °C for 4 h in acetonitrile, the reaction was performed in a DCM/MeCN solution at room temperature. This allowed the reaction to be prepared and conducted entirely within the glovebox. The milder reaction conditions limited product decomposition. The added DCM also increased conversion, since the $P^{Ph}{}_2N^{R'}{}_2$ ligands were more soluble in DCM than MeCN. A reprecipitation from DCM/hexanes resulted in facile removal of any excess ligand, which was the only impurity using this method. Yields were identical to the literature method and the purity was >95% as determined by $^{31}P\{^1H\}$ and ^1H NMR spectroscopy.

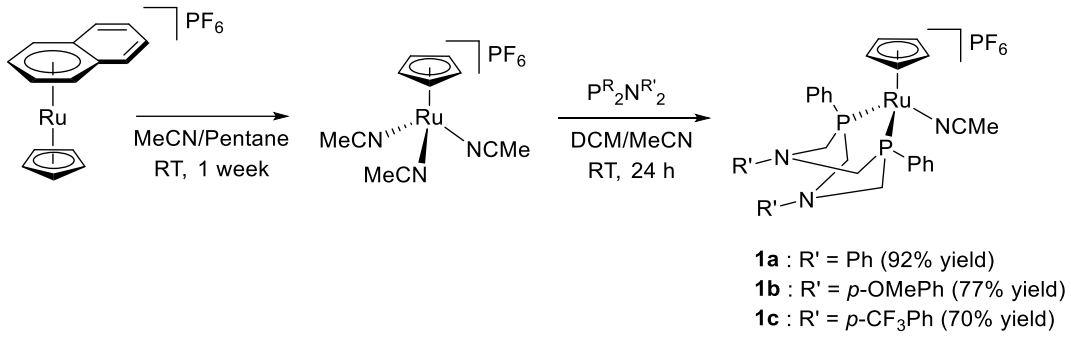

Scheme 2.1. General reaction scheme for the synthesis of the synthesis of $[Ru(Cp)(MeCN)(P^{Ph}{}_2N^{R'}{}_2)]PF_6$ complexes.

2.2 Attempted Syntheses of $FeCl(Cp)(P^{Ph}{}_2N^{Ph}{}_2)$

To test the effect of a different metal center on the selectivity of AD of benzylamine, an iron analogue of **1a** was targeted. The iron complex $[Fe(Cp)(MeCN)(P^{Ph}{}_2N^{Ph}{}_2)]PF_6$ (**3a)** was not synthesized previously, but the Cp* analogue, **3a*** was previously synthesized by our group.[110]

Overall, four synthetic routes were attempted for the synthesis of **3a**. The discussion of all the attempted routes will be included as a reference for future students to use as a resource. The successful synthesis of **3a** is discussed in Section 2.3.

The first synthetic route chosen was based on the synthesis of the Cp* analogue, complex **3a***.[110] This route was a one-pot procedure, where $P^{Ph}{}_2N^{Ph}{}_2$ was reacted with $FeCl_2$ and NaCp to form a chloride intermediate, **2a**. Then, to this reaction mixture, KPF_6 and MeCN was added to promote halide abstraction and ligand coordination, respectively, which should afford the target complex **3a** (Scheme 2.2). The final red solids obtained were analyzed by $^{31}P\{^1H\}$ NMR spectroscopy in CD_2Cl_2. A singlet at δ 57.9 was observed, which was approximately 8 ppm downfield from the Cp* analogue, **3a***. The weaker donor-properties of the Cp ligand indicates that successful halide abstraction and MeCN coordination has occurred. A second signal, which was an AA'BB' pattern at δ 28-36 ppm was observed in a 1:2 ratio to the singlet. This species was hypothesized to be MeCN deficient, and that one of the phosphine or amine groups of a neighboring molecule acts as

a bridging ligand. This would give rise to the AA'BB' pattern that was previously proposed as a minor impurity for the synthesis of **3a***.[111]

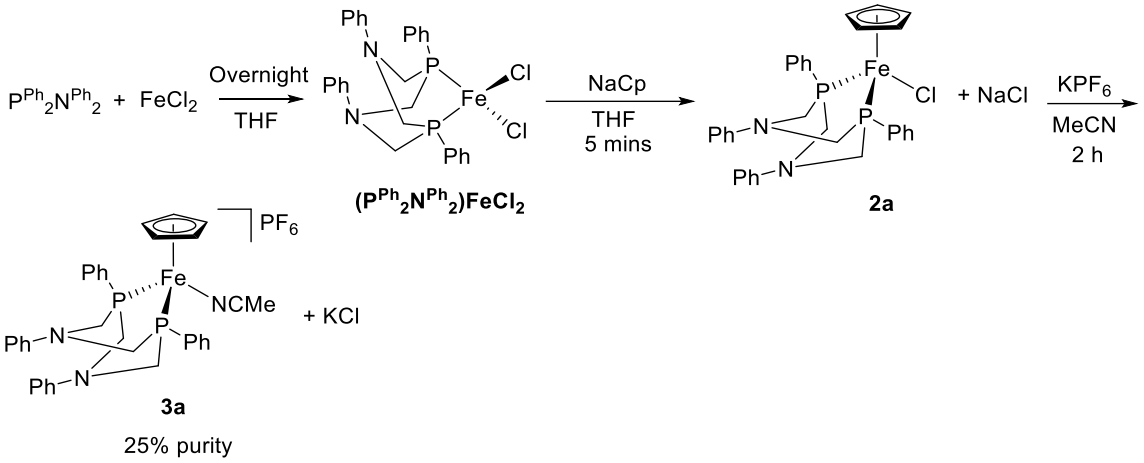

Scheme 2.2. One-pot reaction for the synthesis of compound **3a**.

In an attempt to avoid the formation of the hypothesized MeCN-deficient complex, various tests were conducted in order to reduce the formation of any bimetallic species, such as decreasing the concentration of $FeCl_2$, and increasing the reaction time before the MeCN/KPF_6 addition, but these were not successful in increasing the ratio of product to impurity. Addition of MeCN to the proposed intermediate **2a** prior to KPF_6 addition resulted in a colour change, which was unexpected since the coordinatively saturated complex **2a** should not react with MeCN without a halide abstraction agent.

To identify the product of this reaction, attempts to isolate the intermediate **2a** were made (Scheme 2.3). The $^{31}P\{^1H\}$ NMR spectrum in CD_2Cl_2 after addition of NaCp showed two triplets at 41.4 and 30.3 ppm, and a singlet at –50.5 ppm that corresponds to free $P^{Ph}{}_2N^{Ph}{}_2$ ligand. The reported bis-$P^{Ph}{}_2N^{R'}{}_2$ complex, *cis*-$FeCl_2(P^{Ph}{}_2N^{Bn}{}_2)_2$, gives rise to two multiplets in the $^{31}P\{^1H\}$ NMR spectrum at 45.1 and 31.8 ppm.[112] The identical splitting patterns, as well as the similar chemical shifts observed for the reaction of $FeCl_2$ with $P^{Ph}{}_2N^{Ph}{}_2$, indicate that the major product is *cis*-$FeCl_2(P^{Ph}{}_2N^{Ph}{}_2)_2$ instead of **2a**.

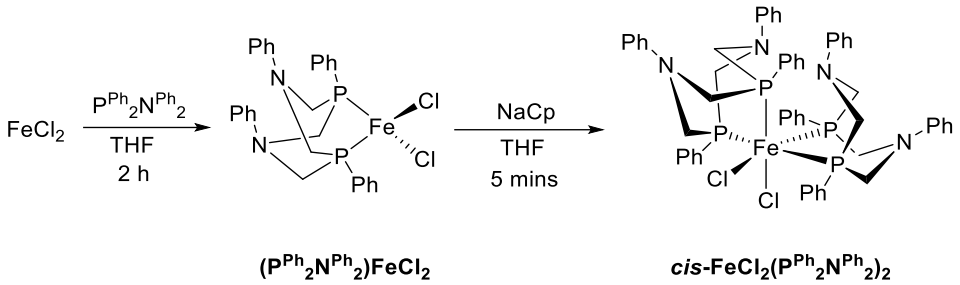

Scheme 2.3. Reaction of $FeCl_2$ with $P^{Ph}{}_2N^{Ph}{}_2$ and NaCp in THF to yield *cis*-$FeCl_2(P^{Ph}{}_2N^{Ph}{}_2)_2$.

To avoid formation of the bis-$P^{Ph}{}_2N^{Ph}{}_2$ complex, $FeCl_2(THF)_{1.5}$ was synthesized to increase solubility of the iron precursor in THF. The increased solubility of $FeCl_2(THF)_{1.5}$ would increase the ratio of $FeCl_2$ to $P^{Ph}{}_2N^{Ph}{}_2$ in solution and would result in more of the mono-ligated $FeCl_2(P^{Ph}{}_2N^{Ph}{}_2)$ species. The newly synthesized $FeCl_2(THF)_{1.5}$ was reacted with NaCp prior to the addition of the $P^{Ph}{}_2N^{Ph}{}_2$ ligand (Scheme 2.4). The $^{31}P\{^1H\}$ NMR spectrum after 30 mins showed no signals, and the ^1H NMR spectrum was broad and had no diagnostic signals to indicate that **2a** was formed, indicating that this method was unsuccessful.

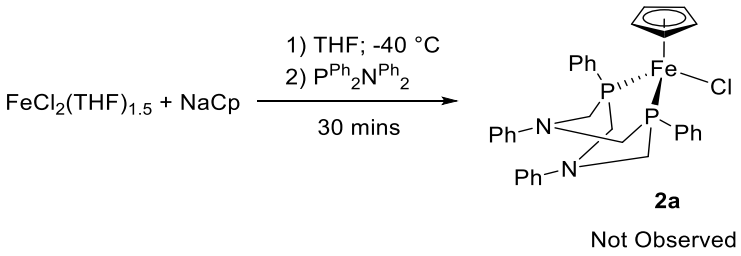

Scheme 2.4. Attempted formation of **2a** by reaction of $FeCl_2(THF)_{1.5}$ with NaCp.

2.3 Successful Synthesis of FeCl(Cp)($P^{Ph}{}_2N^{Ph}{}_2$)

Complex **2a** has been reported by Dubois in 2011, their synthetic route involved photolysis of the precursor compound $FeCl(Cp)(CO)_2$ in the presence of $P^{Ph}{}_2N^{Ph}{}_2$, which afforded **2a** following a recrystallization.[96] This synthetic route was chosen next, as the precursor to **2a**, $FeCl(Cp)(CO)_2$, already has the Cp ligand bound which should avoid any possible formation of a bis-$P^{Ph}{}_2N^{Ph}{}_2$ species. In order to pursue this synthetic route, the precursor $FeCl(Cp)(CO)_2$ was prepared. Synthesis of $FeCl(Cp)(CO)_2$ involved a slightly

modified three-step procedure starting from commercially available $Fe(CO)_5$.[113] The $Fe_2Cp_2(CO)_4$ dimer intermediate was synthesized by heating $Fe(CO)_5$ in a solution of dicyclopentadiene for 20 h, and the product was determined to be pure by IR spectroscopy. $Fe_2Cp_2(CO)_4$ was then dissolved in ethanol, to which 12 M HCl was added, and allowed to stir for 4 days, which formed a crude solution containing $FeCl(Cp)(CO)_2$, as well as some unreacted starting material. Clean $FeCl(Cp)(CO)_2$ was isolated by column chromatography and the compound was determined to be pure by IR spectroscopy.

The literature procedure for the synthesis of **2a** did not specify at which wavelength the photolysis of $FeCl(Cp)(CO)_2$ conducted. The first synthetic attempt was done using a UV-A (400–315 nm) light, and less than 20% product was observed after 48 h. This was likely due to poor solubility of the ligand in the solvent used (toluene) and/or the incorrect UV wavelength was used. To identify the optimal wavelength for the reaction, UV-vis spectra for both reactants were collected (Appendix A.15). The maximum absorbance of $FeCl(Cp)(CO)_2$ was at 354 nm, which was not absorbed by either toluene or $P^{Ph}{}_2N^{Ph}{}_2$. The next attempt at this reaction was performed in a solution of toluene/DCM to increase the solubility of the ligand, and the reaction was conducted in a glass vessel which allowed 354 nm light to be absorbed by the solution (Scheme 2.5). After 4 h, the $^{31}P\{^1H\}$ NMR spectrum showed a major singlet at ~60 ppm, and a minor signal at ~55 ppm. After removal of insoluble grey solids and recrystallization from DCM/hexanes, black crystals were obtained in a 10% yield. The low yield was due to the slow and inconsistent crystallization, which will need to be improved in future synthetic procedures. A $^{31}P\{^1H\}$ NMR spectrum of the crystalline material in CD_2Cl_2 revealed one singlet at 59.3 ppm and the $^{31}P\{^1H\}$ and ^1H NMR spectra were consistent with the literature values. The synthesis of **2a** was improved from the literature procedure by using DCM and 354 nm light, which increased reaction speed from 48 h to 4 h, but the isolation method still needs improvement to achieve acceptable isolated yields. Regardless, a suitable amount of **2a** was obtained to complete the final step to synthesize **3a**.

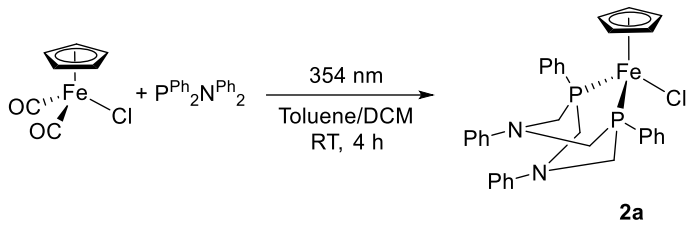

Scheme 2.5. Modified route to the synthesis of **2a** by reaction of $FeCl(Cp)(CO)_2$ with $P^{Ph}{}_2N^{Ph}{}_2$ in toluene/DCM at RT for 4 h.

2.4 Synthesis and Characterization of $[Fe(Cp)(MeCN)(P^{Ph}{}_2N^{Ph}{}_2)]PF_6$

Complex **2a** was treated with KPF_6 in the presence of acetonitrile to generate **3a** (Scheme 2.6). After 3 h, excess KPF_6 was removed by filtration, and the red solids obtained were dissolved in CD_2Cl_2. The $^{31}P\{^1H\}$ NMR spectrum revealed a singlet at 57.8 ppm, and a septet at –144.4 ppm. The singlet was 1.5 ppm upfield from **2a**, and 7.6 ppm downfield from the Cp* substituted complex **3a***.[96,114] The upfield shift compared to **2a** is due to the MeCN ligand being more electron-donating to the Fe center than chloride. The downfield shift compared to **3a*** is because Cp* is much more electron-donating than Cp. A singlet at 2.32 ppm integrates to three relative to a methylene on the $P^{Ph}{}_2N^{Ph}{}_2$ ligand, which was identified as the methyl of the coordinated MeCN ligand. The MALDI-MS of **3a** showed a peak with *m/z* and isotope pattern consistent with $[Ru(Cp)(P^{Ph}{}_2N^{Ph}{}_2)]^+$. This signal is consistent with fragmentation of the molecular cation to release the labile MeCN ligand, which was consistent with all complexes of the type $[M(Cp)(MeCN)(P^{R}{}_2N^{R'}{}_2)]PF_6$, where M = Ru or Fe.[110,109] This new modified procedure avoids the solubility, and conversion issues observed with the previous attempts at synthesizing **2a**, and avoids any of the impurities observed with the other previously attempted methods.

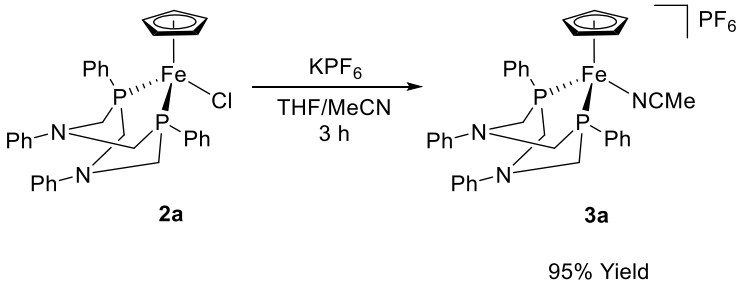

Scheme 2.6. Reaction of **2a** with KPF_6 and MeCN for 3 h to make **3a**.

Chapter 3: Acceptorless Dehydrogenation of Benzylamine Using $[M(Cp/Cp^*)(MeCN)(P^R{}_2N^{R'}{}_2)]PF_6$ Complexes

3.1 Acceptorless Dehydrogenation of Benzylamine with $[Ru(Cp)(MeCN)(P^{Ph}{}_2N^{R'}{}_2)]PF_6$ Complexes: Changes in Secondary Coordination Sphere and Selectivity

To determine the effects of the secondary coordination sphere on catalyst activity, a selection of $[Ru(Cp)(MeCN)(P^{Ph}{}_2N^{R'}{}_2)]PF_6$ complexes were prepared. Ruthenium complexes **1a-d** have different R′ substituents and each of the catalysts were reacted with benzylamine to determine the effect of pendant amine basicity on product distribution (Scheme 3.1). The modification of the pendant amine should have some effect on the catalyst's activity, as the interaction between the base and the substrate is proposed in both an inner and outer sphere pathway. Benzylamine was heated for 48 h at 110 °C in the presence of 3 mol% **1a-d** which were the general conditions used for all catalytic runs in this Chapter, unless otherwise stated. For each catalyst employed, the product distribution of **ADC**:**DAD**:**HB** was quantified by calibrated GC-FID analysis.

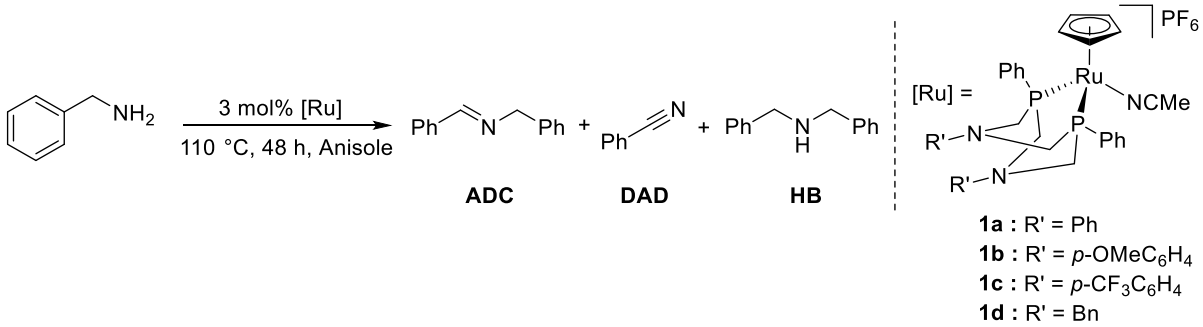

Scheme 3.1. Catalytic acceptorless dehydrogenation of benzylamine using 3 mol% **1a-d**.

The conversion by each catalyst, ranked from highest to lowest, was: **1d** ≈ **1c** > **1a** > **1b**, which corresponds to the R′ trend of Bn ≈ *p*-$CF_3C_6H_4$ > Ph > *p*-$OMeC_6H_4$. For the complexes bearing an aryl-substituted pendant amine, the trend indicates that decreasing the basicity of the pendant amine results in higher conversion. The Bn-substituted complex

is more donating than the Ph and its high conversion does not follow the trends observed with the Ar-substituted complexes.

Table 3.1. Catalyst (**1a-d**) performance and selectivity for the AD of benzylamine.[a]

Entry	Catalyst	%Conv.[b]	%**ADC**	%**DAD**	%**HB**
1	**1a**	59	28	3	20
2	**1b**	45	21	2	26
3	**1c**	70	37	9	17
4[c]	**1d**	76	54	20	3

[a]Conditions: 3 mol% [Ru], 250 mM $BnNH_2$, 110 °C, 48 h. Data was quantified with respect to an internal standard by calibrated GC-FID. Reactions were run in duplicate with the data shown representing the average, which are within 5% error. [b]Conversion calculated by amount of $BnNH_2$ consumed. [c]Data from previously published paper.[80]

To assess catalyst selectivity more easily, the product distribution was plotted for complexes **1a-d** (Figure 3.1). Complex **1d** was the most selective and forms 96% dehydrogenation products **ADC** and **DAD**, and only 4% hydrogenation product **HB**. Thus, the more donating Bn pendant amine results in near-complete dehydrogenation selectivity. Using the Ph-substituted complex **1a** results in 61% dehydrogenation products and 39% hydrogenation products. Switching to an aryl substituent resulted in a 35% decrease in AD product selectivity. Increasing the basicity of the pendant amine, using **1b** results in 53% dehydrogenation and 47% hydrogenation products. The ratios of AD:HB products for **1a** is 3:2 and for **1b** the ratio is 1:1. For the Ar-substituted complexes, increasing the pendant amine basicity resulted in decreased AD product selectivity. Using complex **1c** with reduced pendant amine basicity resulted in 73% dehydrogenation products and 27% hydrogenation product. The ratios of AD:HB products for **1c** is 3:1 which is far more selective for AD products than **1b**, which formed a 1:1 ratio of AD:HB products. By decreasing the pendant amine basicity, a 22% increase in AD product selectivity was observed as compared to **1a**. Overall, Ar-substituted complexes were less selective than the Bn-substituted complex **1d**. However, the selectivity within the aryl-substituted set of

catalysts could be tuned to favour dehydrogenation products by reducing the basicity of the pendant amine.

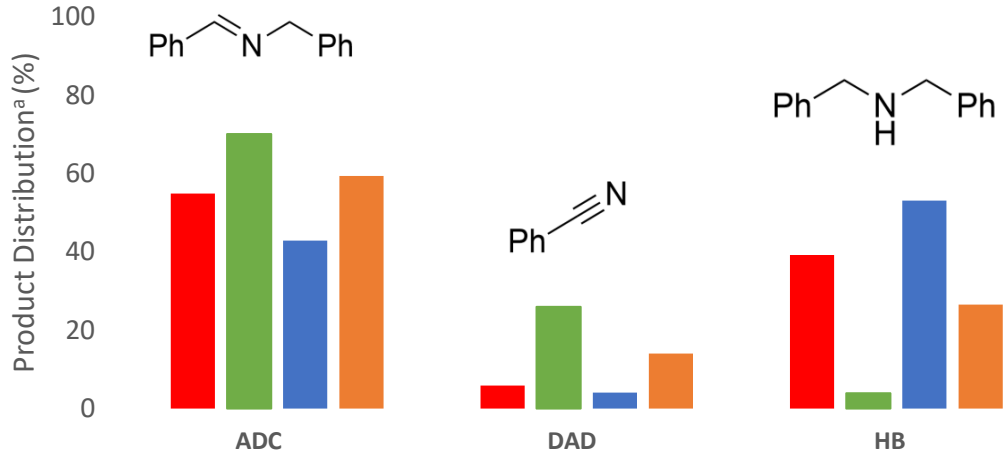

Figure 3.1. Bar graph showing the product distribution of benzylamine dehydrogenation (**ADC** and **DAD**) and hydrogenation (**HB**) products using catalysts **1a** (red), **1b** (blue), **1c** (orange), **1d** (green). [a]Product distribution was calculated by ((%ADC/DAD/HB)/(%ADC+DAD+HB))*100.

The different ratios of AD:HB products using the Ar-substituted complexes can be rationalized by the proposed mechanism shown in Scheme 3.2. Dehydrogenation of benzylamine (outer sphere dehydrogenation depicted) results in an intermediate containing a proton on the pendant amine, and hydride on the metal center (**III**). The Ru–H bond of **III** is protonated by the pendant amine to form an H_2 adduct **IV**. Complexes **IV** and **III** are proposed to exist in equilibrium, which is the case with similar cationic ruthenium and iron $P^{Ph}_2N^{Ph}_2$ complexes.[96,97] Intermediate **IV** can then release H_2 to reform the active catalyst (H_2 release pathway). However, the H_2 release pathway does not account for the observed HB product formed with **1a-c**. In a second pathway, intermediate **III** reacts with **ADC** to form product **HB**, which would also regenerate the active catalyst (hydrogenation pathway). Therefore, turnover can occur from **III** by either H_2 release through intermediate **IV**, or by hydrogenation of product **ADC**. The active catalyst generated from the liberation of H_2 can then either react with a second molecule of benzylamine or possibly react with **Im** to generate benzonitrile (**DAD**). Increasing the basicity of the pendant amine results in a less acidic protonated pendant amine, and intermediate **III** reacts to form **IV** more slowly.

If the equilibrium is shifted towards **III**, more **HB** is formed as a result, as there is more **III** around to hydrogenate **ADC**. By decreasing the basicity of the pendant amine, intermediate **III** has a more acidic protonated pendant amine, and protonolysis can occur faster, shifting the equilibrium towards the formation of **IV**. If **III** reacts more quickly to make **IV**, then there is a lower chance of **ADC** being hydrogenated, which results in less **HB** being formed.

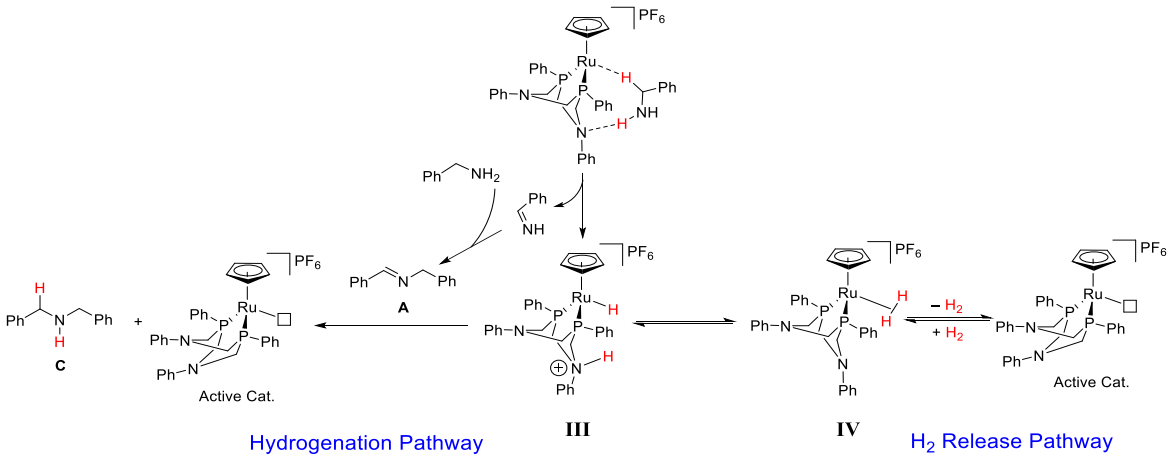

Scheme 3.2. A section of the proposed catalytic mechanism shown for complex **1a**. Complex **III** and **IV** are in equilibrium, and catalytic turnover depends on whether the H_2 release pathway or the hydrogenation pathway occurs.

One possibility for the observation of **HB** in the reaction is the reversible uptake of H_2. The catalytic reactions up until this point have been conducted in sealed vials, where H_2 is unable to escape the system. If uptake of H_2 is reversible, then the active catalyst can bind H_2 to reform intermediate **IV**. As the reaction progresses, and more H_2 is released, the equilibrium between **IV** and **III** will start to shift towards **III**. This would then increase the amount of **HB** produced as a result as there is more **III** around to react with **ADC**. To determine whether H_2 buildup has an effect on the amount of **HB** product formed, a reaction with **1a** and benzylamine will be conducted in the following section.

3.2 Catalytic Acceptorless Dehydrogenation with [Ru(Cp)(MeCN)($P^{Ph}_2N^{R'}_2$)]PF_6 in an Open System

All catalytic reactions under standard conditions (see Scheme 3.1) with **1a** were conducted in a sealed vial. This does not allow H_2 to escape from the system, and this could cause an increase in the amount of **HB** formed as H_2 accumulates in the vessel over time. A reaction with **1a** and benzylamine was conducted under a flow of argon (i.e. ‘open' conditions) to allow H_2 to be removed from the system (Scheme 3.3). The conversion achieved by **1a** in this open system was 33% which was 26% lower than when catalysis was performed in a closed system (Table 3.2, Entry 2). This decrease in conversion could be a result of changing the reaction vessel from a sealed vial in a heating block to a Schlenk flask in an oil bath, which may have resulted in inadequate heating of the solution in the latter case. Despite the decreased conversion, production of **HB** was not suppressed in an open system as compared to a closed system (Figure 3.2). In an open system **1a** gave a 1:2 mixture of **ADC**+**DAD**:**HB**, while in a closed system a 3:2 ratio was observed. The presence of near-equal amounts of **HB** in an open and closed system indicates that the presence of HB in the reaction is not due to H_2 buildup pushing the equilibrium towards the formation of **III**. The formation of **HB** is a result of the competing H_2 release, and hydrogenation pathways, which results in a mixture of both dehydrogenation and hydrogenation products.

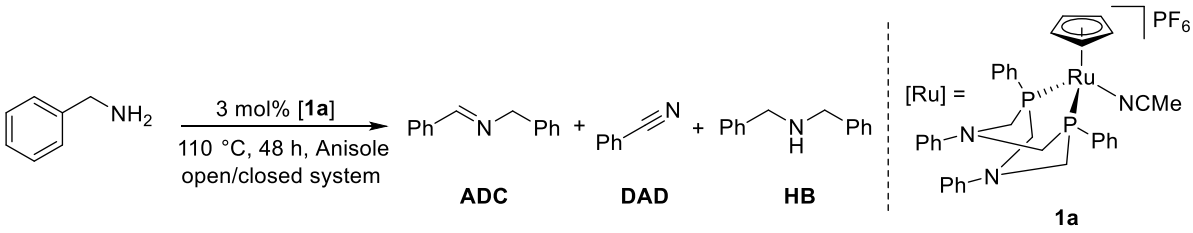

Scheme 3.3. Catalytic AD of benzylamine with **1a** in an open/closed system. Open system: schlenk flask under argon atmosphere. Closed system: sealed vial.

Table 3.2. Comparison of catalyst performance and percent products for the AD of Benzylamine in an open and closed system.[a]

Entry	Catalyst	Open/Closed System	%Conv.[b]	%**ADC**	%**DAD**	%**HB**
1[c]	**1a**	Closed System	59	28	3	20
2[d]	**1a**	Open System	33	9	1	19

[a]Conditions: 3 mol% [Ru], 250 mM $BnNH_2$, 110 °C, 48 h. Data was quantified with respect to an internal standard by calibrated GC-FID. Reactions were run in duplicate with the data shown representing the average. Conversion values were within 5% of each other. [b]Conversion calculated by amount of $BnNH_2$ consumed. [c]Reaction performed in a sealed vial. [d]Reaction performed on a Schlenk line under a constant flow of argon.

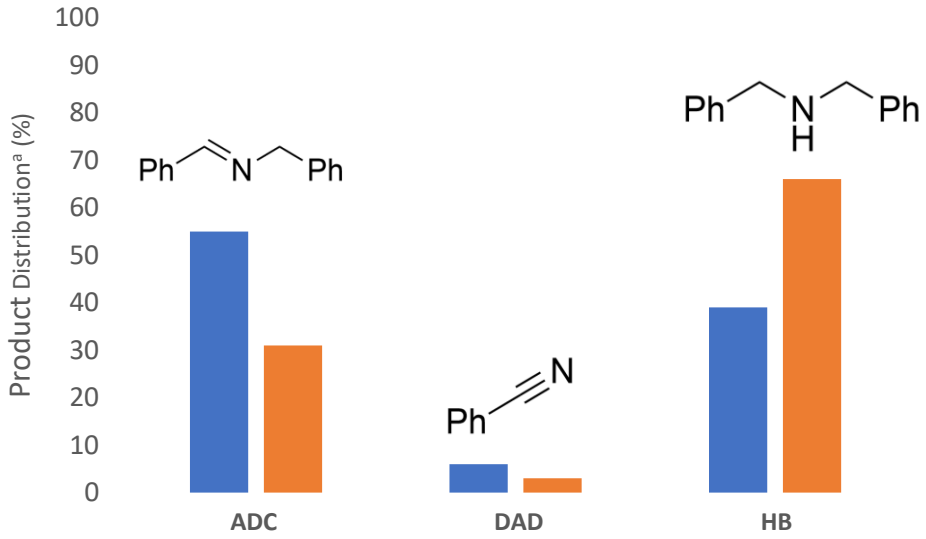

Figure 3.2. Bar graph showing the product distribution of benzylamine dehydrogenation (**ADC** and **DAD**) and hydrogenation (**HB**) products using **1a** in an open system (orange) and closed system (blue). [a]Product distribution was calculated by ((%ADC/DAD/HB)/(%ADC+DAD+HB))*100.

3.3 Acceptorless Dehydrogenation of Benzylamine with [Ru(Cp/Cp*)($P^R_2N^{Ph}_2$)(MeCN)]PF_6 Complexes: Influence of Primary Coordination Sphere and Selectivity

Ruthenium complexes **1a** and **1e** which have different R substituents, and **1a***, which has a bulkier Cp* ligand, were reacted with benzylamine to determine the effect of the primary coordination sphere on product distribution (Scheme 3.4).

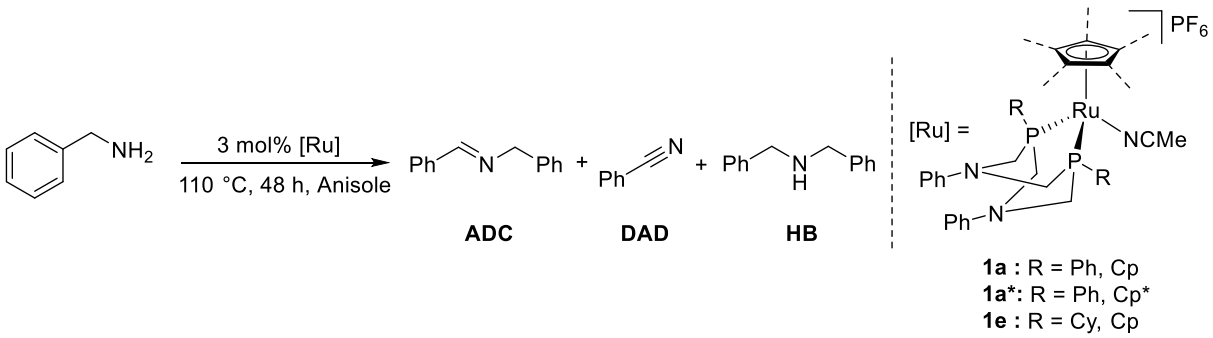

Scheme 3.4. Catalytic acceptorless dehydrogenation of benzylamine using 3 mol% **1a**, **1a***, **1e**.

The highest conversions were obtained with the Cp-bearing complexes **1a** (59%) and **1e** (55%). Changing the donor properties of the phosphine ligand to a slightly more donating cyclohexyl group did not affect conversion. Complex **1a*** achieved 27% conversion, which was 22% less than Cp-analogue **1a**. The decreased conversion with **1a*** indicates that using either a stronger donor, or a larger ancillary ligand decreases conversion.

Table 3.3. Comparison of catalyst performance and percent products formed from AD of benzylamine.[a]

Entry	Catalyst	%Conv.[b]	%**ADC**	%**DAD**	%**HB**
1	**1a**	59	28	3	20
2	**1a***	27	17	3	2
3	**1e**	55	24	3	29

[a]Conditions: 3 mol% [Ru], 250 mM $BnNH_2$, 110 °C, 48 h. Data was quantified with respect to an internal standard by calibrated GC-FID. Reactions were run in duplicate with the data shown representing the average. Conversion values were within 5% of each other. [b]Conversion calculated by amount of $BnNH_2$ consumed.

The product distribution with complexes **1a**, **1a***, and **1e** is shown below in Figure 3.3. Complex **1a*** displays a 10:1 ratio of dehydrogenation to hydrogenation products, while **1a**, which has a 3:2 ratio of (**ADC**+**DAD)**:**HB**. Employing the Cp* ligand results in a drastic increase in product selectivity compared to **1a**. One possible explanation for the decreased amount of **HB** formed with the Cp* analogue is due to the greater steric bulk of the ancillary ligand. Formation of **HB** depends on the reaction of intermediate **III** and **ADC**, and the increased steric bulk may hinder this reaction to a greater extent than the Cp analogue. Catalyst **1e** with R = Cy gives a negligible difference in preference for dehydrogenation over hydrogenation, as compared to **1a** with R = Ph. This would indicate that the identity of the R group has a minimal impact on product selectivity.

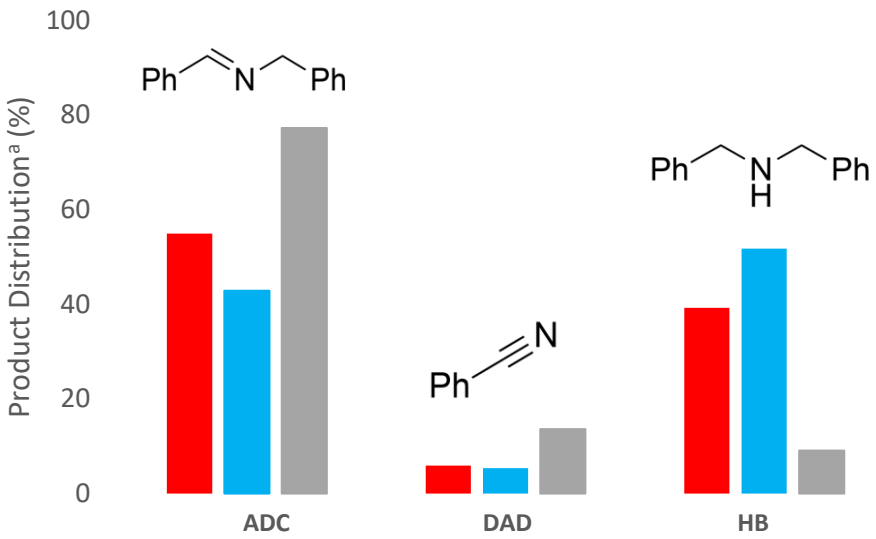

Figure 3.3. Bar graph showing product distribution of benzylamine dehydrogenation (**ADC** and **DAD**) and hydrogenation (**HB**) products using **1a** (red), **1a*** (grey), and **1e** (light-blue). [a]Product distribution was calculated by ((%ADC/DAD/HB)/(%ADC+DAD+HB))*100

3.4 Acceptorless Dehydrogenation of Benzylamine by [Fe(Cp/Cp*)(MeCN)($P^{Ph}_2N^{Ph}_2$)]PF_6 Complexes: Effect of Metal Center on Selectivity

To determine the effect of the metal center on the product distribution for AD of benzylamine, iron analogues of complexes **1a** and **1a*** (**3a** and **3a***, respectively) were tested (Scheme 3.5). Trends in hydride donor-ability for M(H)(Cp)$(CO)_2$ complexes, where M = Fe, Ru, Os, show that the iron-hydride bond was less nucleophilic compared to the ruthenium-hydride bond.[115] This decreased nucleophilicity could potentially lead to decreased reactivity of intermediate **III** with product **ADC**, resulting in lower amounts of **HB** formed. The substrate conversion, as well as the ratios of **ADC**:**DAD**:**HB** were quantified by GC-FID.

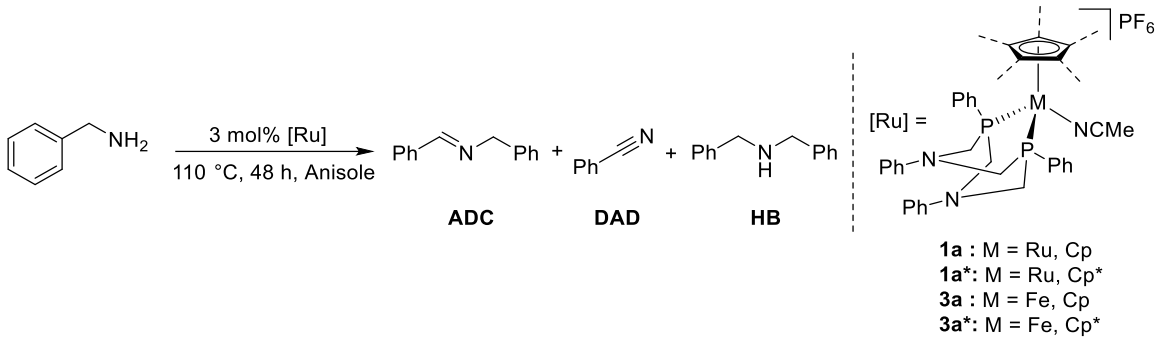

Scheme 3.5. Catalytic acceptorless dehydrogenation of benzylamine using 3 mol% **1a**, **1a***, **3a**, **3a***.

Complex **3a** results in 39% conversion, while **3a*** afforded 21% conversion. Having the Cp* ligand instead of Cp resulted in an 18% decrease in catalyst conversion, which is consistent with the trend with the Ru analogues. Too much steric bulk, or too much electron-donation to the metal center as a result of the Cp* ligand results in decreased conversion. Complex **3a** achieves 30% lower conversion than **1a**, and **3a*** achieves 6% less conversion than **1a***. The iron-analogue of **1a** was noticeably worse, while the difference in conversion between **3a*** and **1a*** is negligible. An increased catalyst loading of **3a** could potentially off-set this decreased activity at 3 mol%, but this has not been tested. Overall, the ruthenium complexes **1a** and **1a*** both resulted in higher conversion than their iron counterparts.

Table 3.4. Comparison of catalyst performance percent products from AD of benzylamine.[a]

Entry #	Complex	%Conv.[b]	%**ADC**	%**DAD**	%**HB**
1	**1a**	59	28	3	20
2	**1a***	27	17	3	2
3	**3a**	39	38	4	0
4	**3a***	21	18	5	0

[a]Conditions: 3 mol% [Ru], 250 mM $BnNH_2$, 110 °C, 48 h. Data was quantified with respect to an internal standard by calibrated GC-FID. Reactions were run in duplicate with the data shown representing the average. Conversion values were within 5% of each other for **1a**/**1a*** and ±7% for **3a**/**3a***. [b]Conversion calculated by amount of $BnNH_2$ consumed.

The product distributions for AD of benzylamine using **1a**, **1a***, **3a**, and **3a*** were plotted to determine the differences in selectivity between each catalyst (Figure 3.4). Complex **3a** formed a 9:1:0 mixture of **ADC**:**DAD**:**HB**, compared to the ruthenium analogue **1a**, which made a 9:1:7 mixture. Complex **3a*** afforded a 4:1:0 ratio of **ADC**:**DAD**:**HB** and use of the ruthenium analogue **1a*** resulted in a 9:2:1 ratio of products. Both iron analogues of **1a** and **1a***, respectively, displays complete AD product selectivity, with no detectable amounts of **HB** formed after 48 h. Additionally, **3a** heavily favors the formation of **ADC**, with a 9:1 ratio of **ADC**:**DAD**, and is the most selective catalyst out of all the complexes tested.

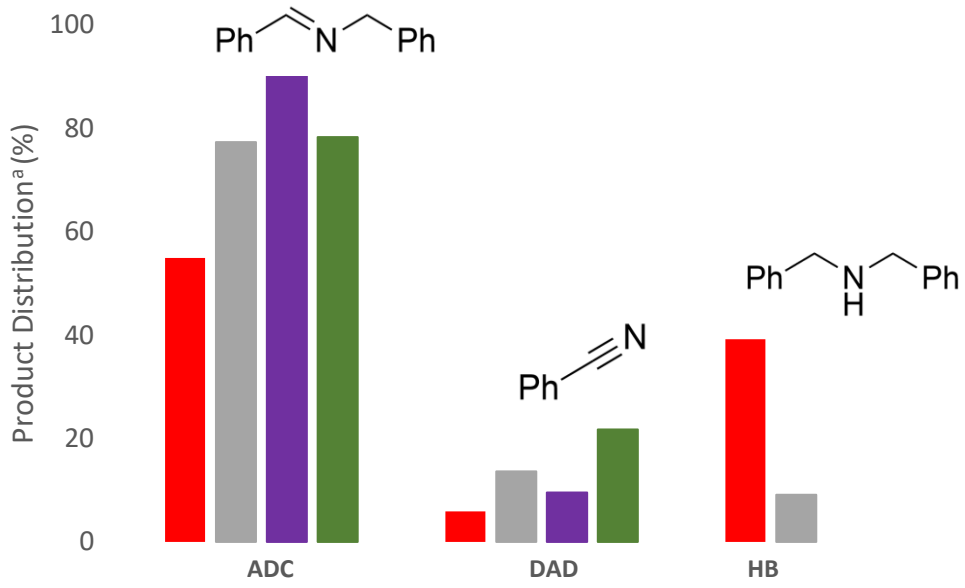

Figure 3.4. Bar graph showing product distribution of benzylamine dehydrogenation/hydrogenation products using **1a** (red), **1a*** (grey), **3a** (purple), **3a*** (green). [a]Product distribution was calculated by ((%ADC/DAD/HB)/(%ADC+DAD+HB))*100.

One possible explanation for the increased selectivity of **3a** towards AD products is due to the decreased hydricity of intermediate **III** where M = Fe (**3a-III**) (Scheme 3.6a). Hydricity is defined as a hydride's donor ability, and is influenced by a variety of factors.[95] If we consider the reaction $[M(H_2)]^+ \rightarrow MH + [H]^+$, the pKa of the dihydrogen species provides information on the hydricity of the conjugate base. In other words, a more acidic

$M(H_2)^+$ complex corresponds to a more hydritic/basic conjugate base, M(H). For example, the pKa of complex $[FeCp(H_2)(P^{Ph}{}_2N^{Bn}{}_2)]^+$ in MeCN is bracketed between 20 and 24, which means that the conjugate base $[Fe(Cp)H(P^{Ph}{}_2N^{Bn}{}_2)]$ is significantly hydritic.[96] Unfortunately, there is no known pKa of $[RuCp(H_2)(P^{Ph}{}_2N^{Bn}{}_2)]^+$, which means that the exact difference in hydricity between **1a** and **3a** cannot be approximated. However, for complexes of the type $[MH(diphosphine)_2]^+$ the hydricity of the complex increases from the first row to the second row. For the reaction of *trans*-$[M(H_2)(H)(dppe)_2]^+$ → *cis*-$M(H)_2(dppe)_2 + H^+$, the pKa of *trans*-$[Fe(H_2)(H)(dppe)_2]^+$ in THF is 11.5, while the pKa of *trans*-$[Ru(H_2)(H)(dppe)_2]^+$ in THF is 14.1.[116] The iron-(H_2) complex is more acidic than the Ru-(H_2) complex, which means that Ru–H is more hydritic than Fe–H. Based on the hydricity trends of the $M(H)_2(dppe)_2$ complexes, it is hypothesized that the M–H bond of **3a** is less hydritic than **1a**. Formation of **HB** is currently proposed to form from the reaction of intermediate **III** with **ADC**, so it is possible that the decreased reactivity of the Fe–H bond in **3a-III** resulted no formation of **HB** (Scheme 3.6b). Instead, the H_2 release is the only pathway possible for **3a**. In the case of **1a**, complex **1a-III** has a more hydritic Ru–H bond, and the reaction of **1a-III** with **ADC** is competing with the H_2 release pathway. This would explain the mixture of dehydrogenation and hydrogenation products formed when **1a** is used.

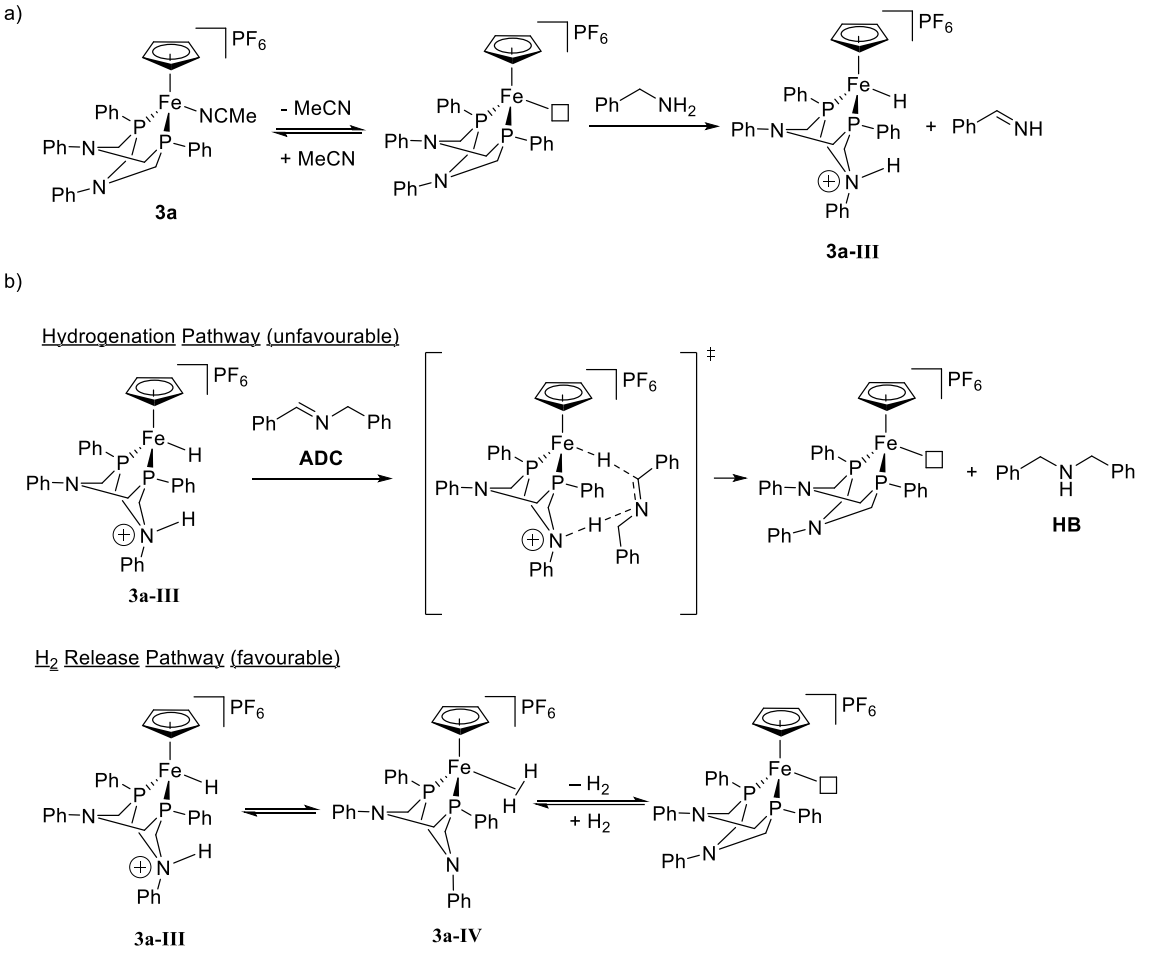

Scheme 3.6. a) Formation of proposed reaction intermediate **3a-III**. b) Two possible reaction pathways starting from **3a-III**, the hydrogenation pathway is proposed to be less favourable due to decreased hydricity of the Fe–H bond.

3.5 Acceptorless Dehydrogenative Coupling of Benzylamine with 1a and 1d

To further explore the differences in selectivity between the $P^{Ph}{}_2N^{Ph}{}_2$ and $P^{Ph}{}_2N^{Bn}{}_2$ ligand-bearing complexes, **1a** was tested towards the acceptorless dehydrogenative coupling (ADC) of benzylamine, with aniline as an additional nucleophile. The same reactions can occur to form **ADC**, **DAD**, and **HB**, but **Im** can also react with aniline to form *N*-phenylbenzenemethanamine (**ADC′**) (Scheme 3.7). Product **ADC′** can also be hydrogenated to form product **HB′**.

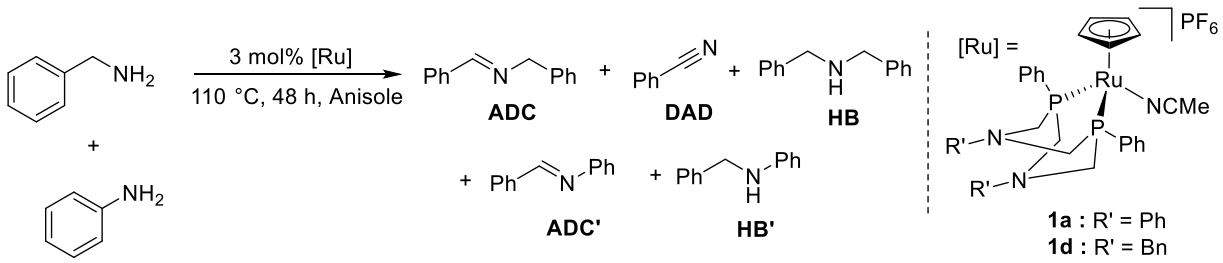

Scheme 3.7. Catalytic AD of benzylamine with aniline using 3 mol% **1a**/**1d**.

Complex **1a** achieved 67% conversion of benzylamine after 48 hours, which was 31% lower than **1d**. Thus, the phenyl-substituted pendant amine results in decreased catalyst activity compared to benzyl-substituted amine which is consistent with the trends observed with benzylamine and no aniline. The ratio of AD:HB products for **1a** was 2:3, and the ratio for **1d** was 1:0. Complex **1a** gave a 5:1:8:0 ratio of **ADC**:**DAD**:**HB**:**ADC′**, while **1d** gave a 2:2:0:1 ratio (Figure 3.5). It was notable that **1a** only gave trace amounts of the aniline-coupled product **ADC′** (less than 1%) which indicates that even in the presence of equimolar amounts of aniline, the homocoupled products were favoured when R = Ph. Benzylamine is a stronger nucleophile than aniline,[117,118] so it is not surprising that **ADC** was the dominant coupled product.

Table 3.5. Comparison of catalyst performance and selectivity for the AD of benzylamine in the presence of aniline.[a]

Entry #	Complex	%Conv[b]	%**ADC**	%**DAD**	%**HB**	%**ADC′**
1	**1a**	67	22	5	40	< 1
2	**1d**[c]	98	42	38	0	19

[a]Conditions: 3 mol% [Ru], 250 mM $BnNH_2$, 250 mM aniline, 110 °C, 48 h. Data was quantified with respect to an internal standard by calibrated GC-FID. Reactions were run in duplicate with the data shown representing the average. Conversion values were within 5% of each other. [b]Conversion calculated by amount of $BnNH_2$ consumed. [c]Data from previously published paper in the group.[80]

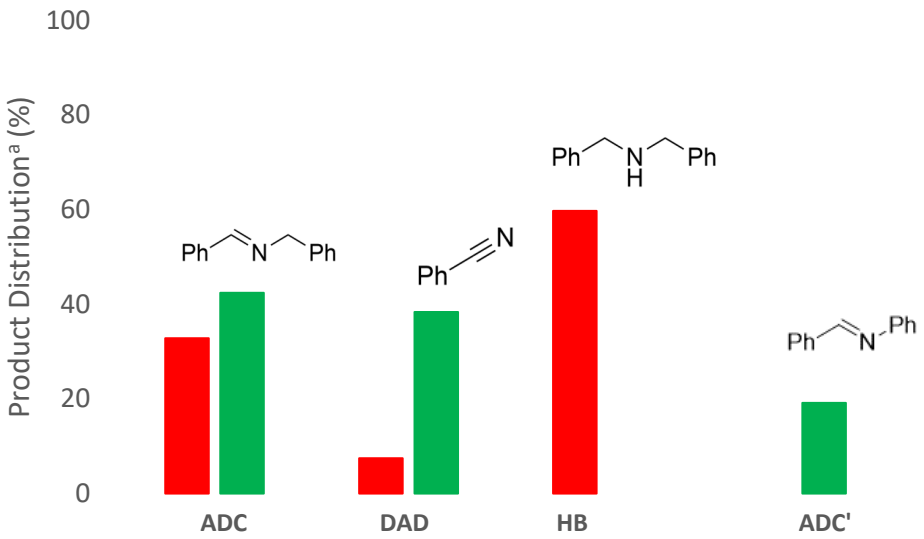

Figure 3.5. Bar graph showing product distribution of benzylamine dehydrogenation/hydrogenation products using **1a** (red), and **1d** (green). [a]Product distribution was calculated by ((%ADC/DAD/HB)/(%ADC+DAD+HB))*100.

3.6 Acceptorless Dehydrogenative Coupling of Benzyl Alcohol with [Ru(Cp)(MeCN)($P^{Ph}_2N^{Ph}_2$)]PF_6

Complex **1a** was used as the catalyst for the acceptorless dehydrogenative coupling of benzyl alcohol with aniline. This was done to probe the differences in activity/selectivity by using a secondary alcohol as the AD substrate instead of an amine (Scheme 3.8). One possible product is formed by oxidation of the alcohol to an aldehyde and subsequent coupling with aniline to form imine **ADC′**, the second possible product is a hydrogenation of the imine to form the hydrogen-borrowed product **HB′**.

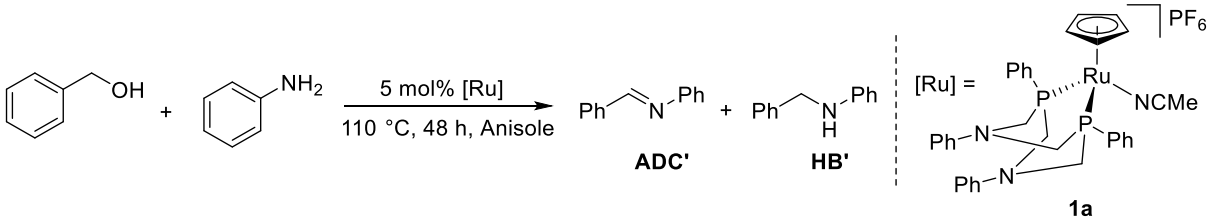

Scheme 3.8. Catalytic ADC of benzyl alcohol with aniline using 5 mol% **1a**.

Complex **1a** afforded 18% conversion of benzyl alcohol, which was 49% lower than when the substrate was benzylamine. This indicates that complex **1a** was much more reactive towards benzylamine than benzyl alcohol as an AD substrate. The pKa of benzylamine in MeCN is 16.92,[119] while the pKa of benzyl alcohol in MeCN is 15.40.[120] If the rate-determining step was outer sphere deprotonation of the substrate, increased acidity of the substrate would result faster reactivity. However, the α-carbon of $BnNH_2$ would be more hydritic than BnOH and would result in an α-CH that is more easily donateable to the metal center. In this case, it seems that a more hydritic α-CH is more important for increased catalyst activity. The amounts of each product observed with **1a** was 2% **ADC′** and 20% **HB′**, indicating high selectivity for HB products with **1a**.

Chapter 4: Mechanistic Studies of [Ru(Cp)(MeCN)($P^{Ph}_2N^{Ph}_2$)]PF_6 for Catalytic Acceptorless Dehydrogenation of Indoline

4.1 Comparing Catalyst Performance of [Ru(Cp)(MeCN)($P^{Ph}_2N^{Ph}_2$)]PF_6 and [Ru(Cp)(MeCN)(dppp)]PF_6 by *In-Situ* IR Spectroscopy

Acceptorless dehydrogenation (AD) was performed on indoline using metal-ligand cooperative complex [Ru(Cp)(MeCN)($P^{Ph}_2N^{Ph}_2$)]PF_6 (**1a**) and non-metal-ligand cooperative complex [Ru(Cp)(MeCN)(dppp)]PF_6 (**4**). The reaction was performed over a 20 h period at 110 °C in anisole and monitored by *in-situ* IR spectroscopy (Scheme 4.1). The expected AD product, indole, has a peak at 1354 cm^{-1} determined by IR spectroscopy that corresponds to a methine C-H stretching frequency, and this signal does not overlap with any signals corresponding to indoline.[121] Catalytic conversion of indoline to indole was monitored by the increase in peak height of the signal at 1354 cm^{-1} . After a 20 h reaction time, the reaction solution was analyzed by GC-FID and the conversion was quantified. The absorbance values at the end of the reaction were then quantified using the GC-FID data, which was used to normalize the IR absorbance values, so that each absorbance value has a corresponding concentration of indole (Figure 4.1). The initial turnover frequencies of complexes **1a** and **4** at 0.5 h were nearly identical (**1a** = 38 h^{-1}, **4** = 42 h^{-1}), however, **1a** reaches 85% conversion over 10 h, while **4** results in 63% conversion in the same amount of time. The turnover numbers (TONs) for **1a** and **4** were 85 and 63, respectively. Comparing TONs revealed that **1a** had 1.3 times higher TONs than **4**. While the catalytic rates were similar between the two complexes, with **1a**, the $P^{Ph}_2N^{Ph}_2$ ligand increases the overall catalyst lifetime, when compared to the non-MLC catalyst **4** with dppp as the ligand. Similar rates between [Ru(Cp)(MeCN)($P^{Ph}_2N^{Bn}_2$)]PF_6 (**1d**) and **4** was observed previously by our group in 2017, where AD of primary amines was studied.[80]

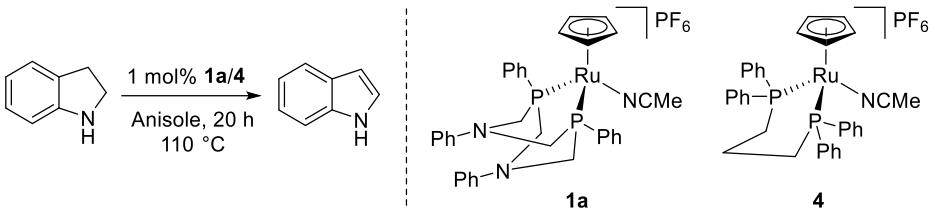

Scheme 4.1. Acceptorless dehydrogenation of indoline to form indole using 1 mol% **1a** or **4**.

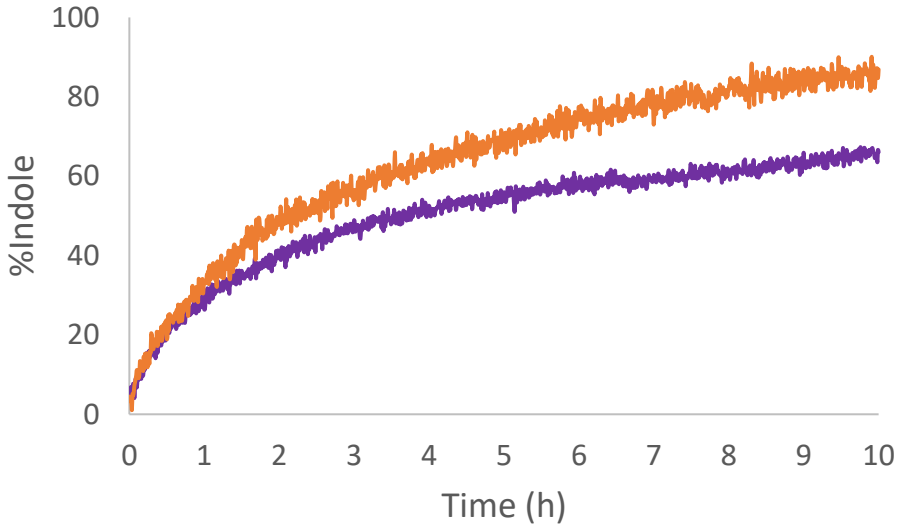

Figure 4.1. Graph depicting the conversion over time monitored by ReactIR. Conversion values were corrected using GC-FID analysis of the reaction solution after 20 h of reaction time (**1a** = orange, **4** = purple). Each data set was run in duplicate, and the overlap between both runs indicates that the results are replicable (Appendix A.21, A.22).

4.2 Mechanistic Studies to Determine the Reaction Rate Order for AD of Indoline using Ru(Cp)(MeCN)($P^{Ph}_2N^{Ph}_2$)]PF_6 (1a)

Variable time normalization analysis (VTNA) for the AD of indoline by catalyst **1a** was conducted to determine the reaction order with respect to substrate concentration (Scheme 4.2).[122] VTNA is a graphical analysis method that can be used to elucidate the reaction rate order of a particular species in a reaction. This method removes the kinetic effect that a component has on a reaction profile, by normalizing the time between each pair of data points in an experiment. The first stage of VTNA is to vary the concentration of substrate, while keeping the concentration of catalyst, and other reaction conditions,

constant. This will allow for the reaction order with respect to substrate concentration to be elucidated, since only the initial substrate concentration changes. Run 1 (R1) and run 2 (R2) were conducted at 110 °C 1 mol% loading of **1a** and monitored over a 20 h period by IR. The initial concentrations of indoline were 250 mM in R1, and 350 mM in R2. The concentration of indoline over time was plotted over the first 10 hours (Figure 4.2). The concentration of indoline in R1 starts at 250 mM and decreases to 25 mM after 10 h, which corresponds to 90% substrate consumption (grey line). The concentration of indoline in R2 starts at 350 mM and decreases down to 145 mM after 10 h and corresponds to 59% substrate consumption (yellow line). Additionally, R2 appears to begin to plateau at 10 h, indicating that the catalyst has become deactivated. To determine whether there was catalyst deactivation during R2, the plot of R1 was time-shifted to a point where the concentrations of indoline would be identical. In this case, after 0.6 h, the concentration of indoline in R2 is 250 mM. Taking R1 and time-shifting the entire plot 0.6 h to the right to where the concentrations of indoline in both reactions are the same (250 mM) will allow for easy comparison of catalyst activity. If the catalyst activity is the same for both R1 and R2, then time shifting R1 onto R2 should result in two overlapping lines from 250 mM indoline to the end of the reaction. Time-shifting the consumption plot of R1 onto R2 reveals that after 100 mM of indoline has been consumed in R2, subsequent consumption of substrate was much slower than R1. This indicates that either catalyst deactivation or product inhibition occurs in R2. Indole has a basic N atom, and a π-bond on the 5-membered ring, that can reversibly bind to the active site of **1a**. As indole accumulates in the reaction, the possibility for product inhibition increases, since there is a higher chance of **1a** and indole interacting.

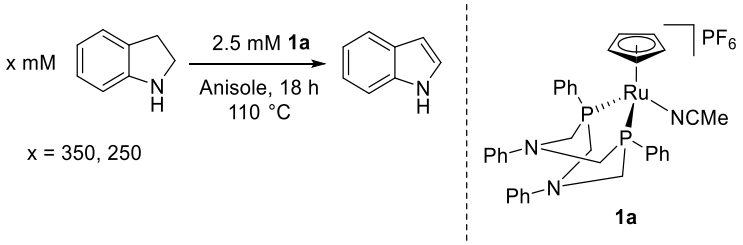

Scheme 4.2. Reaction of 350 mM indoline (R2) and 250 mM indoline (R1) with **1a** to form indole.

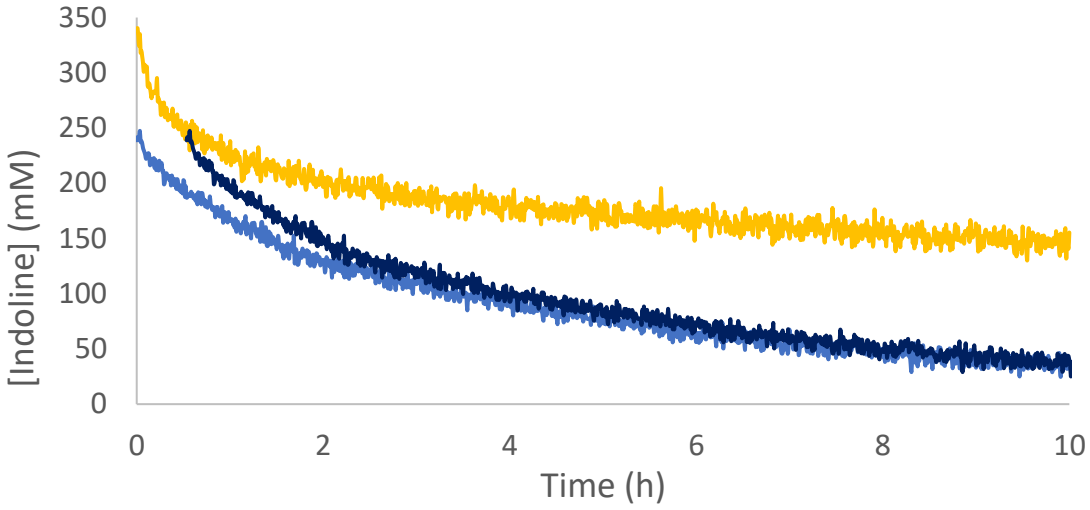

Figure 4.2. Amount of indoline consumed over time for Run 1: 250 mM indoline, 2.5 mM **1a** (light blue) and Run 2: 350 mM indoline, 2.5 mM **1a** (yellow) over 10 h. The dark-blue line represents the time-shifted plot of R1 onto the plot of R2, when the concentrations of indoline were both equal to 250 mM. Concentration values were corrected using GC-FID analysis of the reaction solution after 20 h of reaction time. Each data set was run in duplicate, and the overlap between both runs indicates that the results are replicable (Appendix A.21, A.23).

To test whether indole inhibits product formation, Run 3 (R3) was conducted. A solution containing 250 mM indoline, 2.5 mM **1a**, and 100 mM of indole was subjected to reaction conditions (Scheme 4.3). This run was prepared to mimic the conditions of R2 after consumption of 100 mM of indoline. It was expected that the 100 mM of indole will act as an inhibitor, and that the plots of R2 and R3 should overlap, assuming that product inhibition was occurring. The concentration of indoline in R3 starts at 250 mM and decreases to 46 mM after 10 h, corresponding to 82% consumption of substrate (Figure 4.3, light green line). The initial turnover frequency of R3 at 0.5 h is 69 h^{-1}, while the initial TOF for R2 is 59 h^{-1}. The initial turnover frequency for R3 did not decrease with 100 mM indole added to the reaction. If catalytic rate of **1a** was decreased by interactions with indole, it would be expected that the initial rate of R3 would be lower than R2. Time-shifting the consumption plot of R3 onto R2, at the time when the concentration of indoline was equal to 250 in R2 (green line), shows that the presence of indole did not decrease catalyst activity. This is confirmed by comparing the time-shifted plots of R3 and R1 which

are nearly identical. The consumption of indoline by the catalyst was unaffected by the 100 mM of indole added to the reaction. It is possible that H_2 inhibition is occurring, and that accumulation of H_2 in the reaction results in catalyst deactivation. Another possibility is that catalyst deactivation is occurring because of excess substrate in the reaction, resulting in the formation of off-cycle species. If the substrate binding to the metal is an off-cycle species, then there would be a noticeable increase in indoline-bound catalyst if there was more substrate initially.

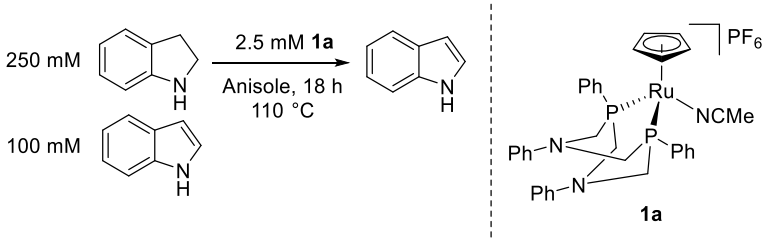

Scheme 4.3. Reaction of 250 mM indoline with **1a** to form indole in the presence of 100 mM indole.

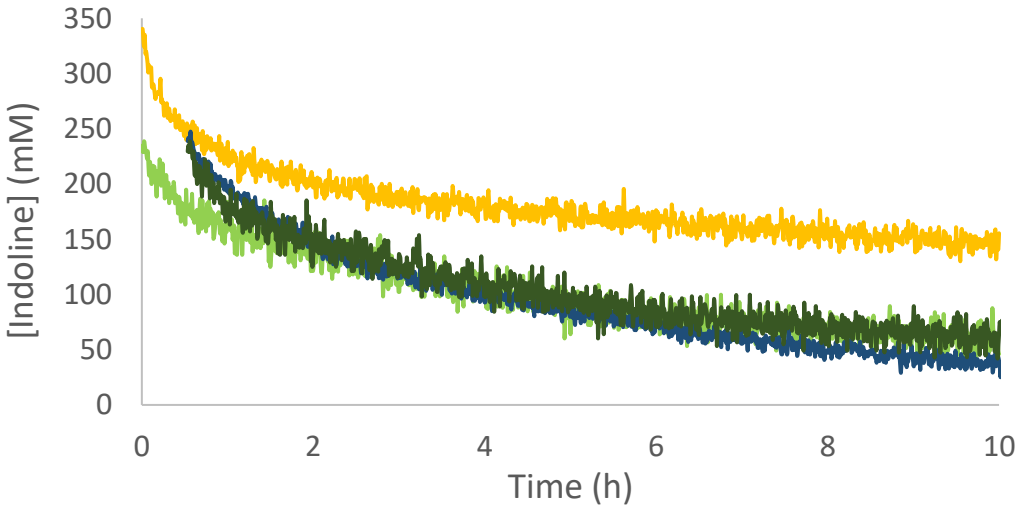

Figure 4.3. Concentration of indoline consumed over time for Run 3: 250 mM indoline + 100 mM indole, 2.5 mM **1a** (light green) and Run 2: 350 mM indoline, 2.5 mM **1a** (yellow) over 10 h. The dark-green line represents the time-shifted plot of R3 onto the plot of R2, when the concentrations of indoline are both equal to 250 mM. The dark-blue line is the time-shifted plot of R1 onto R2 when the concentrations of indoline are both 250 mM. Concentration values were corrected using GC-FID analysis of the reaction solution after 20 h of reaction time. Each data set was run in

duplicate, and the overlap between both runs indicates that the results are replicable (Appendix A.23, A.26).

Due to the catalyst deactivation observed with 350 mM indoline, the reaction order in substrate could not be elucidated by VTNA (Appendix A.28). Instead, a graphical kinetic analysis can be conducted, using integrated rate laws.[123] Plotting the concentration of indoline versus time for R1 (250 mM indoline) results in a decreasing curved line. Performing a linear regression on this data gives a line with the equation: $y = –16x + 171$, with an R square value of 0.878 (Figure 4.4 A). If the trendline for [Indoline] vs. t was a linear trend, then the rate order would be zero order with respect to the concentration of substrate. Next, ln[Indoline] was plotted as a function of time, and the result was a decreasing straight line. Performing a linear regression gives a line with the equation: $y = –0.18x + 5$, with an R square value of 0.972 (Figure 4.4 C). The linear trend observed upon calculating ln[Sub] plotted over time, and higher R^2 indicates that the rate order could be first order, with respect to substrate concentration. The plots of 1/[Indoline] vs. t and $[Indoline]^{1/2}$ vs. t were also calculated and plotted, but neither of the two resulted in a linear trend with a fit as high as with ln[Indoline] vs. t, meaning that the reaction order is unlikely to be second (Figure 4.4 D) or half order (Figure 4.4 B). This implies that the reaction rate order is likely first order with respect to the [Indoline].

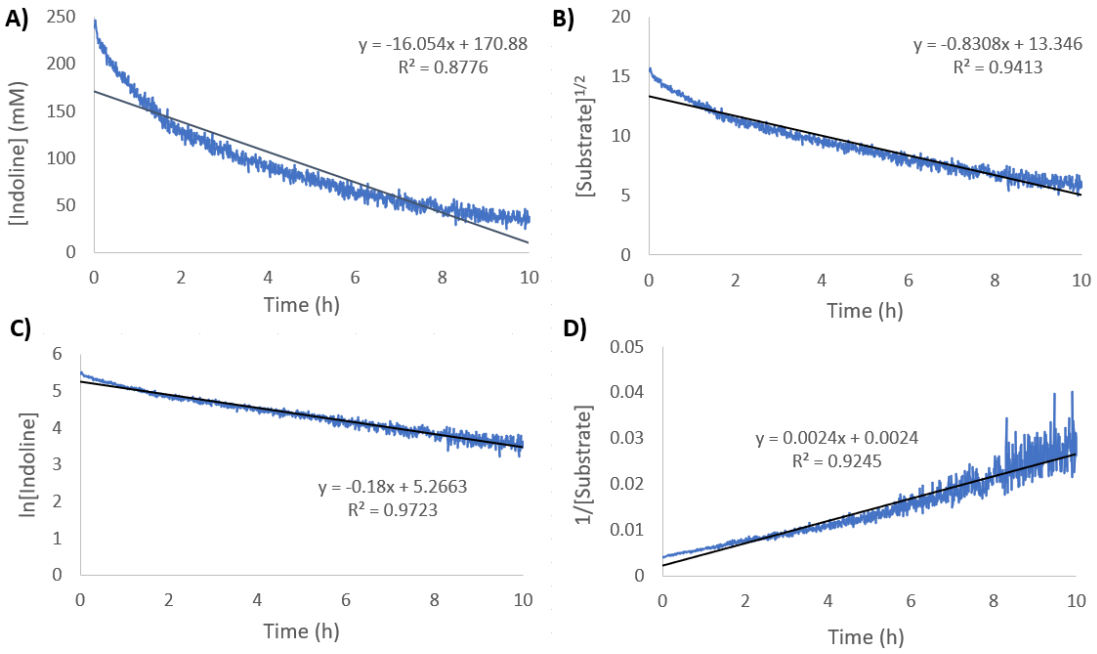

Figure 4.4. A) Plot of [Indoline] over time using 2.5 mM **1a** (run 1). B) Plot of [Indoline]$^{1/2}$ over time using 2.5 mM **1a** (run 1). C) Plot of ln[Indoline] over time using 2.5 mM **1a** (run 1).) D) Plot of 1/[Indoline] over time using 2.5 mM **1a** (run 1). Trendline and equations shown on plots A-D.

4.3 Mechanistic Studies to Determine the Reaction Rate Order of [Ru(Cp)(MeCN)($P^{Ph}_2N^{Ph}_2$)]PF_6 (1a) for AD of Indoline

VTNA for AD of indoline was conducted to determine the reaction rate order with respect to catalyst **1a**. The concentration of indoline was kept constant at 250 mM, and the concentration of **1a** was 2.5 and 1.75 mM in Runs 1 and 2, respectively. The reaction mixture was heated to 110 °C and monitored by *in-situ* IR spectroscopy over a 20-hour period (Scheme 4.4). The production of indole over the first 10 hours is shown (Figure 4.5). Conversion to indole after 10 h using 2.5 mM **1a** after was 87%, while 1.75 mM **1a** was 79%. The conversion when the catalyst concentration was decreased by 0.75 mM was 8% lower, which was not an appreciable difference. The turnover frequencies at 2 h for Run 1 and Run 2 was 9 h^{-1} and 7 h^{-1}, indicating that performances of 2.5 mol% and 1.75 mol% catalyst loading are nearly identical.

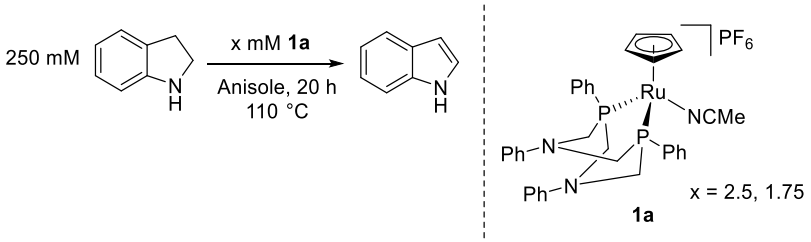

Scheme 4.4. Reaction of indoline (250 mM) with 2.5 or 1.75 mM **1a** to form indole.

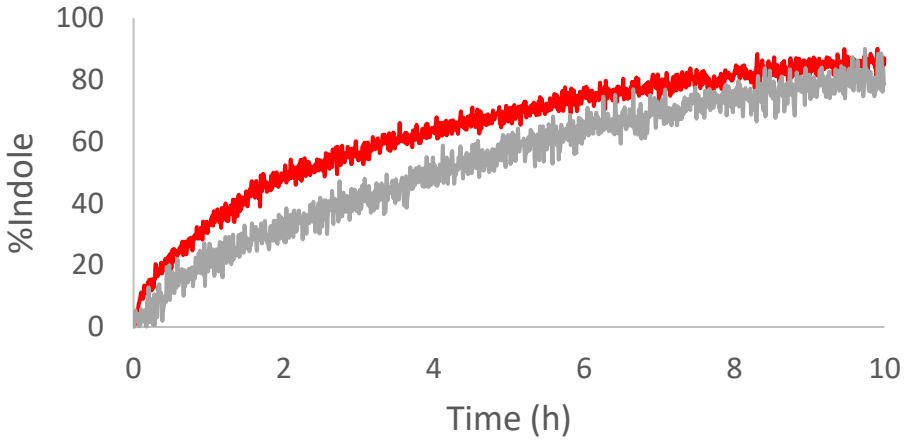

Figure 4.5. Reaction profiles of the %Product over time for run 1: 250 mM indoline, 2.5 mM **1a** (red) and run 2: 250 mM indoline, 1.75 mM **1a** (grey) over 10 h. Conversion values were corrected using GC-FID analysis of the reaction solution after 20 h of reaction time. Each data set was run in duplicate, and the overlap between both runs indicates that the results are replicable (Appendix A.21, A.24).

A variable-time normalization treatment of the data was then conducted to determine the reaction order with respect to catalyst. For both the 1.75 mM and 2.5 mM data sets, the concentration of indole was plotted against $t[cat]^x$, where x is 0, 1 or 2 (Figure 4.6). These x values were selected as zero, first, and second order reactions are common reaction orders. For VTNA, the $t[cat]^x$ term is used to normalize the time component between each data set. This allows for the generation of reaction profiles that can be used to elucidate the reaction rate order with respect to the catalyst concentration. The exponent x corresponds to the reaction rate order of the experiment, and both data sets will visually overlap when raised to the correct exponent. The visual overlap between data sets for each

treatment will allow for an approximation of the reaction rate order, as the data sets will overlap the most when the exponent corresponds to the reaction rate order. The plot of [indole] versus t[cat]^0 resulted in the least overlap between data sets, which indicated that the reaction was very unlikely to be zero order in catalyst. When x = 1, there was good alignment at the beginning and ends of the lines, with a brief divergence when [indole] = 75 to 150 mM. For x = 2, there was excellent overlap up to [indole] = 150 mM, but the lines separate significantly after that point. The VTNA suggests that the rate order for [**1a**] is most likely first order. It could also be that the rate order is more complex, and changes rate order as substrate is consumed over the course of the reaction. Kinetic studies will be described in the subsequent section to provide more insight into the mechanistic behavior of the reaction of **1a** with indoline.

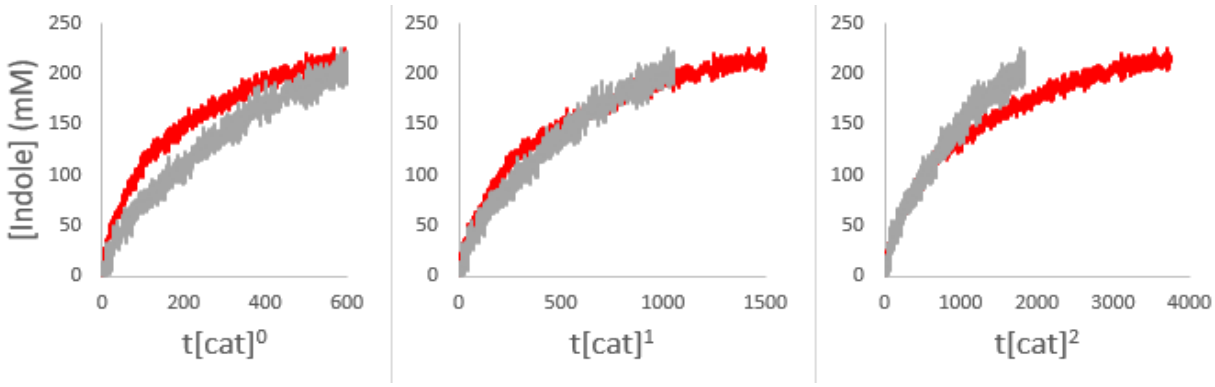

Figure 4.6. Plot of the concentration of indoline as a function of t[cat]^x, where x is 0–2.

4.4 Substrate Inhibition Study of [Ru(Cp)(MeCN)($P^{Ph}_2N^{Ph}_2$)]PF_6 using N-Me Indoline

The decreased activity of [Ru(Cp)(MeCN)($P^{Ph}_2N^{Ph}_2$)]PF_6 (**1a**) at 350 mM substrate concentration prompted a follow-up study to determine if unproductive substrate binding occurs, leading to an off-cycle species that decreases catalytic activity. N-Methyl indoline was chosen as it is close in structure and molecular properties to indoline, and will bind to the metal center of the catalyst similarly to indoline, but due to the lack of an N-H bond, it should not undergo AD. Therefore, it should act as an inhibitor similarly to indoline, but will not be dehydrogenated to form N-methyl indole. A solution of indoline, N-methyl indoline and 2.5 mM **1a** (1 mol%) was heated, and reaction progress was monitored by *in-situ* IR spectroscopy (Scheme 4.5). Run 1 (R1) contained 250 mM indoline and 100 mM

N-methyl indole, while Run 2 (R2) contained 350 mM indoline and no N-Me indoline. The [Indoline] change was monitored over 10 h for R1 and R2 (Figure 4.7). The [Indoline] for R1 starts at 250 mM and decreases to 88 mM indoline before the consumption begins to plateau. The [Indoline] for R2 begins at 350 mM and decreases to 145 mM. Time-shifting R2 onto R1, at the time when the concentration of indoline = 250 mM for both runs, reveals that the presence of N-Me Indoline does not account for the decreased rate of consumption in R2 (orange line).

GC-FID analysis shows that for R1, 66% of the N-methyl indoline in the reaction was converted to N-methyl indole. This indicates that N-methyl indoline was not a suitable substrate analogue, as it too undergoes AD. Overall, it appears as though N-Me indoline was not a suitable substitute for indoline in this test, as N-Me indole was observed. However, the presence of N-Me indole leads to an interesting new substrate to be further tested.

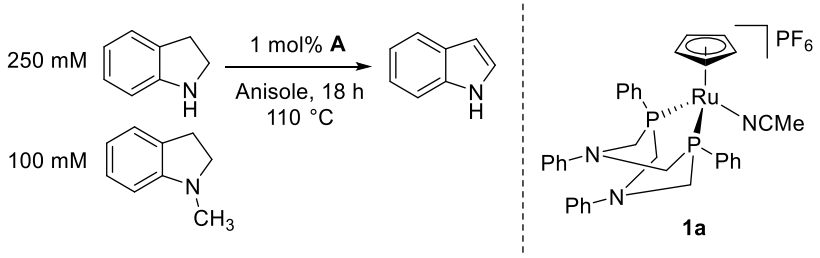

Scheme 4.5. Acceptorless dehydrogenation of indoline to form indole, in the presence of N-methyl indoline, using **1a**.

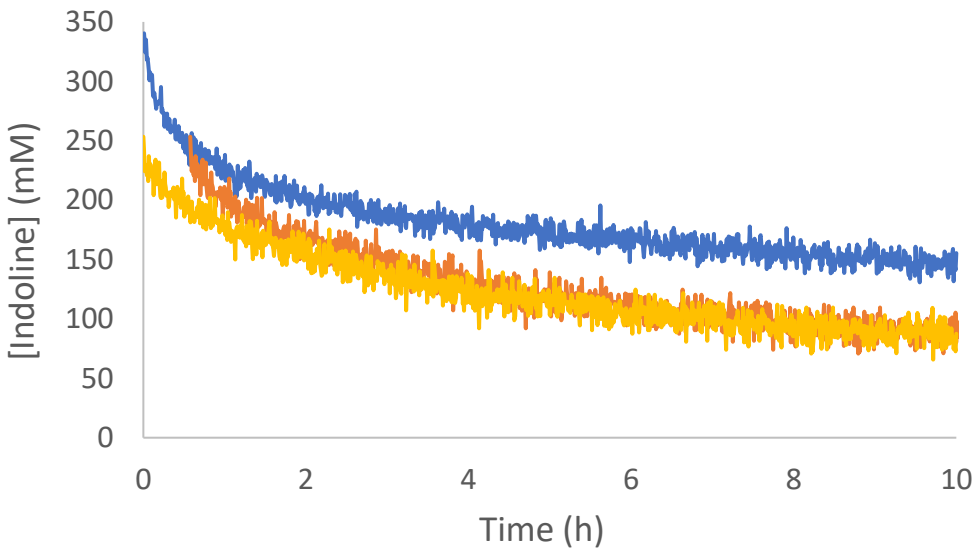

Figure 4.7. Reaction profiles of Run 1: 250 mM indoline, 100 mM N-methyl indoline, 2.5 mM **1a** (yellow) Run 2: 350 mM indoline, 2.5 mM **1a** (blue), and Run 1 time shifted onto run 2, where [Indoline] = 200 mM for run 2 (orange). Concentration values were corrected using GC-FID analysis of the reaction solution after 20 h of reaction time. Each data set was run in duplicate, and the overlap between both runs indicates that the results are replicable (Appendix A.23, A.25).

4.5 Catalytic Assessment of [Ru(Cp)(MeCN)($P^{Ph}_2N^{Ph}_2$)]PF_6 for the AD of N-Me Indoline

Prompted by the attempted catalyst inhibition study in Section 4.4, the AD of N-methyl indoline by catalyst **1a** was tested. The lack of an N-H bond on this substrate initially lead to the conclusion that acceptorless dehydrogenation would not be possible, as there would not be a sufficiently acidic proton in order to react with **1a**. The presence of any N-Me indole would then indicate that dehydrogenation occurs instead at C2 and C3. This is not likely to be an inner sphere mechanism, as there are no labile ligands on the catalyst to open a coordination site for *β*-H elimination to occur from the metal-bound substrate. This means an outer sphere pathway is the most likely mechanism for this substrate. *N*-Methyl indoline (250 mM) and 1 mol% **1a** was heated for 48 h, after which the reaction was analyzed by GC-FID (Scheme 4.6). The sole product observed was *N*-methyl indole in 30% conversion, which was 35% lower than what was observed in Section 4.4 with Run 1 The decrease in conversion could be due to the decrease in catalyst loading by using 250 mM N-Me indoline, or it could be due to decreased activity of the substrate.

This decrease in reactivity could be due to a need for an exogenous base for the C-C dehydrogenation pathway which in the previous case could have been indoline. Regardless, the ability of **1a** to dehydrogenate N-methyl indoline would indicate that this AD mechanism must undergo an outer sphere cooperative pathway, as there is no proton on the amine moiety. The proposed pathway would likely first involve deprotonation of N-methyl indoline at the C2 position, as the presence of the electronegative N atom would render C2 more acidic than C3. Then, a hydride transfer from C3 to the metal center would occur, forming intermediate **III**, and a molecule of N-methyl indole.

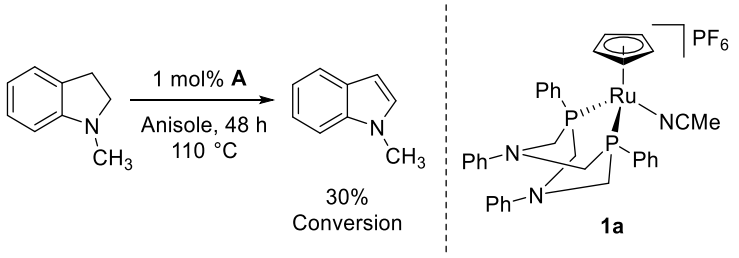

Scheme 4.6. Acceptorless dehydrogenation of N-methyl indoline to form N-methyl indole using **1a**. Conditions: 1 mol% [Ru], 250 mM N-Me indoline, 110 °C, 48 h. Data was quantified with respect to an internal standard by calibrated GC-FID. Reactions were run in duplicate and was within ±5% error. Conversion calculated by amount of N-methyl indoline consumed.

4.6 Kinetic Isotope Effect Experiments: AD of Deuterated Indolines using [Ru(Cp)(MeCN)($P^{Ph}_2N^{Ph}_2$)]PF_6

Two deuterated substrates, N-D indoline and α-D_2 indoline were targeted for synthesis to determine if there is a kinetic isotope effect (KIE) for catalytic AD with **1a** (Scheme 4.7a). The α-D_2 indoline substrate (**Ind-(C2-*d*$_2$)**) was synthesized by literature procedure (Scheme 4.7b).[33] **Ind-(C2-*d*$_2$)** was determined to be 100% deuterated by ^{1}H NMR spectroscopy by disappearance of the methylene triplet signal at 3.56 ppm, as well the multiplicity of the as the methylene signal at 3.03 ppm was a singlet instead of a triplet. The successful deuteration of the C2 methylene was also confirmed by the appearance of a singlet at 3.56 in the ^{2}H NMR spectrum. N-D indoline (**Ind-(N-*d*$_1$)**) was synthesized by a deuterium shake with D_2O (Scheme 4.7b). **Ind-(N-*d*$_1$)** was determined to be 68% deuterated, based on the decreased integration of the N-H signal at 3.76 ppm relative to N-

H indoline in the ^{1}H NMR spectrum. The appearance of a broad signal at 3.76 in the ^{2}H NMR spectrum confirmed that deuteration of the substrate occurred at the N position.

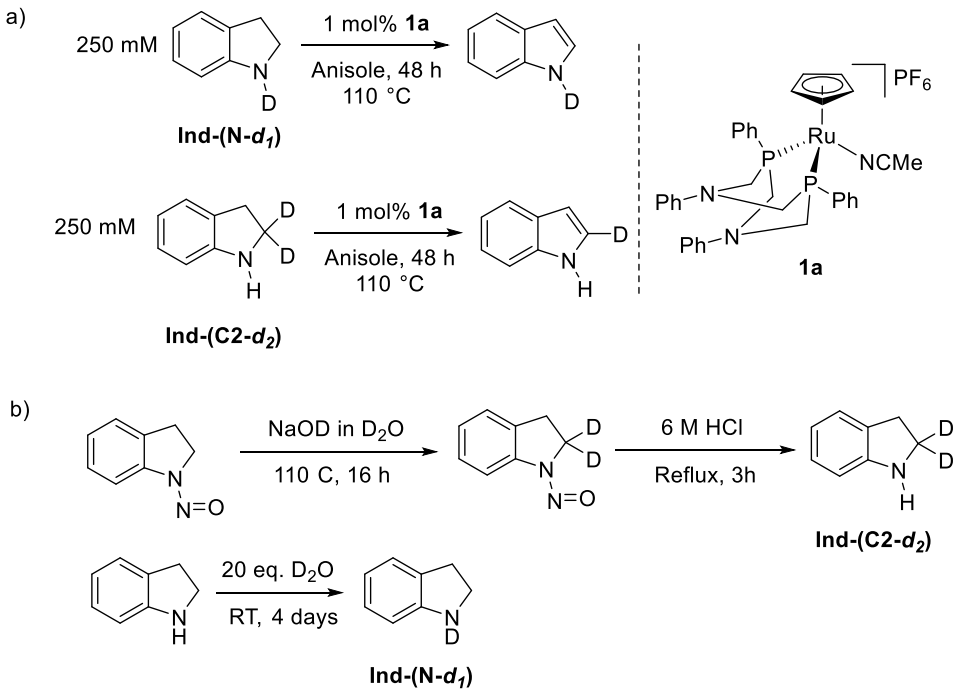

Scheme 4.7. a) Reactions of **Ind-(N-*d*$_1$)** and **Ind-(C2-*d*$_2$)** with 1 mol% **1a** to form N-D indole or α-D indole. b) Synthesis of **Ind-(C2-*d*$_2$)**, and **Ind-(N-*d*$_1$)**.

Several attempts were made to obtain a **Ind-(N-*d*$_1$)** sample with a higher percentage of deuterium incorporation, but none were successful. Therefore, a solution of **Ind-(N-*d*$_1$)**was prepared with 68% deuterium incorporation, and this was subjected to catalytic conditions (Scheme 4.8).

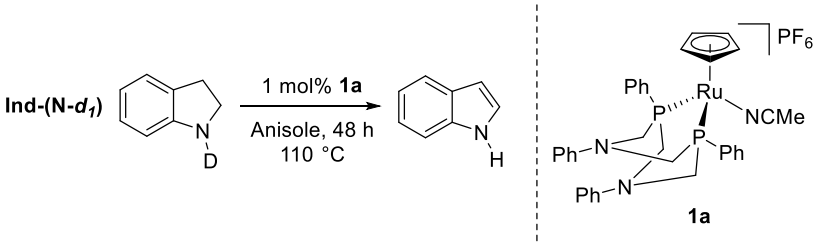

Scheme 4.8. Reaction scheme of **Ind-(N-*d*$_1$)** with 1 mol% **1a**.

If there is a noticeable decrease in catalytic performance using **Ind-(N-*d*$_1$)**, it would indicate that the presence of deuterium at the N position has an effect on the catalytic rate. The conversion of indoline to indole was monitored over a 20 h period, with the first 10 h is shown in Figure 4.8. The percentage of indole begins at 8% and increases to 20% after 1 h of reaction time, and then plateaus. The conversion at 10 h for N-H indoline was 87% after 10 h, which was significantly higher than **Ind-(N-*d*$_1$)**. This indicates that a high kinetic isotope effect was observed, but the presence of protio substrate at the outset means that initial conversion values cannot be included in the rate calculation. Instead, an indirect method without KIE calculations can be used to determine whether or not the decreased conversion observed with **Ind-(N-*d*$_1$)** was due to the presence of the deuterium atom at the N position.

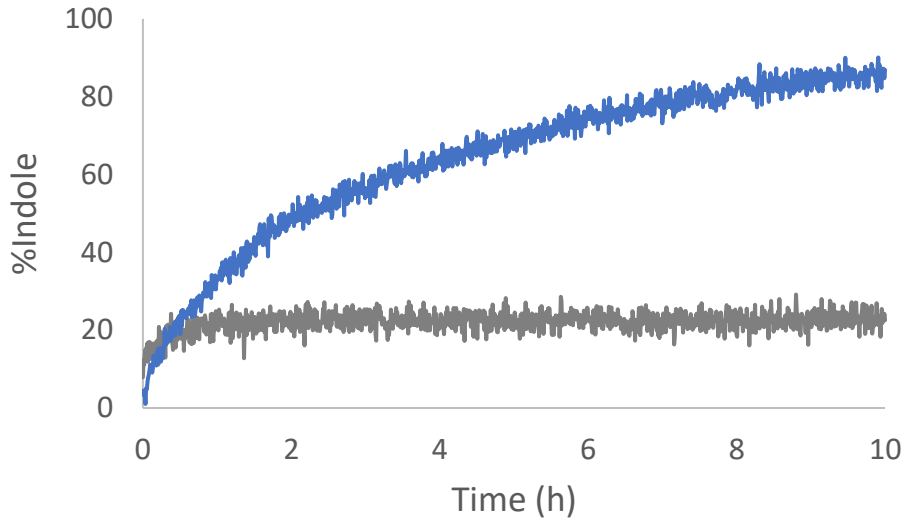

Figure 4.8. Plot of the conversion using 250 mM indoline (blue) using1 mol% **1a**, and 250 mM 68% deuterated **Ind-(N-*d*$_1$)** (grey) using1 mol% **1a**. Conversion values were corrected using GC-FID analysis of the reaction solution after 20 h of reaction time. Each data set was run in duplicate, and the overlap between both runs indicates that the results are replicable (Appendix A.21, A.30).

Two solutions of **Ind-(N-*d*$_1$)** were prepared, solution A was 68% deuterated, as determined by ^{1}H NMR spectroscopy, solution B was 20% deuterated. Solution C, which was composed of >99% protio indoline was also prepared to act as the control. Final

conversions for each solution were quantified by GC-FID. The conversion for solution A was 18% after 6 h, while the conversions for solution B and solution C were 47% and 68%, respectively (Figure 4.9). At zero percent deuteration, the reaction reached 68% in 6 h. Increasing the percent deuteration of the substrate up to 68% lead to a nearly 4-fold decrease in conversion. The presence of the deuterium atom has resulted in a large decrease in conversion. It was likely that the 18% conversion observed with solution A was due complete conversion of the 22% N-H indoline present in the sample.

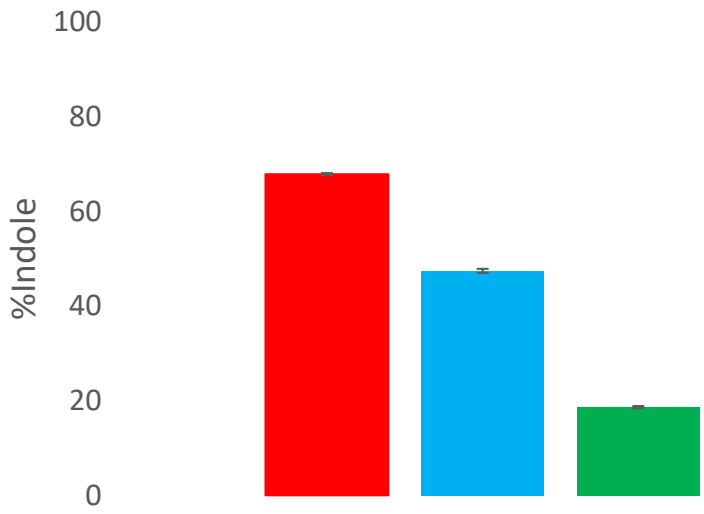

Figure 4.9. Bar graph showing the conversion of solution A (green), solution B (blue) and solution C (red) after 6 h under reaction conditions. Indoline substrate used were 68% deuterated (green), 20% deuterated (blue) and <1% deuterated (red), respectively. Average data between two runs shown, with both runs being within 5% error of each other.

To test the reactivity of indoline when deuterated at the C2 position, **Ind-(C2-*d*$_2$)** was heated to 110 °C in the presence of 1 mol% **1a** and the reaction was monitored by *in-situ* IR spectroscopy over a 20 h period (Scheme 4.10).

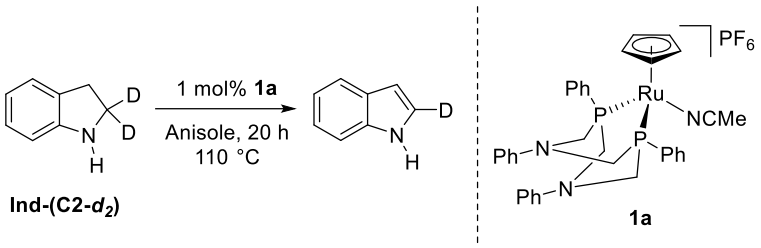

Scheme 4.9. Reaction scheme of **Ind-(C2-*d*$_2$)** with 1 mol% **1a**.

After 20 h, 18% conversion of **Ind-(C2-*d*$_2$)** was quantified by GC-FID. By comparison, a reaction with N-H indoline had a conversion of 97% under the same conditions. Therefore, deuteration at the Cα position resulted in a 79% decrease in substrate conversion. Over time, **Ind-(C2-*d*$_2$)** conversion steadily increases until 10 hours, after which conversion begins to plateau (Figure 4.10). The initial rates for N-H indoline and **Ind-(C2-*d*$_2$)** were determined within the first 40% catalysis (Appendix A.31). The rate was calculated using a linear regression within the 0-1.6 h timeframe for N-H indoline, and 0-10 h for **Ind-(C2-*d*$_2$)**. The rate for N-H indoline was calculated to be 57 mMh^{-1}. The rate for the Cα deuterated analogue **Ind-(C2-*d*$_2$)** was calculated to be 2 mMh^{-1}. The kinetic isotope effect is described as the ratio of the rate constant of the reaction with the protio substrate to the deuterated substrate. If $k_H/k_D > 1$, the deuterated substrate reacts slower than the protio.[123] A primary KIE falls between 1.5 and 10 and indicates the deuterated bond is cleaved in the rate-determining step. The KIE obtained is 29, which is out of the range for a typical primary KIE. A larger KIE value indicates that there could be quantum mechanical tunnelling involved.[124] The high KIE obtained using **Ind-(C2-*d*$_2$)** implies that the transfer step for the Cα hydrogen of the substrate to **1a** was very slow, resulting in a 29-fold decrease in catalyst rate.

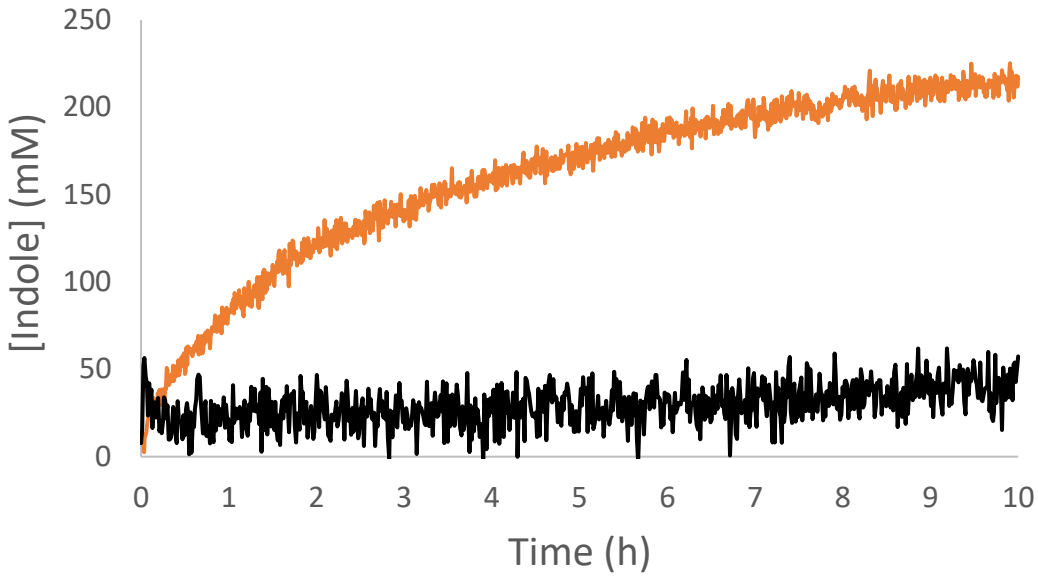

Figure 4.10. Reaction plots of the formation of indole using substrates N-H indoline (orange), **Ind-(C2-*d*$_2$)** (black). Conversion values were corrected using GC-FID analysis of the reaction solution after 20 h of reaction time. Each data set was run in duplicate, and the overlap between both runs indicates that the results are replicable (Appendix A.21, A.29).

Chapter 5: Conclusions and Future Work

5.1 Conclusions

Complexes **1a**, **1b**, **1c**, **3a**, and **4** were synthesized for AD of amines, with **3a** being a new complex. Complexes **1a-e**, **1a***, **3a**, and **3a*** were tested for the AD of benzylamine, and the product distributions of **ADC**, **DAD**, and **HB** were compared. In general, decreasing the basicity of the pendant amine resulted in an overall increase in product selectivity, favouring formation of dehydrogenation products. Conversely, increasing the basicity of the pendant amine resulted in a degradation of product selectivity, resulting in a near-equal distribution between dehydrogenation and hydrogenation products. Modification of the primary coordination sphere through the R groups had no change in product selectivity. Use of the Cp* ligand resulted in an increase in product selectivity, but at the cost of decreased catalyst activity. Complexes **3a** and **3a*** were tested for the AD of benzylamine as well, and both were completely selective for dehydrogenation products, with secondary aldimine **ADC** formed in >80% yield for both complexes. Similarly, changing the ligand from Cp to Cp* resulted in an overall decrease in conversion. While the conversion decreased by 20% using the iron analogue **3a**, the massive increase in selectivity obtained by the iron complexes was far superior to the ruthenium counterparts. Studies of **1a** on the AD of benzylamine in an open system resulted in no noticeable change in dehydrogenation to hydrogenation product formed, which indicated that the reactivity of intermediate **III** with **ADC** determined whether dehydrogenation or hydrogenation products are favoured. Indirect evidence by using the Fe analogue **3a**, as well as the *p*-CF_3Ph complex **1a*** indicated that dehydrogenation products are avoided, when hydricity, and the basicity of the pendant amine was decreased.

Acceptorless dehydrogenative coupling of benzylamine with aniline using **1a** was conducted and compared to **1d** to determine changes in product distribution using a less basic pendant amine. Using the Ph-substituted complex resulted in the formation of both dehydrogenation, and hydrogenation products, notably without any heterocoupled imine products formed. Testing **1a** for the AD of benzyl alcohol in the presence of aniline resulted in the formation of heterocoupled amine *N*-benzyl aniline as the major product, displaying

the first case of selectivity using **1a**, but substantially lower activity compared to benzylamine.

AD of indoline was monitored by *in-situ* IR spectroscopy for **1a** and **4**, which showed that the presence of the $P^{Ph}{}_2N^{Ph}{}_2$ ligand resulted in a 1.3-fold increase in catalytic turnover, resulting in higher conversion values over a 10 h period. Rate studies conducted suggested that the catalyst rate order for AD of indoline with **1a** was first order in catalyst and substrate concentration. Kinetic Isotope Effect studies were conducted, and a high KIE of 32 was calculated. Using either **Ind-(N-*d_1*)** and **Ind-(C2-*d_2*)** resulted in a large decrease in catalyst conversion with **1a**, which provides evidence for the concerted transfer of an equivalent of H_2 to the active catalyst in an outer sphere manner. The AD of N-Me indoline to form N-Me indole was conducted with **1a**, and it was confirmed that N-Me indoline was able to be dehydrogenated by **1a**, which provides evidence for an outer sphere dehydrogenation pathway.

Catalyst **3a** is the first example of a complex of the type $[M(Cp)(MeCN)(P^R{}_2N^{R'}{}_2)]PF_6$ that displays full selectivity for acceptorless dehydrogenation products **ADC** and **DAD**. In addition, **3a** is the first example of an iron catalyst capable of AD of primary amines that is selective for secondary aldimines without the use of an exogenous base.[78] The proposed catalytic mechanism for **3a** is cooperative outer sphere, supported by mechanistic studies conducted with **1a**, and the rate-determining step is hypothesized to be the primary dehydrogenation step, where a hydride and proton are transferred to the catalyst in a concerted manner. Complex **3a** is overall less selective than other established catalysts for this transformation, but further tuning of the ligand system/reaction conditions could increase **ADC** selectivity. Further study could result in the first example of an outer sphere, cooperative non-precious metal catalyst capable of selective acceptorless dehydrogenation of amines.

5.2 Future Work

Optimizations for the synthesis of **3a** are required, specifically the reaction of **2a** with $P^{Ph}{}_2N^{Ph}{}_2$ to form **3a** (Scheme 5.1). Reaction yields never exceeded 15%, and clean **2a** was only able to be isolated twice. Difficulties arose during the recrystallization step, which was the only way to generate clean **2a**. A method of forming clean crystals of **2a** will have to be determined if **3a**, or similar complexes are to be synthesized regularly.

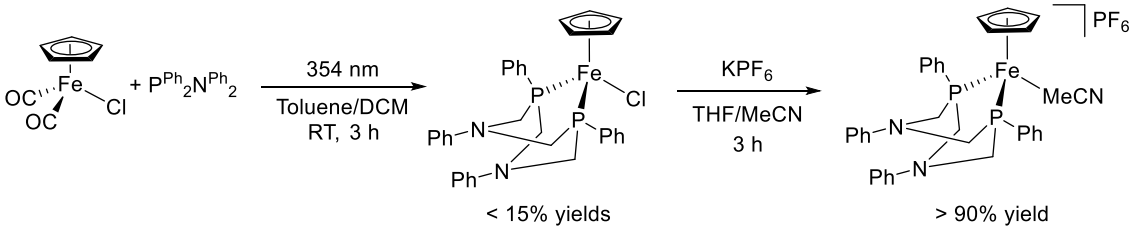

Scheme 5.1. Synthesis of **3a** starting from $Fe(Cl)(Cp)(CO)_2$ and $P^{Ph}{}_2N^{Ph}{}_2$.

Synthesis and assessment of complexes similar to **3a** is essential to developing a more selective catalyst, with high catalytic activity. The formation of dehydrogenation products **ADC** and **DAD** depends on the reactivity of the imine intermediate **Im** and the active catalyst (Scheme 5.2a). Once **3a** dehydrogenates benzylamine to form **Im**, it reacts with either **3a** to form **DAD**, or a molecule of benzylamine to forms **ADC**. Decreasing the reactivity of **3a** with **Im** is a potential approach to decreasing the amount of **DAD** formed. One insight gained in Chapter 3 was that using the *p*-CF_3Ph-substituted complex **1c** for the AD of benzylamine resulted in slightly higher selectivity for dehydrogenation product **ADC**, compared to the Ph-substituted complex **1a**. Additionally, **1c** gave 70% conversion with 3 mol% catalyst loading, which is only 6% lower than the highest performing catalyst, **1d**. Synthesizing the iron-analogue of **1c**, complex **3c**, and testing it for the AD of benzylamine may result in higher conversion, and increased **ADC** product selectivity compared to **3a**. (Scheme 5.2b).

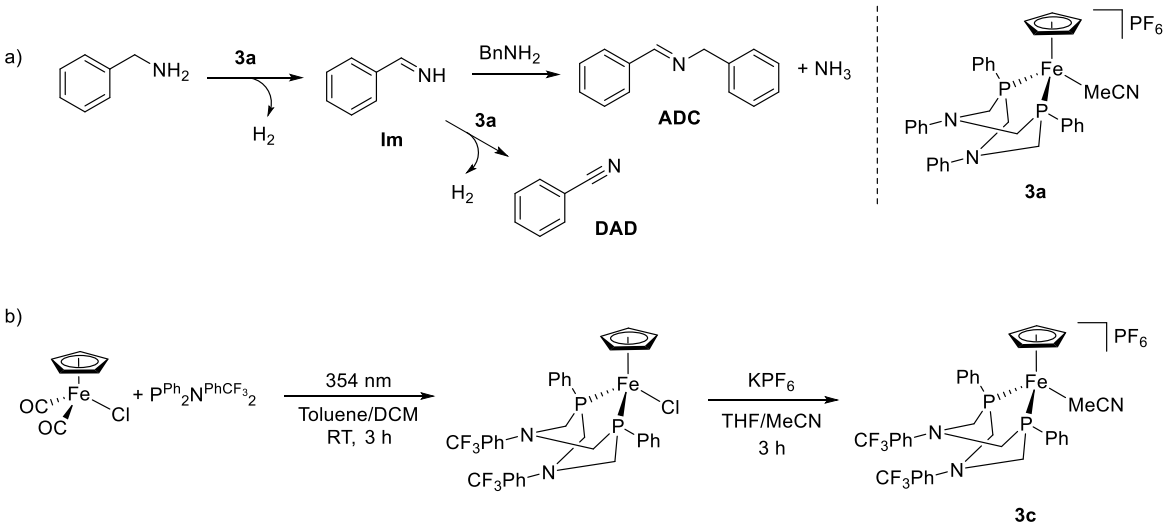

Scheme 5.2. a) Reaction of $BnNH_2$ with **3a** to form intermediate **Im**, which can then react to form product **ADC** or **DAD**. b) Synthesis of **3c** starting from $Fe(Cl)(Cp)(CO)_2$ and $P^{Ph}{}_2N^{PhCF3}{}_2$**.**

Expanding the substrate scope for **3a**, in particular, employing primary amines that are more nucleophilic than benzylamine may increase the AD selectivity of the iron complexes to favour the formation of the ADC product over DAD (Scheme 5.3). Controlling product selectivity by modifying the substrate to a more nucleophilic alkyl-substituted amine, such as *n*-propylamine,[117] could increase the rate of the condensation between the primary imine formed by the first dehydrogenation with **3a** and another molecule of substrate. This could result in complete ADC product selectivity, which would be the first example of a cooperative outer sphere iron catalyst selective for secondary aldimines.

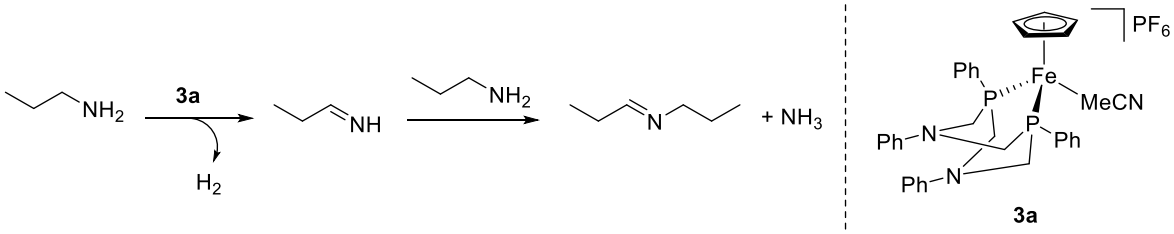

Scheme 5.3. Reaction of *n*-propylamine with **3a** to generate a secondary aldimine.

Further mechanistic insights would be gained by determining the relative hydricities of the M–H bond, where M = Fe/Ru (Scheme 5.4). Synthesis of ruthenium-hydride complex **5a**, and iron-hydride complex **6a**, and reacting each with [HDMF][OTF] in MeCN, will determine the relative hydricities of the M-H bond. Complex **5a** is hypothesized to have a more basic hydride and should react with an acid faster than **6a**. This will be quantified by the formation of **5a-IV** and **6a-IV**, determined by ^{1}H NMR spectroscopy. This would help rationalize why AD of benzylamine forms **HB** when **1a** is used, while no **HB** is formed with **3a**. If the formation of **HB** depends on the reactivity of intermediate **III** with **ADC**, then a less hydritic M-H bond could decrease the reactivity of **III** such that it does not react with **HB**. This would help confirm that the H_2 release pathway is preferred when **3a** is used.

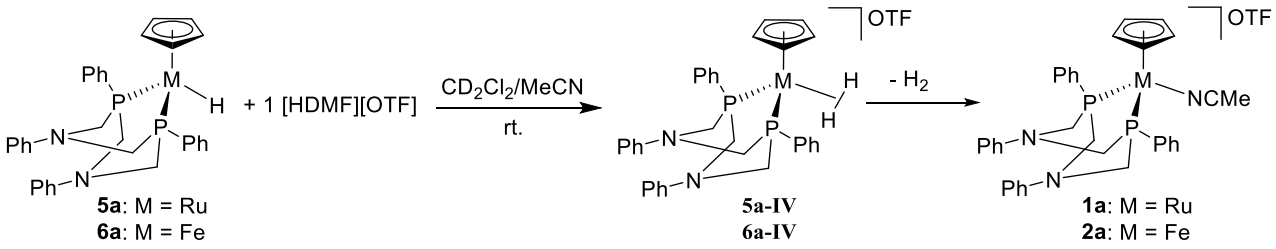

Scheme 5.4. Reaction of M-H complexes **5a**/**6a** with acid [HDMF][OTf] to generate **IV**. Release of H_2 in the presence of MeCN forms **1a**/**3a**.

Another study that should be conducted is confirming whether H_2 uptake is irreversible with **1a** and **3a**. Addition of H_2 to complexes **1a** and **3a** would generate **1a-IV** and **3a-IV** respectively (Scheme 5.5). If the H_2 complexes are not observed, it will help confirm that **HB** is observed with **1a** due to the increased reactivity of **III** with **ADC**, and not a result of reversible H_2 uptake by the catalyst. If the H_2 adducts are formed, then over time and with heating, intermediate **IV** should release the bound H_2, and the active catalyst will bind MeCN to re-form complex **1a** and **3a**. The ease at which H_2 is released, quantified by the reformation of the acetonitrile adducts could be used to explain the reactivity of **III**, and the preferences between H_2 release and **HB** formation pathways.

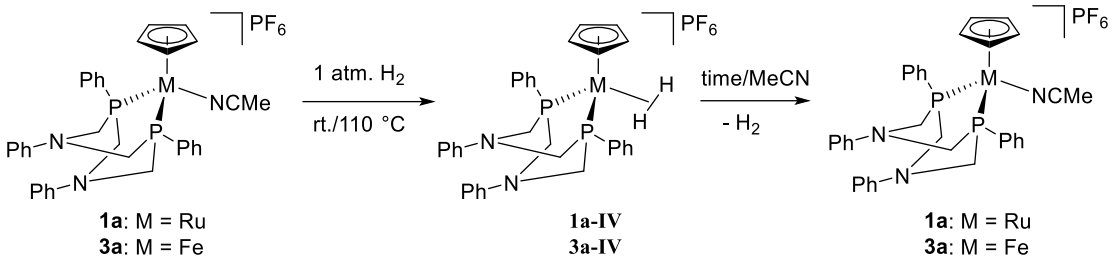

Scheme 5.5. Reaction scheme of **1a**/**3a** with 1 atm H_2 to form **IV**, which will release H_2 over time to reform **1a**/**3a**.

Chapter 6: Experimental Section

6.1 General Experimental Procedure

Unless otherwise stated, all reactions were conducted under an inert argon or nitrogen atmosphere following standard Schlenk or glovebox techniques, respectively. All NMR tubes and glassware were dried in an oven at 150–160 °C for at least 3 h and cooled under inert atmosphere or vacuum before use. All solvents were dried and degassed from an Innovative Technology 400-5 Solvent Purification system and stored over 4 Å molecular sieves for at least 24 h before use, unless otherwise stated. THF was dried with calcium hydride, distilled, and stored on 4 Å molecular sieves under inert atmosphere. Ethanol was stored over 3 Å sieves and degassed on a Schlenk line. All other reagents were purchased from commercial sources and used without any further purification. For experimental procedures, RT = 26°C, which is the temperature of the gloveboxes and lab. The ligand $P^{Ph}{}_2N^{Ph}{}_2$ was synthesized following a modified literature procedure that used a 37% w/w aqueous paraformaldehyde solution instead of solid paraformaldehyde,[109,111] and the $^{31}P\{^1H\}$ and ^1H NMR chemical shifts of the isolated compound matched the literature values.[109] $[Ru(Cp)(MeCN)_3]PF_6$ was synthesized following a literature procedure and ^1H NMR chemical shifts of the isolated compound matched the literature values.[107] $[Ru(Cp)(dppp)(MeCN)][PF_6]$ (**4**) was synthesized following a previously established procedure and the NMR values matched what was previously obtained.[106] The product was determined to be 92% pure by $^{31}P\{^1H\}$NMR spectroscopy, with a minor impurity at 42.1 ppm. Preliminary catalyst tests with indoline determined that the impurity did not have an effect on the performance of **4** and was used without further purification (93% yield). $[Ru(Cp)(P^{Cy}{}_2N^{Ph}{}_2)(MeCN)][PF_6]$ (**1e**) and $[Ru(Cp^*)(P^{Ph}{}_2N^{Ph}{}_2)(MeCN)][PF_6]$ (**1a***) were synthesized by group member Devon Chapple and each was >95% pure by $^{31}P\{^1H\}$ and ^1H NMR spectroscopy and the samples were used without further purification. Complex $[Fe(Cp^*)(P^{Ph}{}_2N^{Ph}{}_2)(MeCN)][PF_6]$ (**3a***) was synthesized by group member Benjamin Bridge, was >95% pure by $^{31}P\{^1H\}$ and ^1H NMR spectroscopy. The synthesis of $[Ru(Cp)(MeCN)_3]PF_6$ was performed following a literature procedure.[107,108] $FeCl(Cp)(CO)_2$ was synthesized following a literature procedure, and formation of product and purity was determined by IR spectroscopy (Appendix A.1-A.3), the values obtained

matched the literature.[113] *N*-Methyl indoline was prepared following a literature procedure, and ^{1}H NMR shifts matched the literature values.[125,126] **Ind-(C2-*d*$_2$)** was synthesized from indoline following literature procedures, and the ^{1}H and ^{2}H NMR values obtained for each intermediate matched the literature.[127] **Ind-(N-*d*$_1$)** was synthesized following a modified literature procedure.[128]

All NMR spectra were recorded on a Bruker 400 MHz spectrometer at 25 °C unless stated otherwise. ^{1}H NMR spectra were referenced internally to TMS (0 ppm) based on residual solvent signals. ^{13}C{^{1}H} NMR spectra were referenced internally to TMS (0 ppm) by solvent carbon signals: $CDCl_3$ (77.2 ppm). ^{31}P{^{1}H} NMR spectra were referenced externally in protio solvents and internally in deuterated solvents to 85% phosphoric acid (0 ppm). Assigned multiplicities are abbreviated as: singlet (s), doublet (d), triplet (t), quartet (q), and multiplet (m). Catalytic performance was measured using an Agilent 7890a gas chromatograph instrument with flame ionization detector (GC-FID), fitted with an HP-5 column. The amount of substrate and product for each catalytic experiment was quantified using area counts that were corrected with a response factor referenced to an internal standard. Catalytic studies monitored by in situ IR spectroscopy were conducted using a METTLER TOLEDO ReactIR 15, using a SiComp DST Series AgX Fiber Conduit probe. Conversion values were determined by analyzing the solution by GC-FID after 18-20 hours of reaction time. Absorbance values for the peak of interest was then corrected using the conversion values obtained by GC-FID and applied to all peak height values collected by the instrument to generate a plot of % product versus time. The UV light source used for the synthesis of $FeCl(Cp)(P^{Ph}{}_2N^{Ph}{}_2)$ (**2a**) was a medium-pressure Hg arc streetlamp.

6.2 Modified Synthesis of [Ru(Cp)($P^{Ph}_2N^{R'}_2$)(MeCN)][PF_6] Complexes, Where R′ = Ph, *p*-$OMeC_6H_4$, and *p*-$CF_3C_6H_4$

The synthesis of [Ru(Cp)($P^{Ph}_2N^{p\text{-}OMeC_6H_4}$)(MeCN)][$PF_6$] (**1b**) and [Ru(Cp)($P^{Ph}_2N^{p\text{-}CF_3C_6H_4}_2$)(MeCN)][$PF_6$] (**1c**) followed the method reported,[109] with modifications to the reaction solvent, temperature, and subsequent workup. The complete method used is provided here.

In the glovebox, [Ru(Cp)$(MeCN)_3$]PF_6 (60 mg, 0.138 mmol) was added to a 20 mL screw-cap vial with a stir bar. MeCN (4 mL) was added, followed by $P^{Ph}_2N^{R'}_2$ (66 mg, 0.146 mmol, 1.06 equiv). To the resulting orange suspension, DCM (8 mL) was added, which gave a total volume of 12 mL. The reaction was stirred for an additional 24 h, during which a clear yellow solution had formed. The solvent was removed under vacuum, which gave a yellow residue. The residue was re-dissolved in DCM (0.5 mL), and cold pentane (5 mL) was added to precipitate a yellow solid. The solvent was removed via decanting and the solid was washed with room-temperature pentane (3 × 5 mL) to yield a yellow powder, which was dried under vacuum. Yields: 66-89%, ^{1}H and ^{31}P{^{1}H} NMR spectroscopy values matched those obtained in the literature.[109]

6.3 Modified Synthesis of FeClCp)($P^{Ph}_2N^{Ph}_2$) (2a)

In the glovebox, FeCl(Cp)$(CO)_2$ (349 mg, 1.64 mmol, 1.05 equiv) was added to a 20 mL glass screw-cap vial containing toluene (6 mL) and a stir bar. To the cloudy red solution, $P^{Ph}_2N^{Ph}_2$ (648 mg, 1.56 mmol) was added, followed by DCM (6 mL). The solution was allowed to stir for 5 min, or until the solution became clear. Approximately 0.8 mL was taken up by pipette and transferred to an NMR tube. The NMR tube and 20 mL vial was then sealed and brought out of the box, where they were both fixed by a clamp one inch from a UV lamp (354 nm), which was then activated. The solution was not stirred. The solution slowly changed from clear red to clear and black over the course of the reaction. After the time required for complete disappearance of free $P^{Ph}_2N^{Ph}_2$ ligand as judged by ^{31}P{^{1}H} NMR spectroscopy (2.5-3.5 h), the vial and NMR tube were brought back into the glovebox. The NMR tube solution was recombined with the 20 mL vial. The solution was pumped to dryness, redissolved in diethyl ether, and passed through a

microfibre plug to remove insoluble solids. The black solution was pumped to dryness, and the black solids were dissolved in 10 mL DCM. To this, 8 mL of pentane was added, or until solids barely begin to form. The resulting solution was left for 2-3 days, or until black crystals began to form. These crystals were then collected, washed with pentane (3×5 mL) and the resulting solids were dried under vacuum. Yield 110 mg (12%). The $^{31}P\{^{1}H\}$ and ^{1}H NMR values matched literature values.[96]

6.4 Synthesis of [Fe(Cp)($P^{Ph}_2N^{Ph}_2$)(MeCN)]PF_6 (3a)

In the glovebox, FeCl(Cp)($P^{Ph}_2N^{Ph}_2$) (**2a**) (50 mg, 0.082 mmol) was dissolved in 3 mL THF in a 20 mL screw cap vial with a stir bar. A solution of KPF_6 (23 mg, 0.123 mmol) in MeCN (1.5 mL) was added to the stirring solution of **2a**. The vial that contained the KPF_6 solution was rinsed with 1.5 mL acetonitrile, which was also added to the solution of **2a**. The reaction was allowed to stir for 2 h, during which the colour changed from black to clear and red. The solution was pumped to dryness, and the residue was dissolved in 0.2 mL DCM. 5 mL of pentane was added, which reprecipitated bright red solids. The solvent was removed by pipette, and the solids were washed with pentane (2×5 mL) and diethyl ether (5 mL). The red solids were dried under vacuum yielding the final product. Yield: 60 mg (97%), red solid. ^{1}H (400 MHz, CD_2Cl_2) δ: 8.05-7.95 (m, Ph-*H*, 4 H), 7.77-7.63 (m, Ph-*H*, 6H), 7.37-7.21 (m, Ph-*H*, 4 H), 7.10-7.02 (m, Ph-*H*, 2 H), 7.00-6.90 (m, Ph-*H*, 4 H), 4.39 (s, Cp-*H*, 5 H), 4.30-4.23 (m, P-*CH*$_2$-N, 2H), 4.18-4.12 (m, P-*CH*$_2$-N, 2H), 3.89-3.79 (m, P-*CH*$_2$-N, 2H), 3.35-3.21 (m, P-*CH*$_2$-N, 2H), 2.32 (s, NC-C*H*$_3$, 3H). $^{13}C\{^{1}H\}$ (101 MHz, CD_2Cl_2) δ: 151.8 (t, $^{3}J_{C\text{-}P}$ = 7.5 Hz, C^{Ar}-N), 151.7 (t, $^{3}J_{C\text{-}P}$ = 8.6 Hz, C^{Ar}-N), 134.5 (s, Fe-N*C*CH$_3$), 133.7 (ABX, P-C^{Ar}), 131.6 (s, C^{Ar}), 131.2 (s, C^{Ar}), 129.8 (s, C^{Ar}), 129.7 (s, C^{Ar}), 129.6 (s, C^{Ar}), 122.1 (s, C^{Ar}), 121.7 (s, C^{Ar}), 118.1 (s, C^{Ar}), 117.7 (s, C^{Ar}), 79.6 (s, C_5-(H)$_5$), 51.8 (ABX, P-*C*H$_2$-N), 50.5 (ABX, P-*C*H$_2$-N), 5.0 (s, Fe-NC*C*H$_3$). $^{31}P\{^{1}H\}$ (162 MHz, CD_2Cl_2) δ: 57.8 (s, *P*-Ph), –144.4 (sept, $^{1}J_{P\text{-}F}$ = 710.8 Hz, *P*F$_6$). MALDI MS (pyrene matrix): Calc. *m/z* 575.2 [Fe(Cp)($P^{Ph}_2N^{Ph}_2$)]$^+$, Obs. *m/z* 575.1. ATR-FTIR (cm^{-1}) 1596 (C=C, phenyl ring), 1264 (C-N stretch).

6.5 Modified Synthesis of Ind-(N-d_1)

The following synthesis was performed by modifying a previous literature procedure.[128] A 20 mL screw-cap vial was charged with indoline (0.988g, 8.39 mmol), deuterium oxide (10 mL 555 mmol, 66 equiv), and a stir bar, and the reaction was stirred for 3 days. DCM (5 mL) was then added, and the reaction was extracted with DCM (3×5 mL). The combined DCM layers were dried with $MgSO_4$, and the solids were removed by gravity filtration. Removal of the solvent via rotary evaporation yields N-D indoline as a grey oil. Yield: 0.975 g, 97%. The solution was determined to be 58% deuterated by ^1H NMR spectroscopy, and deuteration was confirmed by the appearance of a signal at 3.73 ppm in the ^2H NMR spectrum, as well as the ^1H NMR spectrum matched the literature values.[127]

6.6 Representative Procedure for the Catalytic AD/ADC of Indoline/Benzylamine using [Ru] Complexes, with Quantification by GC-FID

In the glovebox, the following two stock solutions were prepared in anisole: 1) internal standard tetrahydronaphthalene (200 mM) with substrate benzylamine, benzyl alcohol or indoline (500 mM); and 2) **1a/1a*/1b/1c/1e** (15 mM). Two 4 mL screw-cap vials containing stir bars were charged with 250 μL of tetrahydronaphthalene/substrate solution, and 250 μL of catalyst solution giving a final volume of 500 μL. The concentration in each vial was: 250 mM substrate, 100 mM tetrahydronaphthalene and 7.5 mM **1a/1a*/1b/1c/1e** (3 mol%). A final vial, that was used as the time = 0 sample, which was charged with 250 μL of the tetrahydronaphthalene/substrate solution, and 250 μL of anisole. The reaction vials were then capped and removed from the glovebox, sealed with tape, and heated to 110 °C in an aluminum heating block with stirring. After the solution was heated for the required time, the vials were removed from the heat, cooled, and exposed to air to quench the catalyst. An aliquot (20 μL) from each vial (including the time = 0 vial) was diluted to 5 mM by adding acetonitrile (980 μL) and the solutions were analyzed by calibrated GC-FID.

6.7 Representative Procedure for the Catalytic AD of Benzylamine/Benzyl Alcohol with Aniline Using [Ru] Complexes, with Quantification by GC-FID

In the glovebox, the following two stock solutions were prepared in anisole: 1) internal standard tetrahydronaphthalene (200 mM) and benzyl alcohol/benzylamine (500 mM) and aniline (500 mM); and 2) **1a** (15 mM). Two 4 mL screw-cap vials containing stir bars were charged with 250 μL of tetrahydronaphthalene/substrate/aniline solution, and 250 μL of the solution containing **1a** giving a final volume of 500 μL. The concentration in each vial was: 250 mM substrate, 250 mM aniline, 100 mM tetrahydronaphthalene and 7.5 mM **1a** (3 mol%). A final vial, that was used as the time = 0 sample, which was charged with 250 μL of the tetrahydronaphthalene/substrate/aniline solution, and 250 μL of anisole. The reaction vials were then capped and removed from the glovebox, sealed with tape, and heated to 110 °C in an aluminum heating block with stirring. After the solution was heated for the required time, the vials were removed from the heat, cooled, and exposed to air to quench the catalyst. An aliquot (20 μL) from vial (including the time = 0 vial) was diluted to 5 mM by adding acetonitrile (980 μL) and the solutions were analyzed by calibrated GC-FID.

6.8 Representative Procedure for the Catalytic AD of Benzylamine in an Open System Using [Ru] Complexes, with Quantification by GC-FID

In the glovebox, the following two stock solutions were prepared in anisole: 1) internal standard tetrahydronaphthalene (200 mM) and benzylamine (500 mM), and 2) **1a** (15 mM). Two 250 mL three-neck Schlenk flasks containing stir bars were charged with 1.5 mL of the benzylamine/tetrahydronaphthalene solution, and 1.5 mL of catalyst giving a final volume of 3 mL. The concentration in each flask was: 250 mM substrate,100 mM tetrahydronaphthalene and 7.5 mM **1a** (3 mol%). A 4 mL screw-cap vial was used as the time = 0 sample, which was charged with 250 μL of the tetrahydronaphthalene/benzylamine solution, and 250 μL of anisole. The Schlenk flasks were brought out of the box and connected to the Schlenk line and were equipped with reflux condensers and heated to 110 °C in an oil bath with stirring. After the solution was heated for the required time, the flasks were removed from the heat, cooled, and exposed to air to quench the catalyst. An aliquot (20 μL) from each flask (and the time = 0 vial) was

diluted to 5 mM by adding acetonitrile (980 μL) and the solutions were analyzed by calibrated GC-FID.

6.9 Representative Procedure for the Catalytic Acceptorless Dehydrogenation of Benzylamine Using [Fe] Complexes, with Quantification by GC-FID

In the glovebox, the following two stock solutions was prepared: 1) tetrahydronaphthalene (100 mM) and substrate (250 mM) in anisole; and 2) **3a** (12.50 mM) in DCM. From the stock solution of **3a**, 0.5 mL was transferred to each of two 4 mL screw-cap vials containing stir bars, and the DCM was removed via reduced pressure until dryness. The two vials were charged with 500 μL of tetrahydronaphthalene/substrate solution giving a final volume of 500 μL. The concentration in each vial was: 250 mM substrate, 100 mM tetrahydronaphthalene and 12.5 mM catalyst (5 mol%). A final vial, that was used as the time = 0 sample, was charged with 500 μL of the tetrahydronaphthalene and substrate solution. The reaction vials were then capped and removed from the glovebox, sealed with tape, and heated to 110 °C with stirring. After the solution was heated for the required time, the vials were removed from heat, cooled, and exposed to air to quench the catalyst. A 20 μL aliquot from each vial (including the time = 0 vial) was diluted to 5 mM by adding 980 μL acetonitrile and the solutions were analyzed by calibrated GC-FID.

6.10 Representative Procedure for the Catalytic AD of Indoline/Indoline-d_2/*N*-d-indoline Monitored by *In Situ* IR Spectroscopy

In the glovebox the following two stock solutions were prepared in anisole: 1) indoline (500 mM) and tetrahydronaphthalene (200 mM); and 2) **1a** (5 mM). To 250 mL three-neck round-bottom flask with stir bar, was added 1.5 mL of the indoline/tetrahydronaphthalene stock solution. To a 25 mL round-bottom flask, 2 mL of the **1a** stock solution was added. Both round-bottoms were then sealed with rubber septa. To a separate 4 mL screw-cap vial was added 0.5 mL of the indoline/tetrahydronaphthalene stock solution and 0.5 mL of anisole, to act as the time = 0 sample. The 250 mL three-neck flask was removed from the glovebox and affixed above an oil bath. The oil bath was then heated to 110 °C. To the three-neck round-bottom, a reflux condenser was equipped to the

middle neck, the ReactIR SiComp probe was inserted into a side-neck of the reaction flask, and the final neck was sealed with a septum. A portion of the catalyst stock solution (1.5 mL) was added to the now stirring solution by syringe through the septum on the third neck, bringing the volume of the reaction to 3 mL. The final concentrations in the solution was 250 mM substrate, 100 mM tetrahydronaphthalene and 2.5 mL **1a** (1 mol%). The reaction flask was placed into the oil bath which was now 110 °C, and the ReactIR experiment was initiated. Data acquisition was 1 scan every 30 seconds, for 20 h. Peak height increase of a diagnostic peak for the product at 1354 cm^{-1} was monitored over this time period. After the reaction time had elapsed, a 20 μL aliquot of the reaction and separately of the time = 0 vial were both diluted to 5 mM by adding 980 μL acetonitrile and the solutions were analyzed by calibrated GC-FID. This allowed the amount of indole after 20 h to be quantified. This was then used to determine the exact amount of indole that one peak height unit corresponded to in the IR experiment, which was then applied to all other peak height values obtained by the instrument to obtain a plot of %indole produced as a function of time.

Appendices

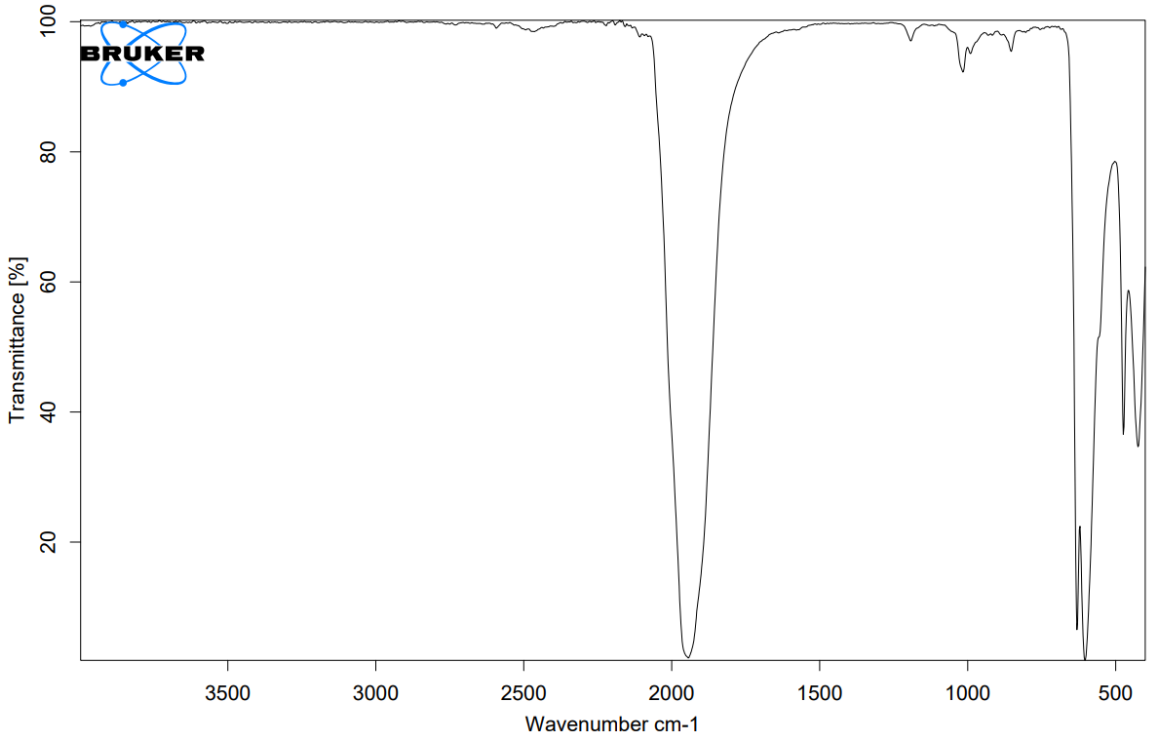

Appendix A.1. ATR-FTIR spectrum of $FeCO_5$ in DCM.

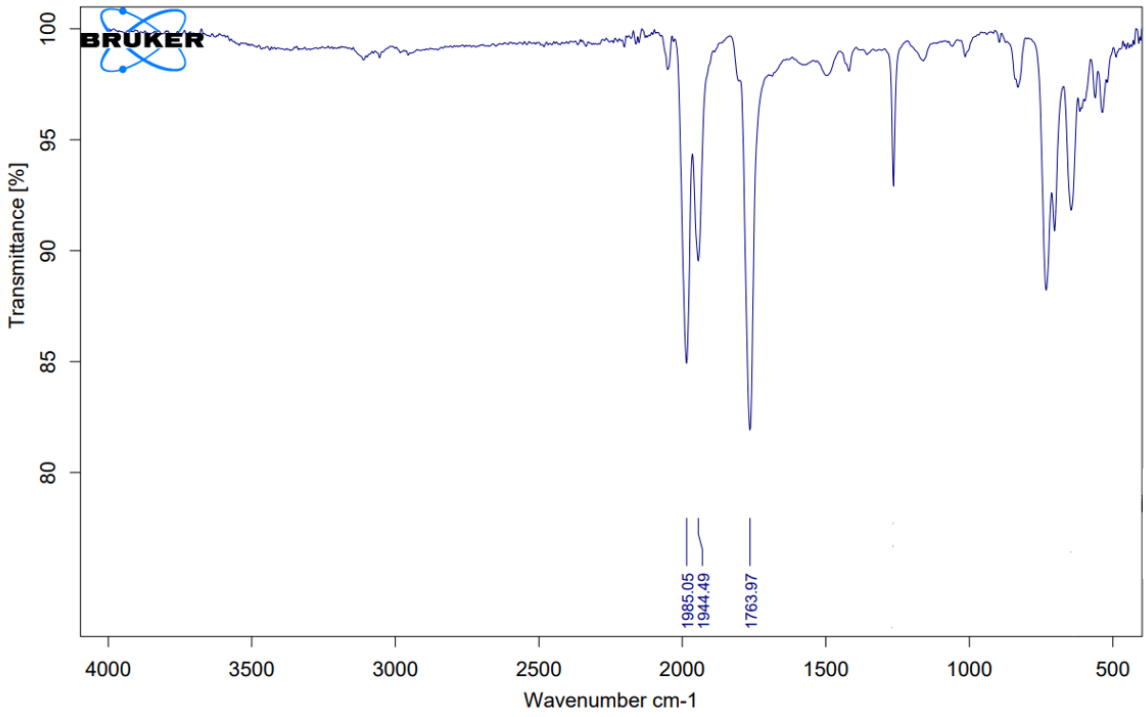

Appendix A.2. ATR-FTIR spectrum of $Fe(Cp)_2(CO)_4$ in DCM. $\nu_{CO}(cm^{-1})$ = 1985, 1995, 1764.[113]

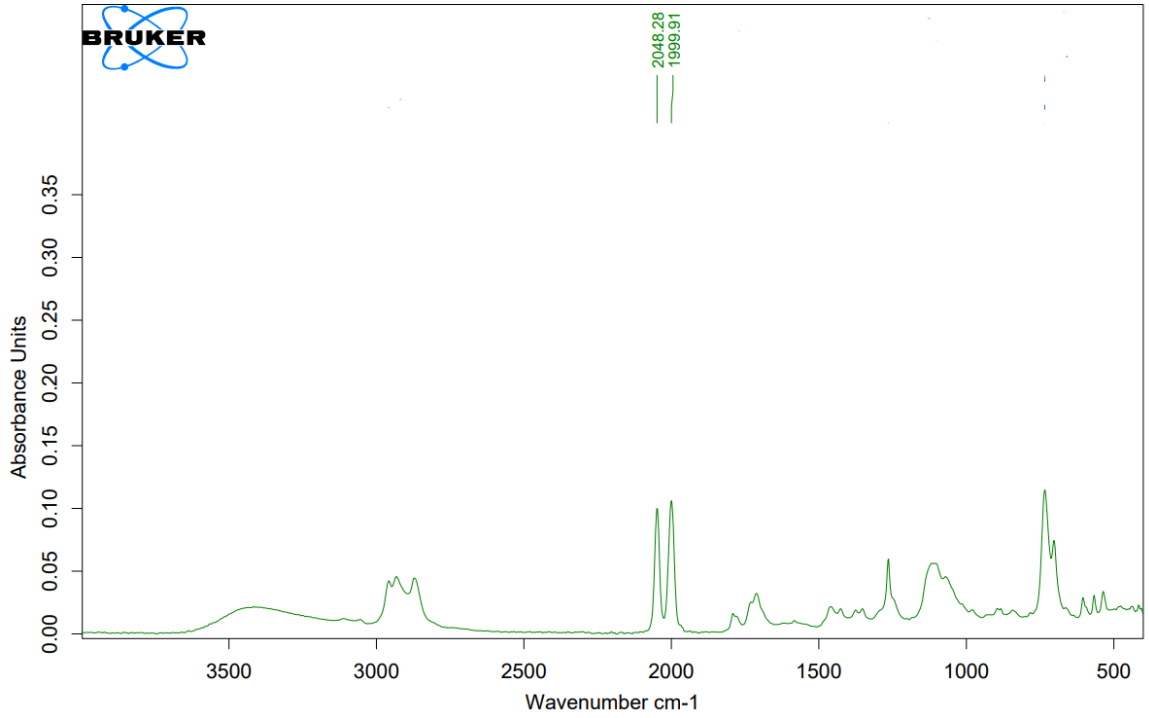

Appendix A.3. ATR-FTIR spectrum of $FeCl(Cp)(CO)_2$ in DCM. $\nu_{CO}(cm^{-1})$ = 2048, 1999.[113]

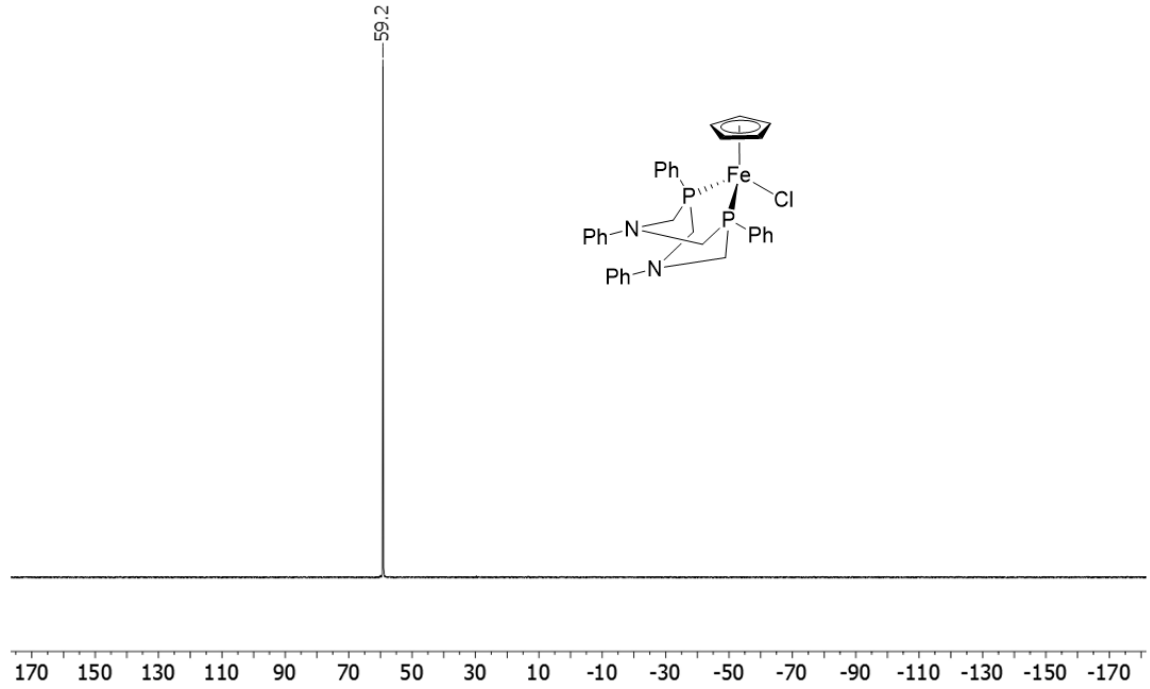

Appendix A.4. $^{31}P\{^1H\}$ NMR spectrum of **2a** (162 MHz, CD_2Cl_2).

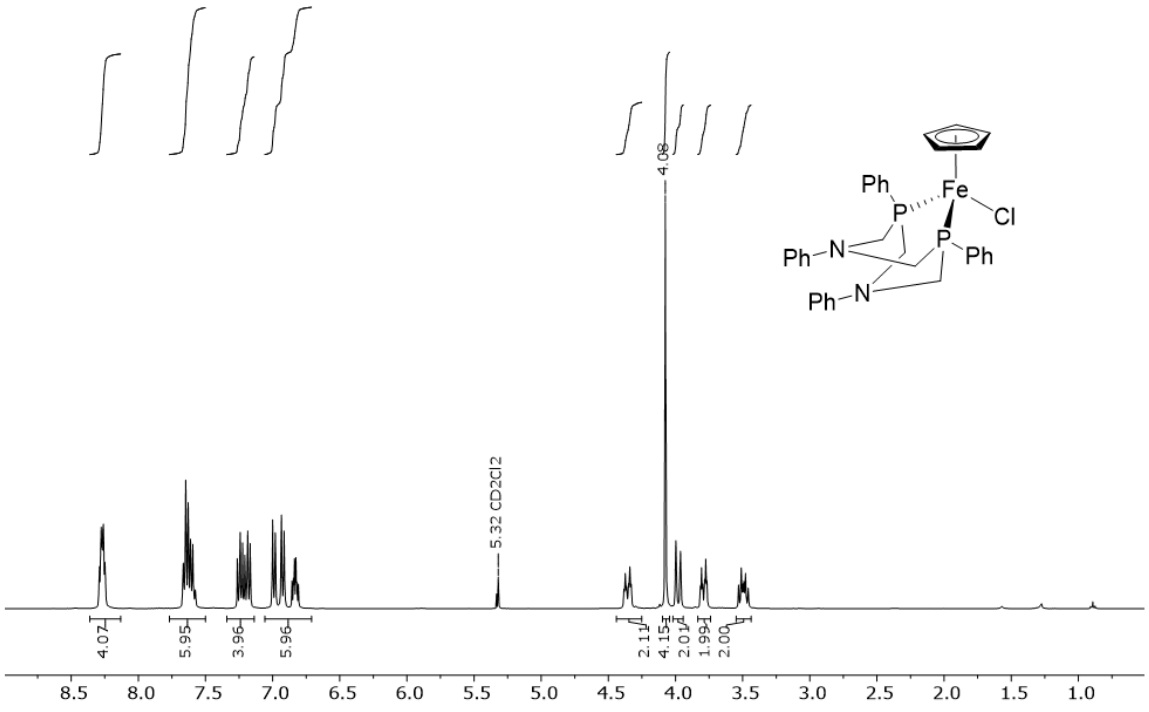

Appendix A.5. ^{1}H NMR spectrum of **2a** (400 MHz, CD_2Cl_2).

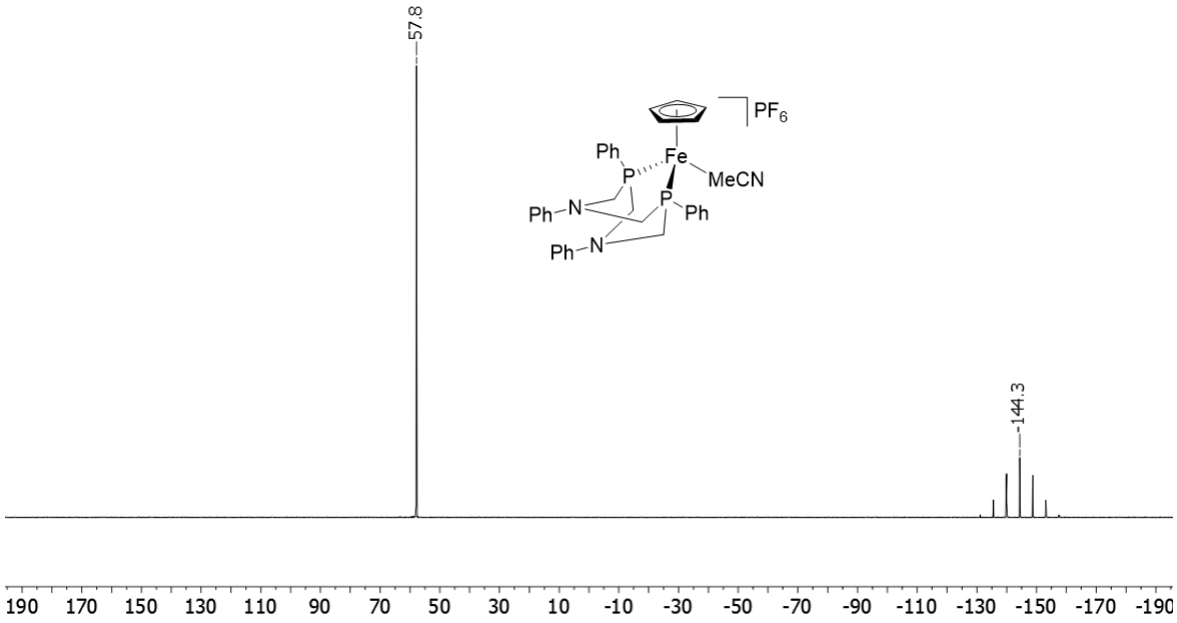

Appendix A.6. $^{31}P\{^{1}H\}$ NMR spectrum of **3a** (162 MHz, CD_2Cl_2).

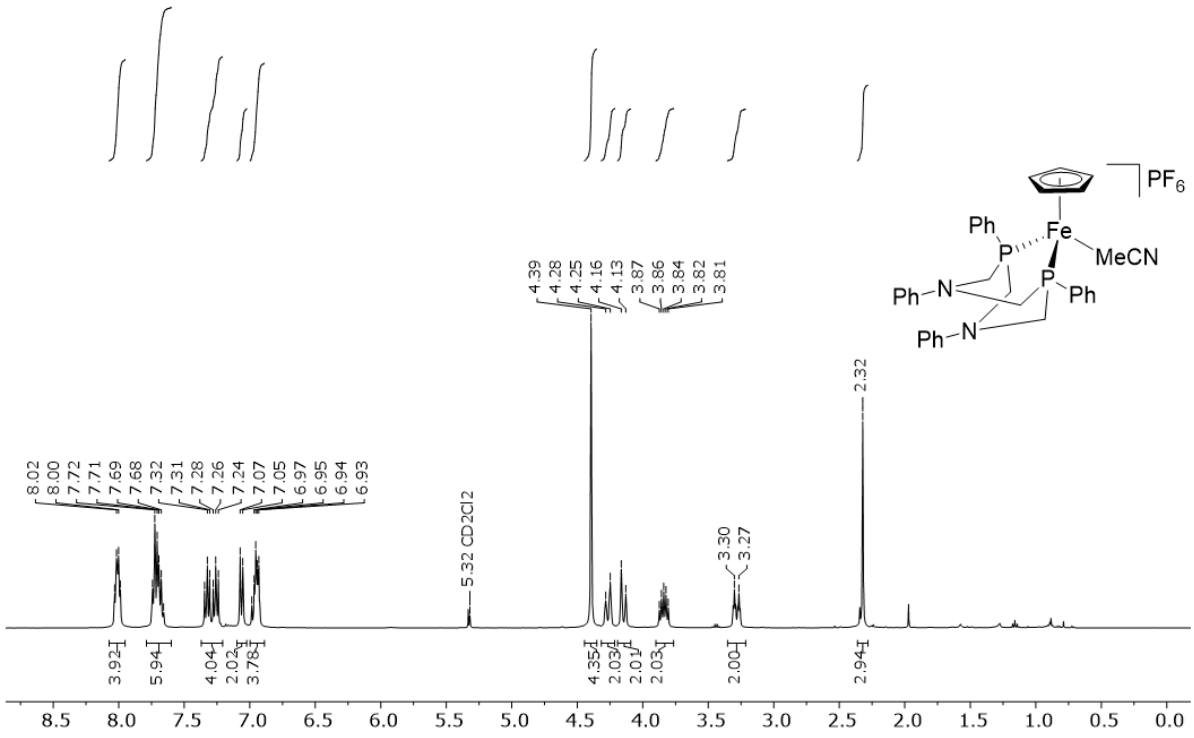

Appendix A.7. ^{1}H NMR spectrum of **3a** (400 MHz, CD_2Cl_2).

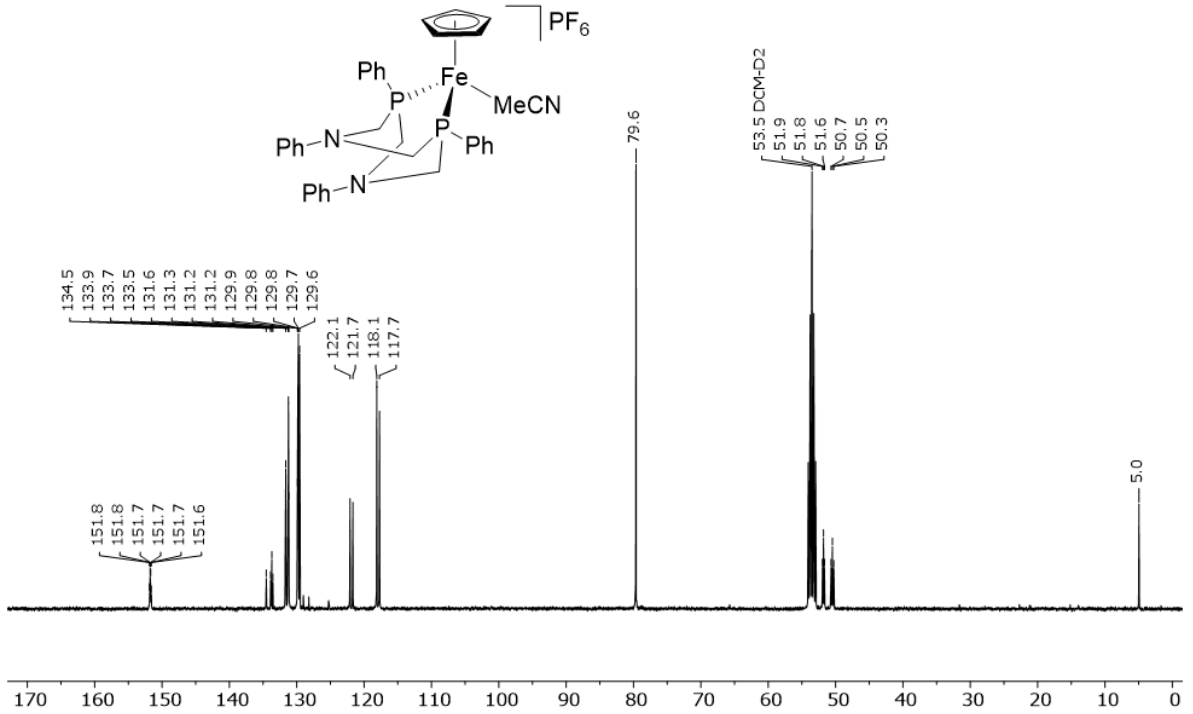

Appendix A.8 $^{13}C\{^{1}H\}$ NMR spectrum of **3a** (101 MHz, CD_2Cl_2).

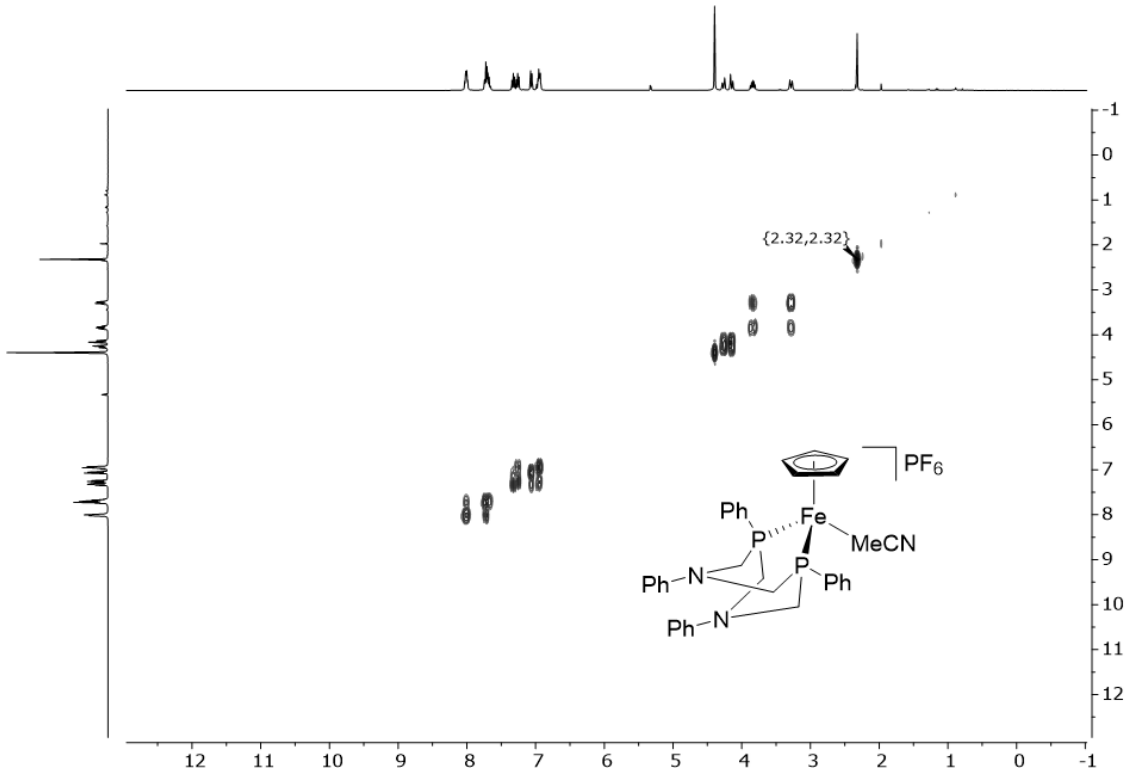

Appendix A.9. ^{1}H-^{1}H COSY spectrum of **3a** (400 MHz, CD_2Cl_2).

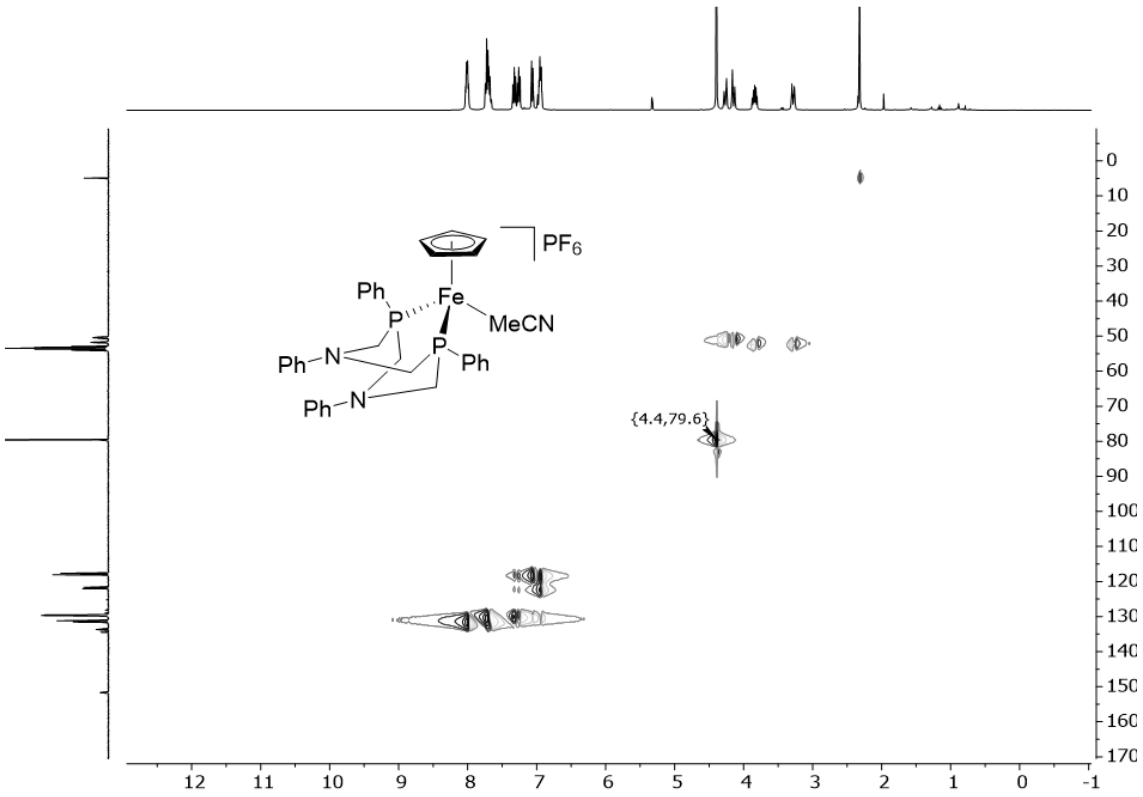

Appendix A.10. ^{1}H-^{13}C HSQC spectrum of **3a** (400 MHz, CD_2Cl_2).

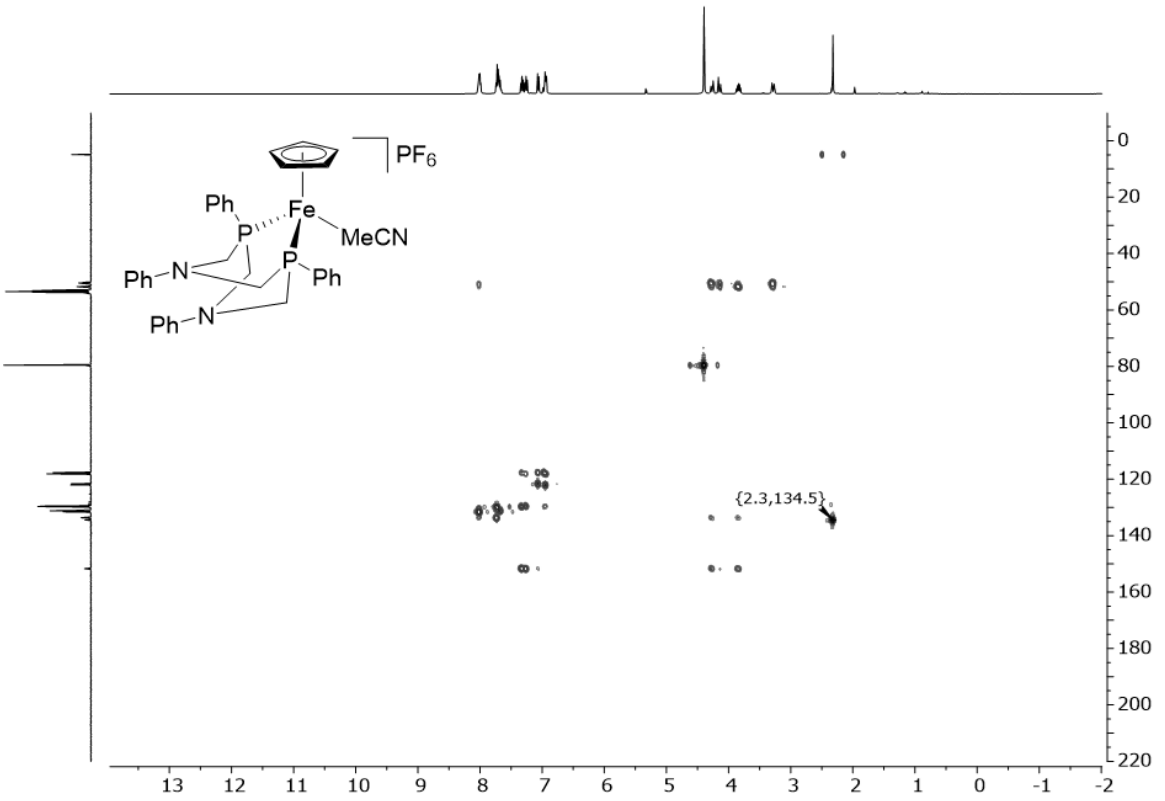

Appendix A.11. ^{1}H-^{13}C HMBC spectrum of **3a** (400 MHz, CD_2Cl_2).

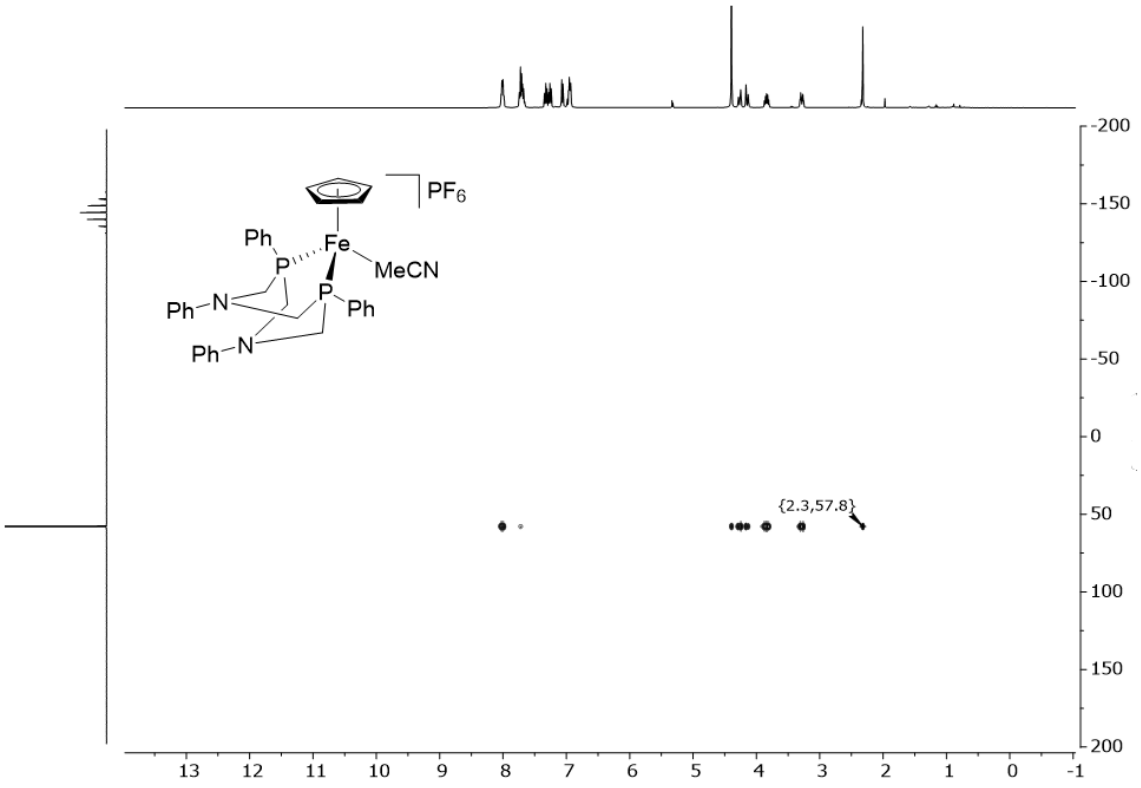

Appendix A.12. ^{1}H-^{31}P HMBC spectrum of **3a** (400 MHz, CD_2Cl_2).

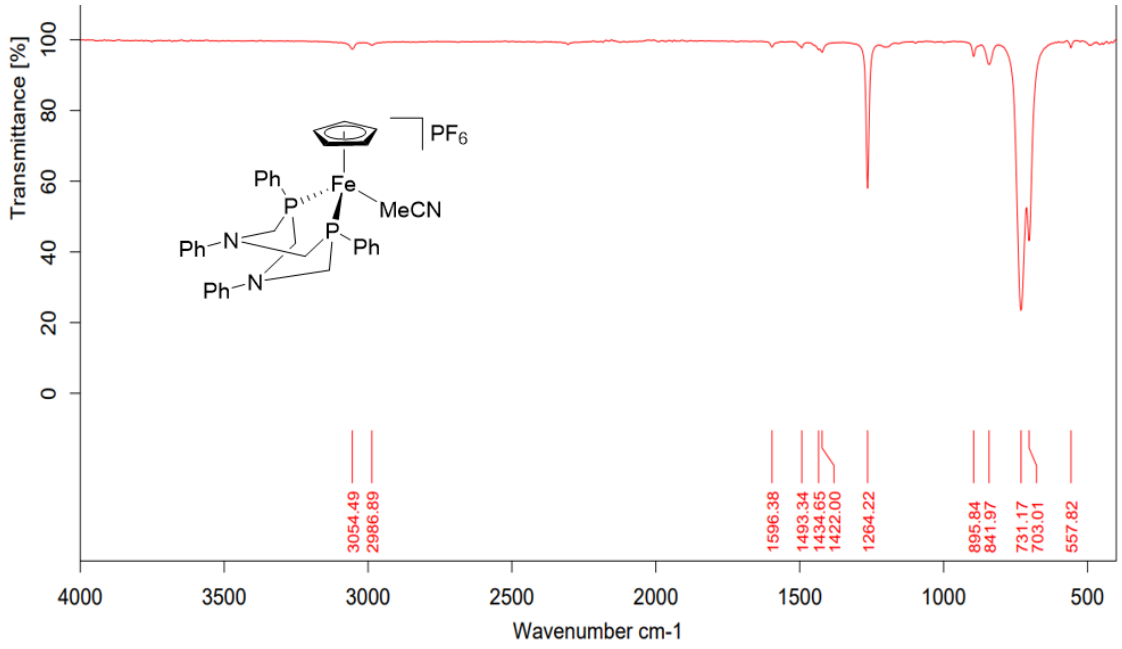

Appendix A.13. ATR-FTIR spectrum of **3a** in DCM.

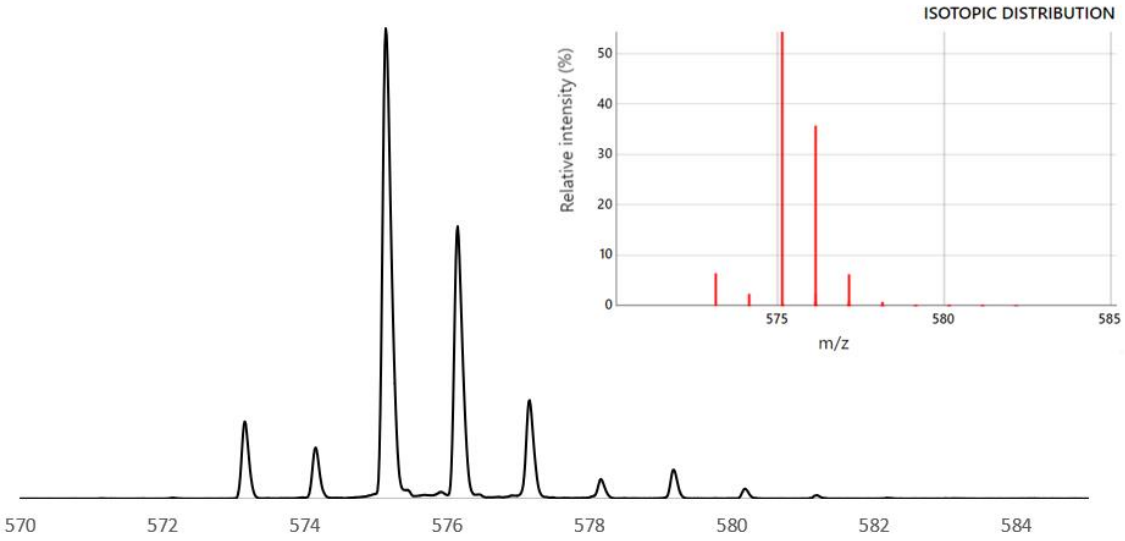

Appendix A.14. MALDI-MS data for complex **3a**, collected using a pyrene matrix. The top right picture shows the predicted isotope patterns,[129] while the bottom spectrum is the observed patterns. The isotope pattern corresponds to [**3a**-MeCN-PF_6]$^+$ (*m/z* = 575.1).

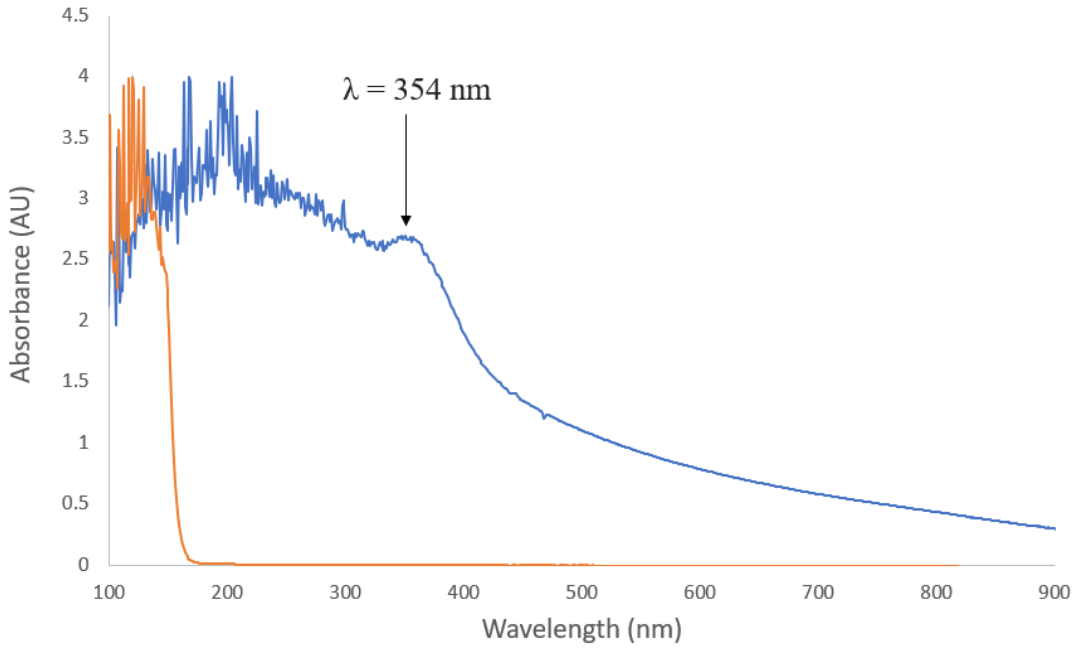

Appendix A.15. UV-vis spectrum of **2a** (blue) and $P^{Ph}{}_2N^{Ph}{}_2$ (orange) in DCM/Toluene.

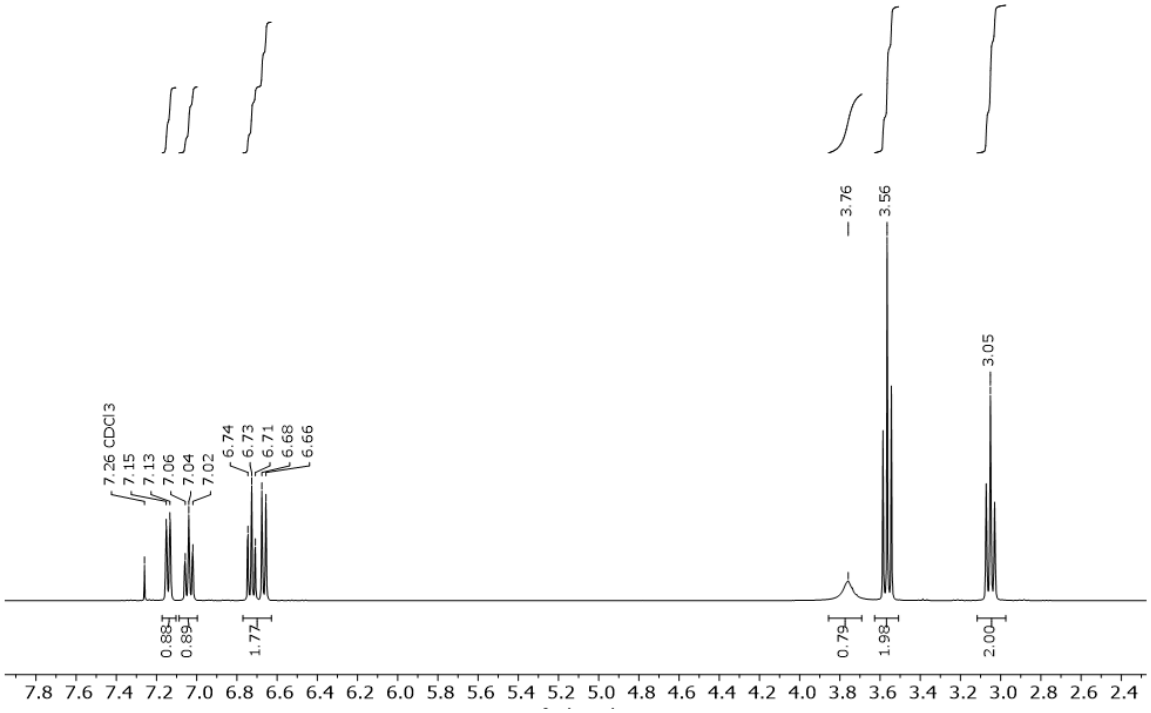

Appendix A.16. ^{1}H NMR spectrum of indoline (400 MHz, $CDCl_3$).

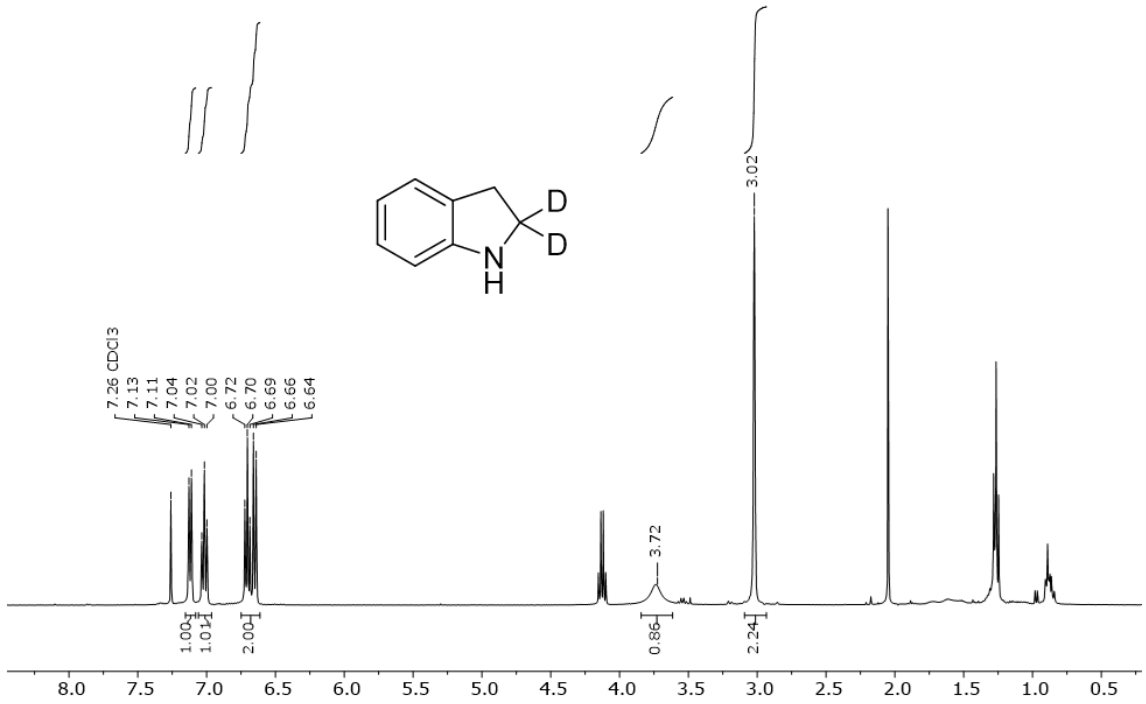

Appendix A.17. ^{1}H NMR spectrum of indoline-(C2-d_2) (400 MHz, $CDCl_3$). Substrate was dried over reduced pressure for 3 days prior to catalytic studies.

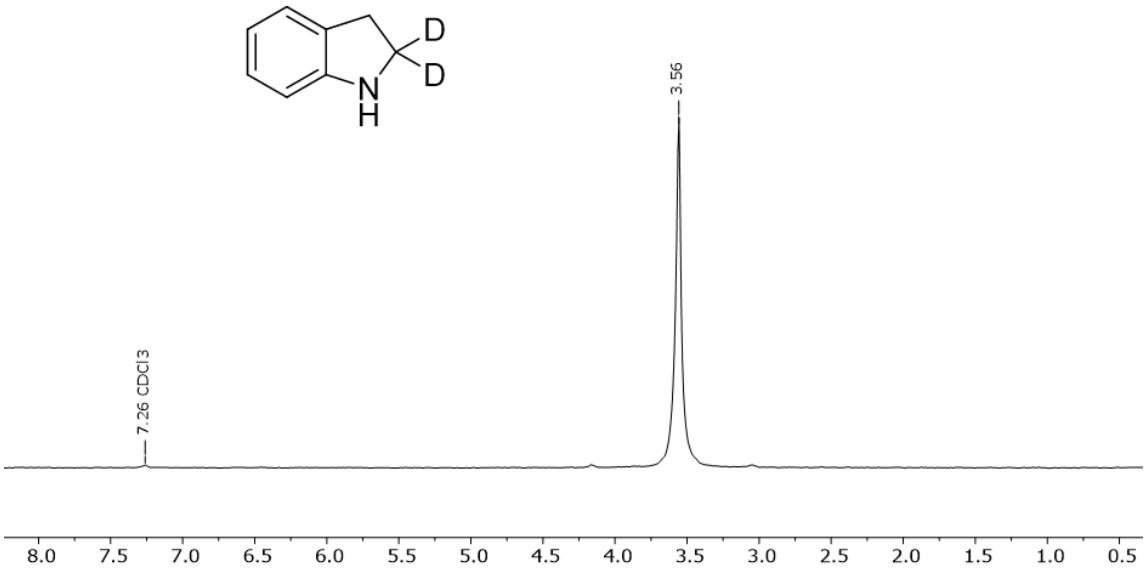

Appendix A.18. ^{2}H NMR spectrum of indoline-(C2-d_2) (400 MHz, $CDCl_3$).

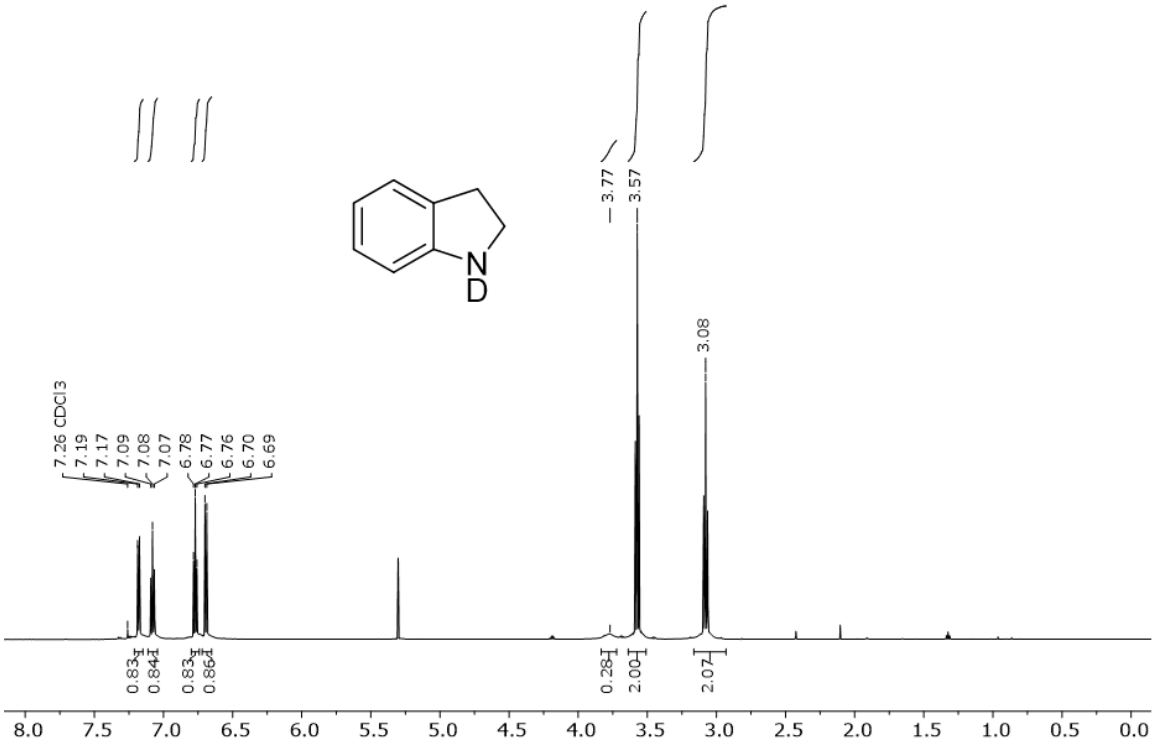

Appendix A.19. ^{1}H NMR spectrum of indoline-(N-d_1) (400 MHz, $CDCl_3$). Substrate was dried over reduced pressure for 3 days prior to catalytic studies.

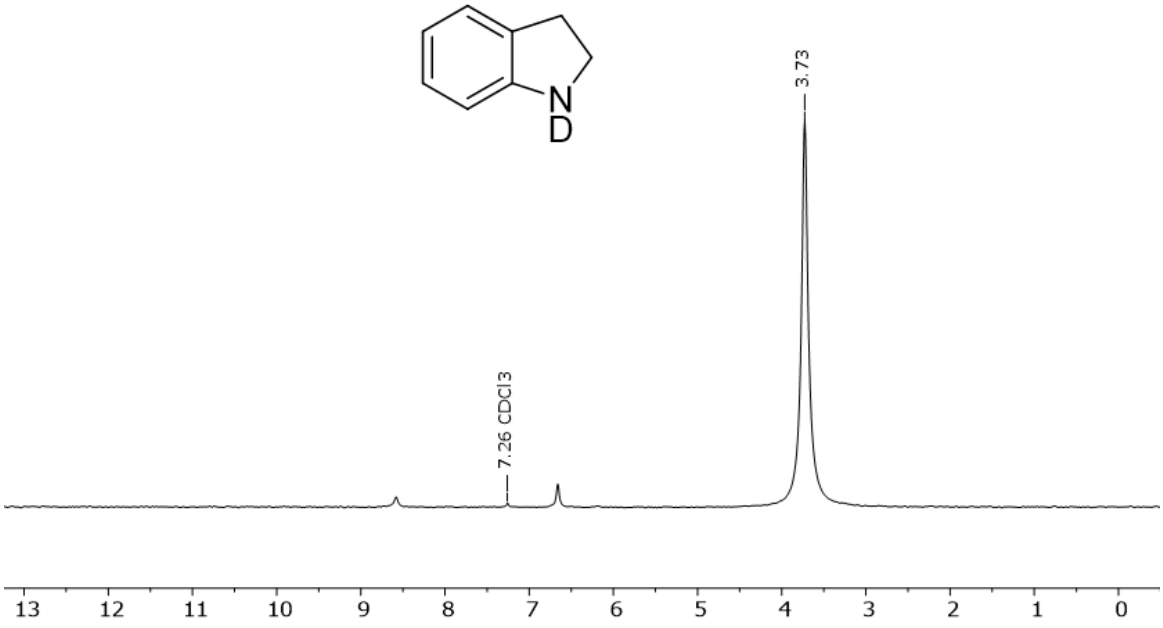

Appendix A.20. ^{2}H NMR spectrum of indoline-(N-d_1) (400 MHz, $CDCl_3$).

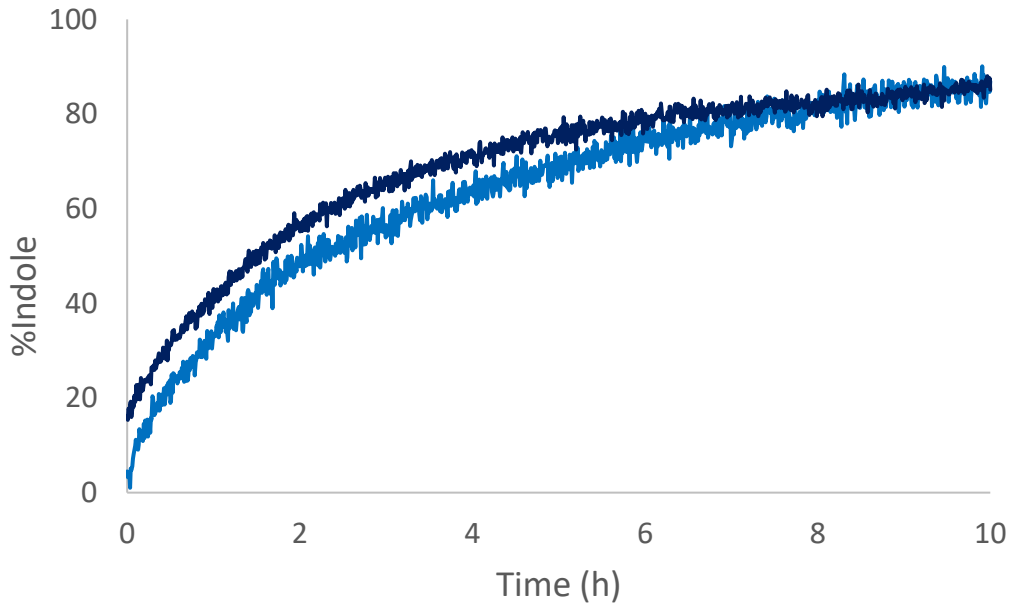

Appendix A.21. Percentage of indole formed over time using 250 mM indoline and 2.5 mM **1a** (1 mol%), monitored by *in-situ* IR spectroscopy. Reaction conditions: 110 °C, in anisole. Experiment was run in duplicate, and the overlap between the two runs indicate that the reaction is replicable.

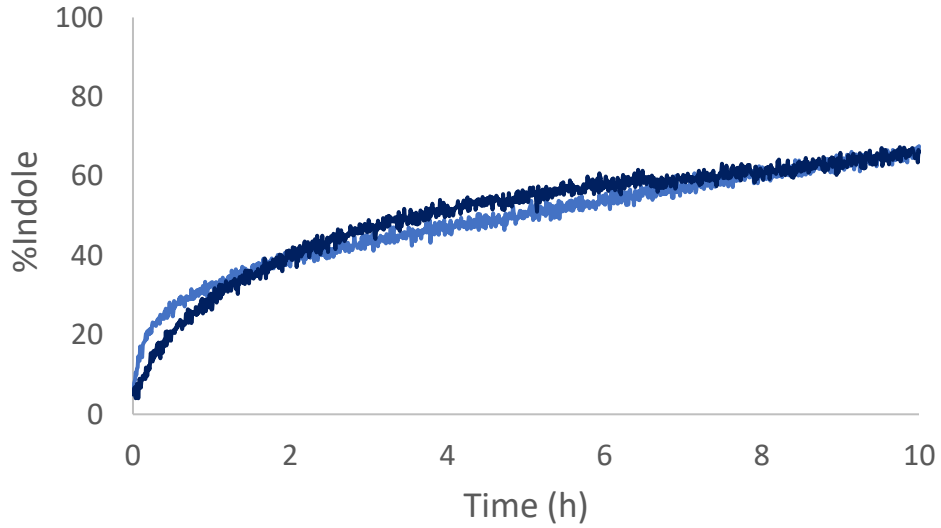

Appendix A.22. Percentage of indole formed over time using 250 mM indoline and 2.5 mM **4** (1 mol%), monitored by *in-situ* IR spectroscopy. Reaction conditions: 110 °C, in anisole. Experiment was run in duplicate, and the overlap between the two runs indicate that the reaction is replicable.

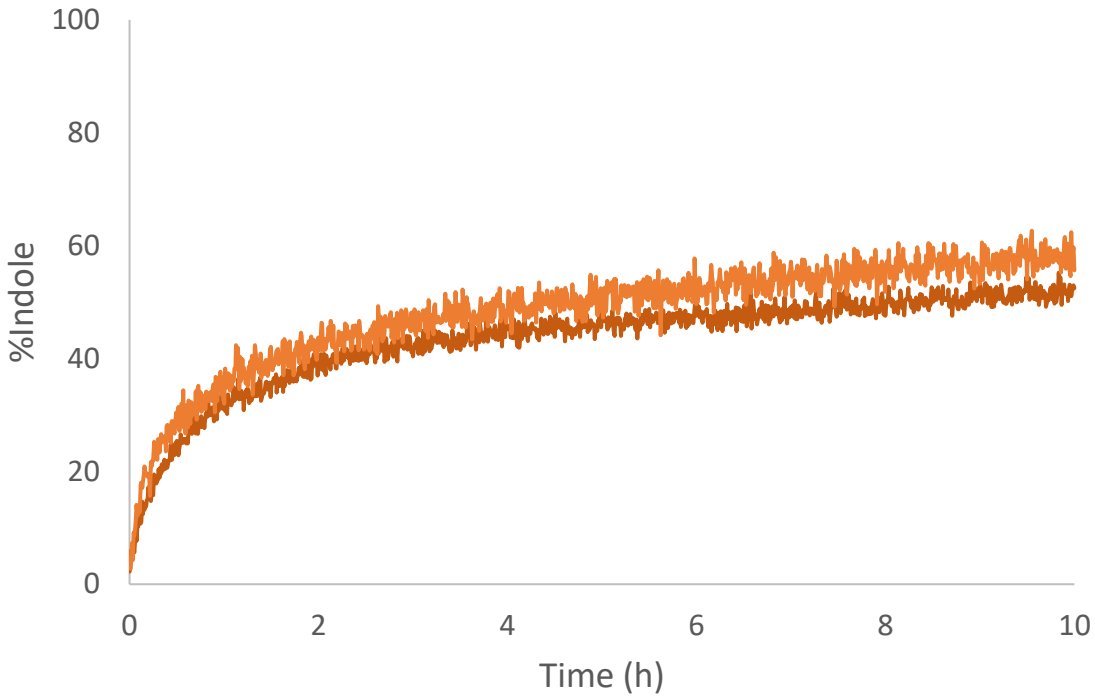

Appendix A.23. Percentage of indole formed over time using 350 mM indoline and 2.5 mM **1a** (0.7 mol%), monitored by *in-situ* IR spectroscopy. Reaction conditions: 110 °C, in anisole. Experiment was run in duplicate, and the overlap between the two runs indicate that the reaction is replicable.

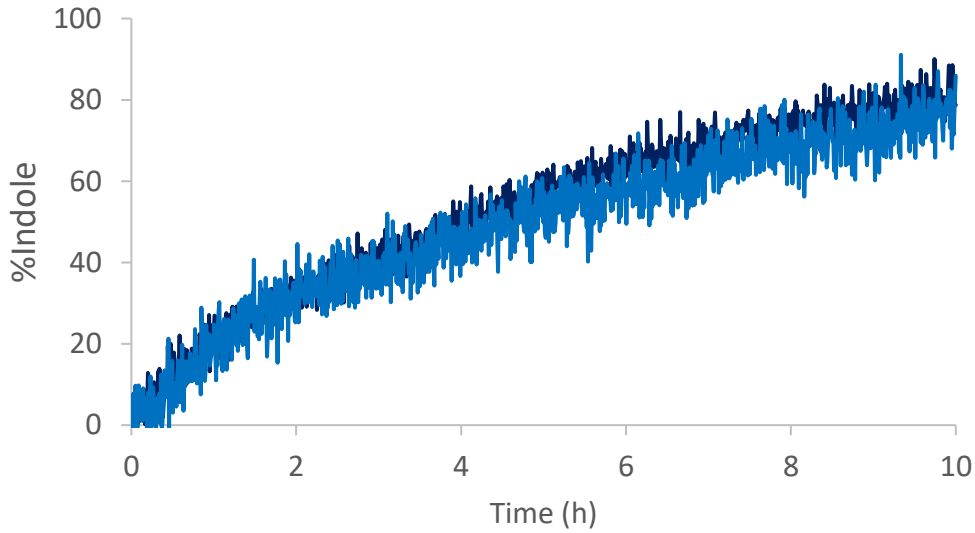

Appendix A.24. Percentage of indole formed over time using 250 mM indoline and 1.75 mM **1a** (0.7 mol%), monitored by *in-situ* IR spectroscopy. Reaction conditions: 110 °C, in anisole.

Experiment was run in duplicate, and the overlap between the two runs indicate that the reaction is replicable.

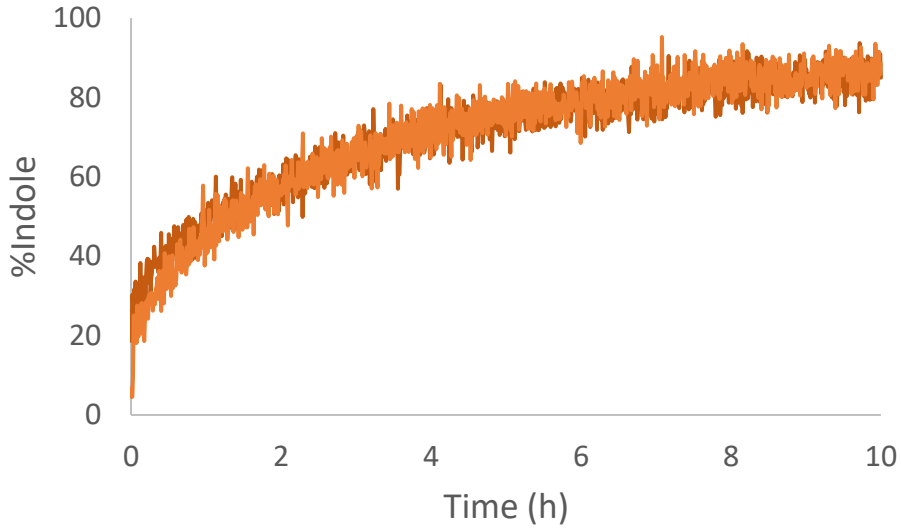

Appendix A.25. Percentage of indole formed over time using 250 mM indoline, 100 mM N-Me indoline, and 2.5 mM **1a** (1 mol% relative to indoline), monitored by *in-situ* IR spectroscopy. Reaction conditions: 110 °C, in anisole. Experiment was run in duplicate, and the overlap between the two runs indicate that the reaction is replicable.

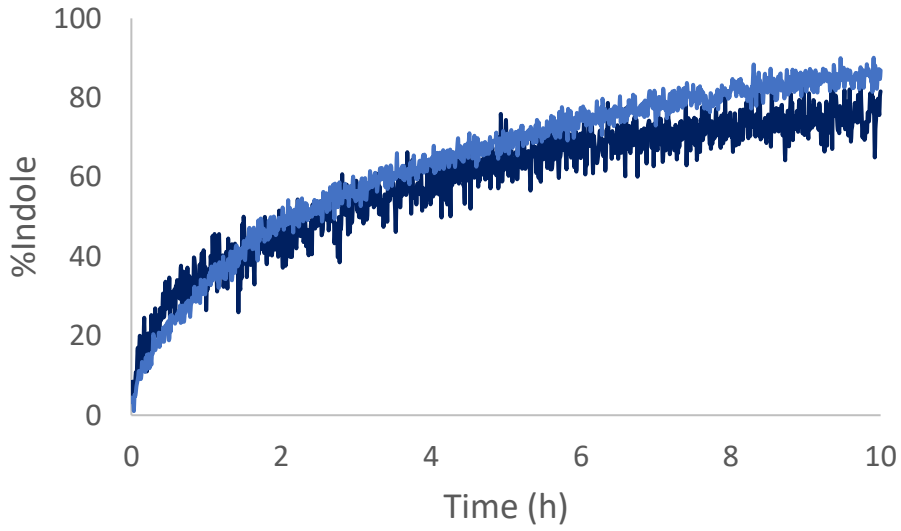

Appendix A.26. Percentage of indole formed over time using 250 mM indoline, 100 indole, and 2.5 mM **1a** (1 mol% relative to indoline), monitored by *in-situ* IR spectroscopy. Reaction conditions:

110 °C, in anisole. Experiment was run in duplicate, and the overlap between the two runs indicate that the reaction is replicable.

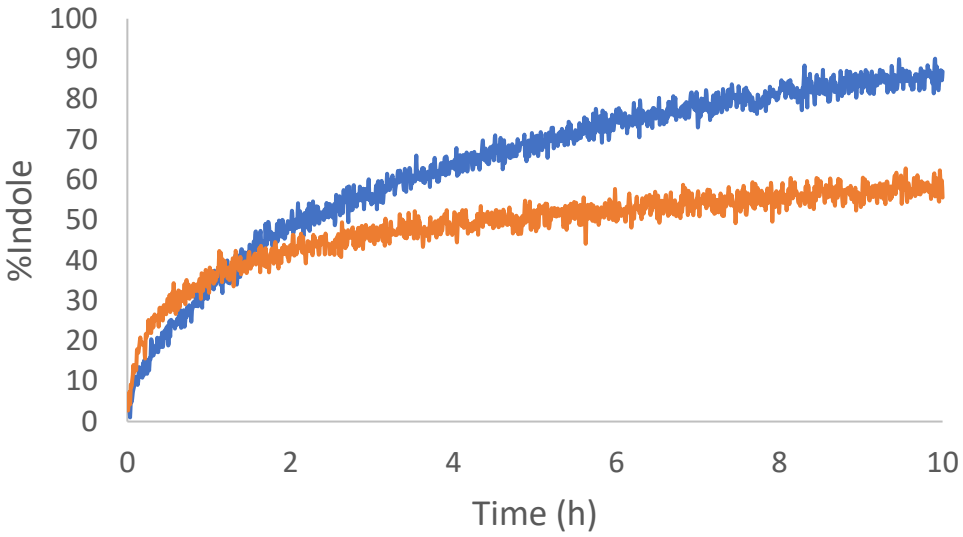

Appendix A.27. Percentage of indole formed over time for Run 1: 350 mM indoline, 2.5 mM **1a** (orange) and Run 2: 250 mM indoline, 2.5 mM **1a** (blue) over 10 h.

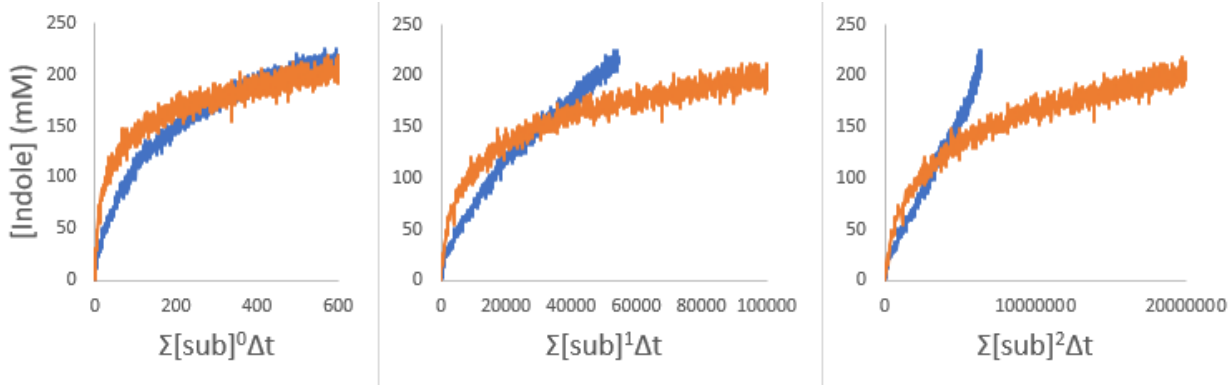

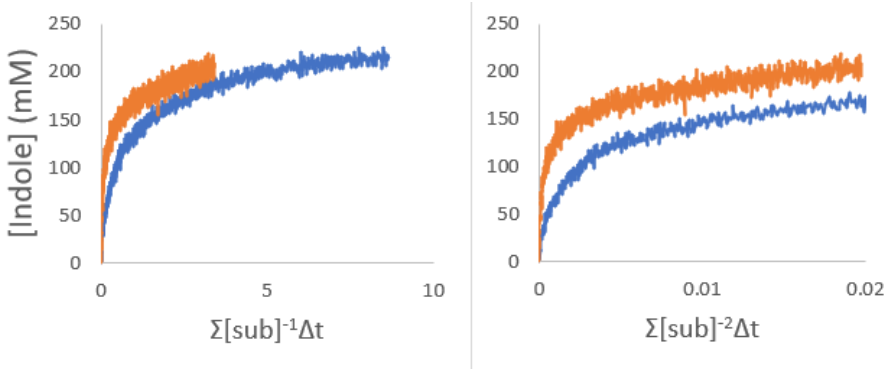

Appendix A.28. Plot of the concentration of indoline as a function of t[cat]^{x}, where x is -2 to +2. Rate order of [indoline] was unable to be concluded by VTNA. Orange data set = 350 mM indoline, 2.5 mM **1a**. Blue data set = 250 mM indoline, 2.5 mM **1a**.

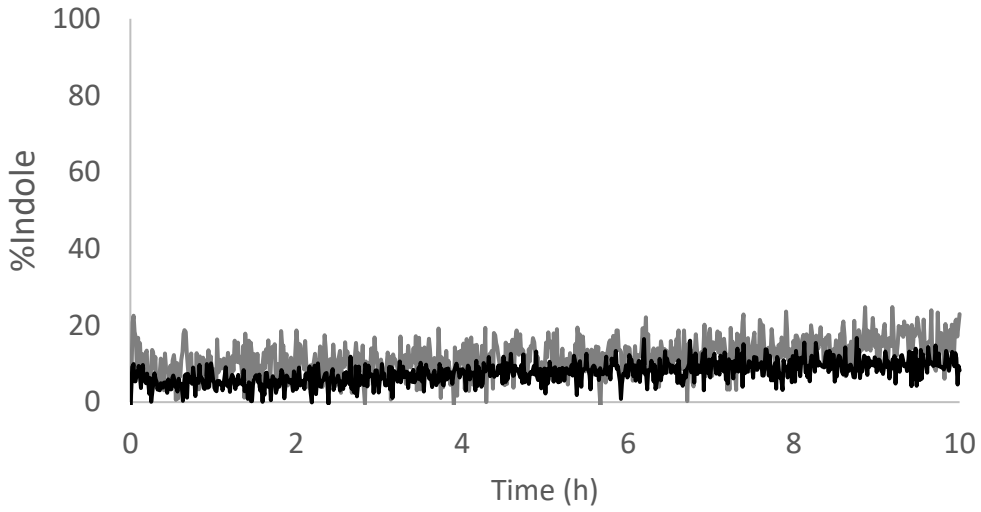

Appendix A.29. Percentage of indole formed over time using indoline-α-d_2. Reaction conditions: 250 mM indoline-α-d_2, 2.5 mM **1a**, 110 °C in anisole. Experiment was run in duplicate, and the overlap between the two runs indicate that the reaction is replicable.

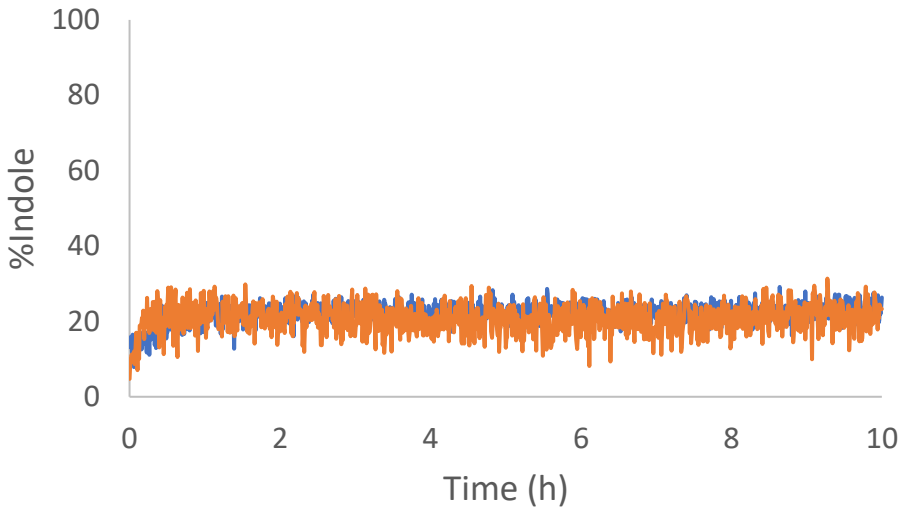

Appendix A.30. Percentage of indole formed over time using indoline-N-d_1 (68% deuterated). Reaction conditions: 250 mM indoline-N-d_1, 2.5 mM **1a**, 110 °C in anisole. Experiment was run in duplicate, and the overlap between the two runs indicate that the reaction is replicable.

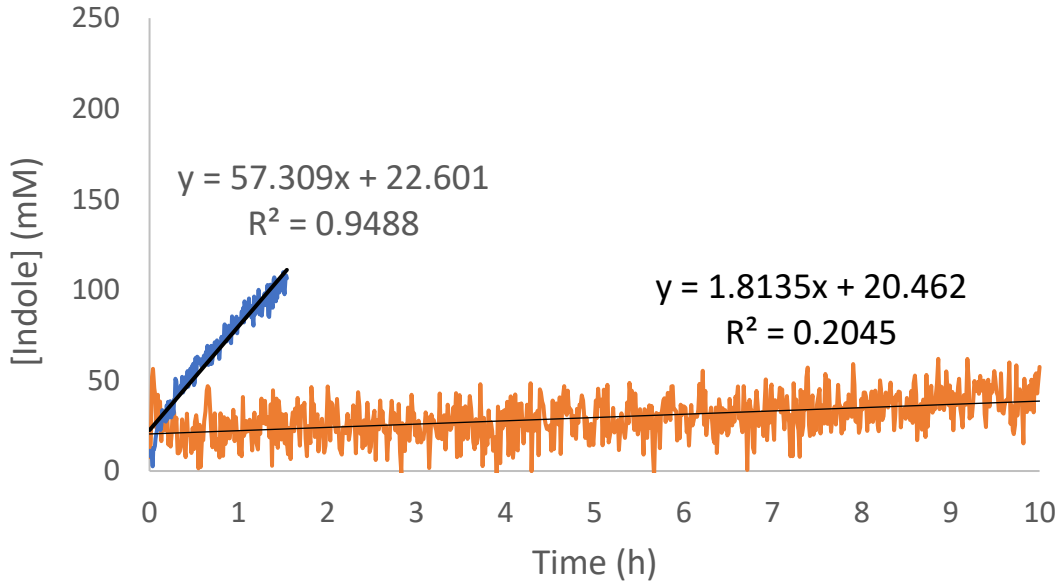

Appendix A.31. Plot of concentration of indole over time for indoline (blue) and indoline-α-d_2 (orange), for the first 40% of conversion. Trendlines and line equations (with R square values) generated using Microsoft excel (linear regression).

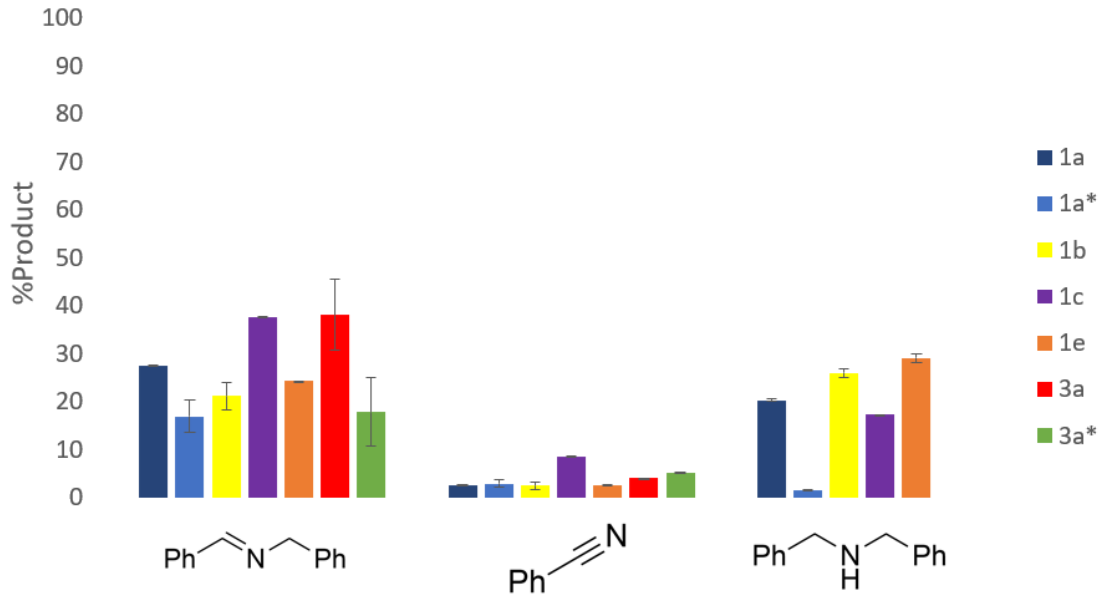

Catalyst	Conversion	ADC	Error ADC	DAD	Error DAD	HB	Error HB
1a	59	27.62194173	0.1461146	2.697294972	0.022707397	20.11980918	0.48991256
1a*	27	16.9356494	3.4352163	2.920902136	0.70424687	1.577458561	0.02914157
1b	45	21.14379391	2.935323	2.450209069	0.673285916	26.0741815	0.91907808
1c	70	37.7367052	0.0371618	8.672294611	0.004329653	17.25908773	0.00861662
1e	55	24.26188745	0.1067886	2.622730818	0.040422877	29.11088569	0.87752568
3a	43	38.14068902	7.4072324	4.03223895	0.067484552	0	
3a*	22	17.87331347	7.0868437	5.14674219	0.217343674	0	

Appendix A.32. Percent product formation for catalysts **1a-1c**, **1e**, **3a**, **3a*** for AD of benzylamine to form **ADC**, **DAD**, and **HB**. Bars display an average of two runs with the error bars showing the difference between the two runs. Raw data shown in table.

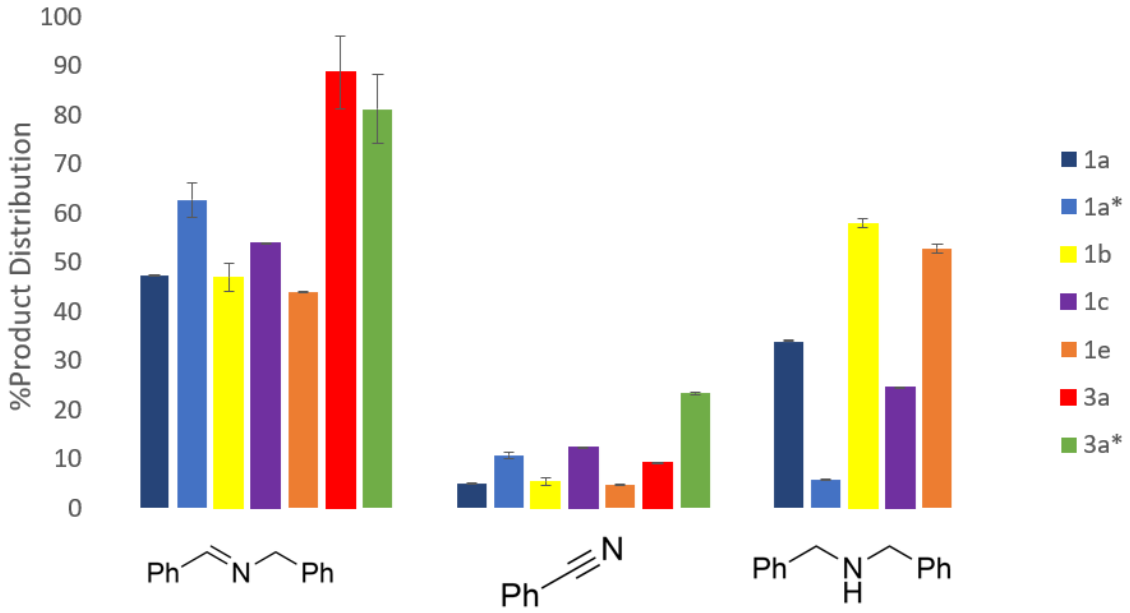

Appendix A.33. Product distribution for catalysts **1a-1c**, **1e**, **3a**, **3a*** for AD of benzylamine to form **ADC**, **DAD**, and **HB**. Bars display an average of two runs with the error bars showing the difference between the two runs. Product distribution = [(%ADC or %DAD or %HB)/(ADC+DAD+HB)]*100

References

(1) Crabtree, R. H. *The Organometallic Chemistry of the Transition Metals: Sixth Edition*, 6th ed.; John Wiley & Sons, Inc., 2014; Vol. 9781118138.

(2) Berton, G.; Leeuwen, P. W. N. M. Van. *Homogeneous Catalysis: Understanding the Art*; 2008.

(3) Cornils, B.; Herrmann, W. A. *J. Catal.* **2003**, *216* (1–2), 23–31.

(4) Kozuch, S.; Martin, J. M. L. *ACS Catal.* **2012**, *2* (12), 2787–2794.

(5) Ye, S.; Ding, C.; Li, C. *Artificial Photosynthesis Systems for Catalytic Water Oxidation*, 1st ed.; Elsevier Inc., 2019; Vol. 74.

(6) Fleming, F. F.; Yao, L.; Ravikumar, P. C.; Funk, L.; Shook, B. C. *J. Med. Chem.* **2010**, *53* (22), 7902–7917.

(7) Martin, S. F. *Pure Appl. Chem.* **2009**, *81* (2), 195–204.

(8) Fleming, F. F. *Nat. Prod. Rep.* **1999**, *16*, 597–606.

(9) Vitaku, E.; Smith, D. T.; Njardarson, J. T. *J. Med. Chem.* **2014**, *57* (24), 10257–10274.

(10) Belowich, M. E.; Stoddart, J. F. *Chem. Soc. Rev.* **2012**, *41* (6), 2003–2024.

(11) Layer, R. W. *Chem. Rev.* **1963**, *63* (5), 489–510.

(12) Schiff, H. *Justus Liebigs Ann. Chem.* **1864**, *131* (1), 118–119.

(13) Patil, R. D.; Adimurthy, S. *Asian J. Org. Chem.* **2013**, *2* (9), 726–744.

(14) Naeimi, H., Sharghi, H., Salimi, F., Rabiei, K. *Heteroat. Chem.* **2008**, *19* (1), 43–47.

(15) Nicolaou, K. C.; Mathison, C. J. N.; Montagnon, T. *Angew. Chemie - Int. Ed.* **2003**, *42* (34), 4077–4082.

(16) Aoyama, T.; Sonoda, N.; Yamauchi, M.; Toriyama, K.; Anzai, M.; Ando, A.; Shioiri, T. *Synlett* **1998**, No. 1, 35–36.

(17) Luca, O. R.; Wang, T.; Konezny, S. J.; Batista, V. S.; Crabtree, R. H. *New J. Chem.* **2011**, *35* (5), 998–999.

(18) Onto, K.; Hatakeyama, T.; Uchiito, S.; Tokuda, M.; Suginome, H. *Tetrahedron* **1998**, *54* (29), 8403–8410.

(19) Gunanathan, C.; Milstein, D. *Science*. American Association for the Advancement of Science July 19, 2013.

(20) Ell, A. H.; Samec, J. S. M.; Brasse, C.; Bäckvall, J.-E. *Chem. Commun.* **2002**, *33* (35), 1144–1145.

(21) Grasselli, R. K. *Catal. Today* **1999**, *49* (1–3), 141–153.

(22) Hodgson, H. H. *Chem. Rev.* **1947**, *40* (2), 251–277.

(23) Chakraborty, S.; Patel, Y. J.; Krause, J. A.; Guan, H. *Angew. Chemie - Int. Ed.* **2013**, *52* (29), 7523–7526.

(24) Velcicky, J.; Soicke, A.; Steiner, R.; Schmalz, H. G. *J. Am. Chem. Soc.* **2011**, *133* (18), 6948–6951.

(25) Falk, A.; Göderz, A. L.; Schmalz, H. G. *Angew. Chemie - Int. Ed.* **2013**, *52* (5), 1576–1580.

(26) Ishihara, K.; Furuya, Y.; Yamamoto, H. *Angew. Chemie - Int. Ed.* **2002**, *41* (16), 2983–2986.

(27) Yamaguchi, K.; Fujiwara, H.; Ogasawara, Y.; Kotani, M.; Mizuno, N. *Angew. Chemie - Int. Ed.* **2007**, *46* (21), 3922–3925.

(28) Verbindung, D.; Rosenmund, K. W.; Struck, E.; Mitteilung, I.; Berlin, U.; Hilfe, M.; Verfahrens, K.; Wasser, K. *Ber. Ber. Dtsch. Chem. Ges. B* **1919**, *52*, 1749–1756.

(29) Ellis, G. P.; Romney-Alexander, T. M. *Chem. Rev.* **1987**, *87* (4), 779–794.

(30) Gu, X. Q.; Chen, W.; Morales-Morales, D.; Jensen, C. M. *J. Mol. Catal. A Chem.* **2002**, *189* (1), 119–124.

(31) Jensen, C. M. *Chem. Commun.* **1999**, *3* (24), 2443–2449.

(32) Gupta, M.; Hagen, C.; Flesher, R. J.; Kaska, W. C.; Jensen, C. M. *Chem. Commun.* **1996**, *36* (17), 2083–2084.

(33) Chae, S. Y.; Do, W. L. *Organometallics* **2009**, *28* (4), 947–949.

(34) Gnanaprakasam, B.; Zhang, J.; Milstein, D. **2010**, 1468–1471.

(35) Gunanthan, C., Ben-David, Y., Milstein, D. *Science (80-.).* **2007**, *317* (August), 2005–2008.

(36) Crabtree, R. H. **2017**, *9246* (1).

(37) Borghs, J. C.; Azofra, M.; Biberger, T.; Linnenberg, O. *ChemSusChem* **2019**, 3083–3088.

(38) Chai, H.; Yu, K.; Liu, B.; Tan, W.; Zhang, G. *Organometallics* **2020**, *39*, 217–226.

(39) Saha, B.; Rahaman, S. M. W.; Daw, P.; Sengupta, G.; Bera, J. K. *Chem. Eur. J.* **2014**, *20*, 6542–6551.

(40) Das, K.; Mondal, A.; Pal, D.; Srivastava, H. K.; Srimani, D. *Organometallics* **2019**, *38*, 1815–1825.

(41) Donthireddy, S. N. R.; Pandey, V. K.; Rit, A. *J. Org. Chem.* **2021**, No. 86, 6994–7001.

(42) Miao, Y.; Samuelsen, S. V; Madsen, R. *Organometallics* **2021**, *40*, 1328–1335.

(43) Bottaro, F.; Madsen, R. *ChemCatChem* **2019**, *11*, 2707–2712.

(44) Azizi, K.; Akrami, S.; Madsen, R. *Chem. Eur. J.* **2019**, *25* (Iii), 6439–6446.

(45) Mondal, R.; Herbert, D. E. *Organometallics* **2020**, *39*, 1310–1317.

(46) Huang, M.; Liu, J.; Li, Y.; Lan, X.; Su, P.; Zhao, C. *Catal. Today* **2021**, *370* (July 2020), 114–141.

(47) Zhang, G.; Hanson, S. K. *Org. Lett.* **2013**, No. 11, 10325–10328.

(48) Tseng, K. N. T.; Kampf, J. W.; Szymczak, N. K. *ACS Catal.* **2015**, *5* (9), 5468–5485.

(49) Eisenstein, O.; Crabtree, R. H. *New J. Chem.* **2013**, *37* (1), 21–27.

(50) Hale, L. V. A.; Malakar, T.; Tseng, K. N. T.; Zimmerman, P. M.; Paul, A.; Szymczak, N. K. *ACS Catal.* **2016**, *6* (8), 4799–4813.

(51) Dub, P. A.; Gordon, J. C. *ACS Catal.* **2017**, *7* (10), 6635–6655.

(52) Blum, Y.; Czarkle, D.; Rahamlm, Y.; Shvo, Y. *Organometallics* **1985**, *4* (8), 1459–1461.

(53) Noyori, R. *Angew. Chemie - Int. Ed.* **2002**, *41* (12), 2008–2022.

(54) Prades, A.; Peris, E.; Albrecht, M. *Organometallics* **2011**, *30* (5), 1162–1167.

(55) Wang, Z.; Belli, J.; Jensen, C. M. *Faraday Discuss.* **2011**, *151*, 297–305.

(56) Bernskoetter, W. H.; Brookhart, M. *Organometallics* **2008**, *27* (9), 2036–2045.

(57) Zhang, Y.; Chen, C.; Ghosh, S. C.; Li, Y.; Hong, S. H. *Organometallics* **2010**, *29* (6), 1374–1378.

(58) Ho, H. A.; Manna, K.; Sadow, A. D. *Angew. Chemie - Int. Ed.* **2012**, *51* (34), 8607–8610.

(59) He, L. P.; Chen, T.; Gong, D.; Lai, Z.; Huang, K. W. *Organometallics* **2012**, *31* (14), 5208–5211.

(60) Li, H.; Gonçalves, T. P.; Lupp, D.; Huang, K. W. *ACS Catal.* **2019**, *9* (3), 1619–1629.

(61) Zhang, J.; Gandelman, M.; Shimon, L. J. W.; Rozenberg, H.; Milstein, D. *Organometallics* **2004**, *23* (17), 4026–4033.

(62) Tseng, K. N. T.; Rizzi, A. M.; Szymczak, N. K. *J. Am. Chem. Soc.* **2013**, *135* (44), 16352–16355.

(63) Ventura-Espinosa, D.; Marzá-Beltrán, A.; Mata, J. A. *Chem. - A Eur. J.* **2016**, *22* (49), 17758–17766.

(64) Valencia, M.; Pereira, A.; Müller-Bunz, H.; Belderraín, T. R.; Pérez, P. J.; Albrecht, M. *Chem. - A Eur. J.* **2017**, *23* (37), 8901–8911.

(65) Kannan, M.; Barteja, P.; Devi, P.; Muthaiah, S. *J. Catal.* **2020**, *386*, 1–11.

(66) Kannan, M.; Muthaiah, S. *Synlett* **2020**, *31* (11), 1073–1076.

(67) Achard, T.; Egly, J.; Sigrist, M.; Maisse-François, A.; Bellemin-Laponnaz, S. *Chem. - A Eur. J.* **2019**, *25* (58), 13271–13274.

(68) Takallou, A.; Habibi, A.; Halimehjan, A. Z.; Balalaie, S. *Appl. Organomet. Chem.* **2020**, *34* (3), 1–8.

(69) Klarner, M.; Hammon, S.; Feulner, S.; Kümmel, S.; Kador, L.; Kempe, R. *ChemCatChem* **2020**, *12* (18), 4593–4599.

(70) Nie, X.; Zheng, Y.; Ji, L.; Fu, H.; Chen, H.; Li, R. *J. Catal.* **2020**, *391*, 378–385.

(71) Bottaro, F.; Takallou, A.; Chehaiber, A.; Madsen, R. *European J. Org. Chem.* **2019**, *2019*

(42), 7164–7168.

(72) Chakraborty, S.; Leitus, G.; Milstein, D. *Angew. Chemie - Int. Ed.* **2017**, *56* (8), 2074–2078.

(73) Kannan, M.; Muthaiah, S. *Organometallics* **2019**, *38* (19), 3560–3567.

(74) Tseng, K. N. T.; Szymczak, N. K. *Synlett* **2014**, *25* (17), 2385–2389.

(75) Prades, A.; Peris, E.; Albrecht, M. *Organometallics* **2011**, *30*, 1162–1167.

(76) Chen, W.; Egly, J.; Poblador-Bahamonde, A. I.; Maisse-Francois, A.; Bellemin-Laponnaz, S.; Achard, T. *Dalt. Trans.* **2020**, *49* (10), 3243–3252.

(77) Pretorius, R.; Olguín, J.; Albrecht, M. *Inorg. Chem.* **2017**, *56* (20), 12410–12420.

(78) Nazarahari, M.; Azizian, J. *Chem. Pap.* **2021**, *75* (11), 5705–5710.

(79) Dutta, I.; Yadav, S.; Sarbajna, A.; De, S.; Hölscher, M.; Leitner, W.; Bera, J. K. *J. Am. Chem. Soc.* **2018**, *140* (28), 8662–8666.

(80) Stubbs, J. M.; Hazlehurst, R. J.; Boyle, P. D.; Blacquiere, J. M. *Organometallics* **2017**, *36* (9), 1692–1698.

(81) Niu, X.; Yang, L. *Adv. Synth. Catal.* **2021**, *363* (17), 4209–4215.

(82) Talwar, D.; Gonzalez-De-Castro, A.; Li, H. Y.; Xiao, J. *Angew. Chemie - Int. Ed.* **2015**, *54* (17), 5223–5227.

(83) Chakraborty, S.; Brennessel, W. W.; Jones, W. D. *J. Am. Chem. Soc.* **2014**, *136* (24), 8564–8567.

(84) Zhang, D.; Iwai, T.; Sawamura, M. *Org. Lett.* **2020**, *22* (13), 5240–5245.

(85) Sánchez, P.; Hernández-Juárez, M.; Rendón, N.; López-Serrano, J.; Santos, L. L.; Álvarez, E.; Paneque, M.; Suárez, A. *Dalt. Trans.* **2020**, *49* (28), 9583–9587.

(86) Balayeva, N. O.; Mamiyev, Z.; Dillert, R.; Zheng, N.; Bahnemann, D. W. *ACS Catal.* **2020**, *10* (10), 5542–5553.

(87) Ryabchuk, P.; Agapova, A.; Kreyenschulte, C.; Lund, H.; Junge, H.; Junge, K.; Beller, M. *Chem. Commun.* **2019**, *55* (34), 4969–4972.

(88) Buil, M. L.; Esteruelas, M. A.; Gay, M. P.; Gómez-Gallego, M.; Nicasio, A. I.; Oñate, E.; Santiago, A.; Sierra, M. A. *Organometallics* **2018**, *37* (4), 603–617.

(89) Sawatlon, B.; Surawatanawong, P. *Dalt. Trans.* **2016**, *45* (38), 14965–14978.

(90) Cooksey, J. P.; Saidi, O.; Williams, J. M. J.; Blacker, A. J.; Marsden, S. P. *Tetrahedron* **2021**, *78*, 131785.

(91) Muthaiah, S.; Hong, S. H. *Adv. Synth. Catal.* **2012**, *354* (16), 3045–3053.

(92) Sahoo, M. K.; Balaraman, E. *Green Chem.* **2019**, *21* (8), 2119–2128.

(93) Hu, H., Wodrich, M. D. *Nat. Rev. Chem.* **2018**, *2*.

(94) Hale, L. V. A.; Szymczak, N. K. *ACS Catal.* **2018**, *8* (7), 6446–6461.

(95) Bullock, R. M.; Helm, M. L. *Acc. Chem. Res.* **2015**, *48* (7), 2017–2026.

(96) Liu, T.; Chen, S.; O'Hagan, M. J.; Rakowski Dubois, M.; Bullock, R. M.; Dubois, D. L. *J. Am. Chem. Soc.* **2012**, *134* (14), 6257–6272.

(97) Liu, T.; Dubois, M. R.; Dubois, D. L.; Bullock, R. M. *Energy Environ. Sci.* **2014**, *7* (11), 3630–3639.

(98) Liu, T.; Wang, X.; Hoffmann, C.; Dubois, D. L.; Bullock, R. M. *Angew. Chemie - Int. Ed.* **2014**, *53* (21), 5300–5304.

(99) Liu, T.; Dubois, D. L.; Bullock, R. M. *Nat. Chem.* **2013**, *5* (3), 228–233.

(100) Zong, J.; Mague, J. T.; Pascal, R. A. *J. Am. Chem. Soc.* **2013**, *135* (36), 13235–13237.

(101) Kilgore, U. J.; Stewart, M. P.; Helm, M. L.; Dougherty, W. G.; Kassel, W. S.; Dubois, M. R.; Dubois, D. L.; Bullock, R. M. *Inorg. Chem.* **2011**, *50* (21), 10908–10918.

(102) Wiese, S.; Kilgore, U. J.; Dubois, D. L.; Bullock, R. M. *ACS Catal.* **2012**, *2* (5), 720–727.

(103) Weiss, C. J.; Das, P.; Miller, D. L.; Helm, M. L.; Appel, A. M. *ACS Catal.* **2014**, *4* (9), 2951–2958.

(104) Raugei, S.; Helm, M. L.; Hammes-Schiffer, S.; Appel, A. M.; O'Hagan, M.; Wiedner, E. S.; Bullock, R. M. *Inorg. Chem.* **2016**, *55* (2), 445–460.

(105) Stubbs, J.M., Hoffman, M.D., El-Zouki, E., Blacquiere, J. M. *Manuscr. Prep.* **2020**.

(106) Stubbs, J. M.; Bow, J. P. J.; Hazlehurst, R. J.; Blacquiere, J. M. *Dalt. Trans.* **2016**, *45* (43), 17100–17103.

(107) Kündig, E. P.; Monnier, F. R. *Adv. Synth. Catal.* **2004**, *346* (8), 901–904.

(108) Mercier, A.; Yeo, W. C.; Chou, J.; Chaudhuri, P. D.; Bernardinelli, G.; Kündig, E. P. *Chem. Commun.* **2009**, No. 35, 5227–5229.

(109) Stubbs, J. M.; Chapple, D. E.; Boyle, P. D.; Blacquiere, J. M. *ChemCatChem* **2018**, *10* (17), 3694–3702.

(110) Bridge, B. J.; Boyle, P. D.; Blacquiere, J. M. *Organometallics* **2020**.

(111) Bridge, B. J. *MSc. Thesis* **2020**.

(112) Liao, Q.; Liu, T.; Johnson, S. I.; Klug, C. M.; Wiedner, E. S.; Morris Bullock, R.; Dubois, D. L. *Dalt. Trans.* **2019**, *48* (15), 4867–4878.

(113) Rong, B.; Zhong, W.; Gu, E.; Long, L.; Song, L.; Liu, X. *Electrochim. Acta* **2018**, *283*, 27–35.

(114) Bridge, B. J.; Boyle, P. D.; Blacquiere, J. M. *Organometallics* **2020**, *39* (14), 2570–2574.

(115) Cheng, T. Y.; Bullock, R. M. *Organometallics* **2002**, *21* (11), 2325–2331.

(116) Abdur-Rashid, K.; Fong, T. P.; Greaves, B.; Gusev, D. G.; Hinman, J. G.; Landau, S. E.; Lough, A. J.; Morris, R. H. *J. Am. Chem. Soc.* **2000**, *122* (38), 9155–9171.

(117) Kanzian, T.; Nigst, T. A.; Maier, A.; Pichl, S.; Mayr, H. *European J. Org. Chem.* **2009**, No. 36, 6379–6385.

(118) Brotzel, F.; Ying, C. C.; Mayr, H. *J. Org. Chem.* **2007**, *72* (10), 3679–3688.

(119) Tshepelevitsh, S.; Kütt, A.; Lõkov, M.; Kaljurand, I.; Saame, J.; Heering, A.; Plieger, P. G.; Vianello, R.; Leito, I. *European J. Org. Chem.* **2019**, *2019* (40), 6735–6748.

(120) Nakagawa, Y.; Uehara, K.; Mizuno, N. *Inorg. Chem.* **2005**, *44* (24), 9068–9075.

(121) Majoube, M.; Vergoten, G. *J. Raman Spectrosc.* **1992**, *23* (8), 431–444.

(122) Burés, J. *Angew. Chemie - Int. Ed.* **2016**, *55* (52), 16084–16087.

(123) Meek, S. J.; Pitman, C. L.; Miller, A. J. M. *J. Chem. Educ.* **2016**, *93* (2), 275–286.

(124) Meisner, J.; Kästner, J. *Angew. Chemie - Int. Ed.* **2016**, *55* (18), 5400–5413.

(125) Banjare, S. K.; Nanda, T.; Ravikumar, P. C. *Org. Lett.* **2019**, *21* (19), 8138–8143.

(126) Ahlbrecht, H.; Düber, E. O.; Epsztajn, J.; Marcinkowski, R. M. K. *Tetrahedron* **1984**, *40* (7), 1157–1165.

(127) Ohwada, T.; Miura, M.; Tanaka, H.; Sakamoto, S. **2001**, 10164–10172.

(128) Fung, B. M.; Wei, I. Y. *J. Am. Chem. Soc.* **1970**, *92* (6), 1497–1501.

(129) Patiny, L.; Borel, A. *J. Chem. Inf. Model.* **2013**, *53* (5), 1223–1228.